AD-A151 703 MEASUREMENT OF THE LINEWIDTHS OF HYDROGEN FLUORIDE Q-TRANSITIONS USING CO.. (U) AIR FORCE INST OF TECH WRIGHT-PATTERSON AFB OH SCHOOL OF ENGI.. R A CLEIS

1/2

UNCLASSIFIED DEC 83 AFIT/GEO/PH/83D-2 F/G 7/4 NL

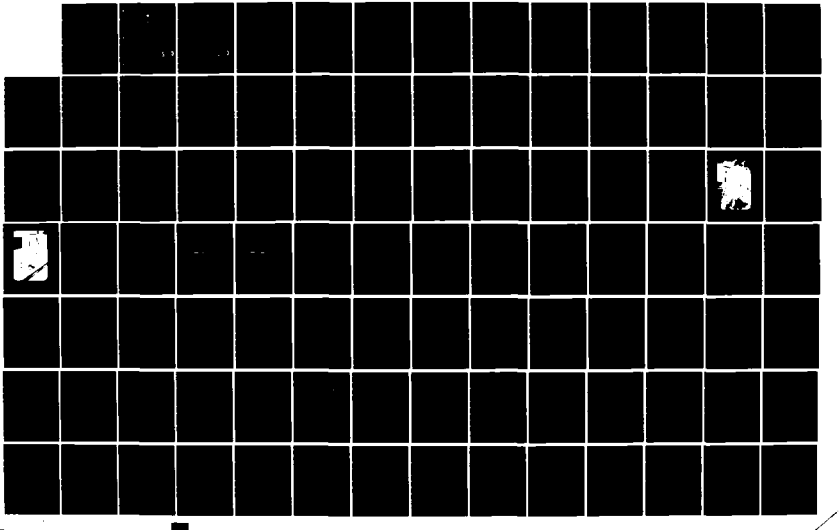

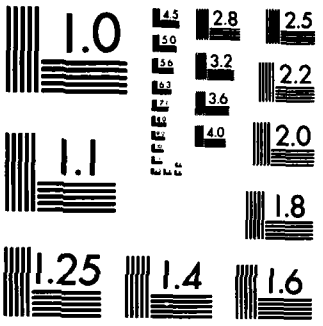

MEASUREMENT OF THE LINEWIDTHS OF HYDROGEN FLUORIDE Q-TRANSITIONS USING COHERENT ANTI-STOKES RAMAN SPECTROSCOPY

THESIS

Richard A. Cleis
Second Lieutenant, USAF

AFIT/GEO/PH/83D-2

DEPARTMENT OF THE AIR FORCE
AIR UNIVERSITY
AIR FORCE INSTITUTE OF TECHNOLOGY

Wright-Patterson Air Force Base, Ohio

MEASUREMENT OF THE LINEWIDTHS OF HYDROGEN FLUORIDE Q-TRANSITIONS USING COHERENT ANTI-STOKES RAMAN SPECTROSCOPY

THESIS

Richard A. Cleis
Second Lieutenant, USAF

AFIT/GEO/PH/83D-2

Approved for public release; distribution unlimited

AFIT/GEO/PH/83D-2

MEASUREMENT OF THE LINEWIDTHS OF HYDROGEN FLUORIDE Q-TRANSTIONS USING COHERENT ANTI-STOKES RAMAN SPECTROSCOPY

THESIS

Presented to the Faculty of the School of Engineering

of the Air Force Institute of Technology

Air University

In Partial Fulfillment of the

Requirements for the Degree of

Master of Science in Electrical Engineering

Richard A. Cleis, B.S.

Second Lieutenant, USAF

December 1983

Preface

The purpose of this project was to measure with CARS equipment the linewidths of Raman transitions in HF. A similar analysis of DF was planned since both gases are used in high energy lasers. Unfortunate circumstances prevented the study of DF, but the procedures developed for the HF experiments and analyses should apply to DF with little modification.

I could not have successfully completed this project without the guidance of my faculty advisor, Won B. Roh., who's patience knows no bounds. Larry P. Goss also provided invaluable assistance and contributed much of the software required for the analysis. Their years of previous effort made the present project possible.

Richard A. Cleis

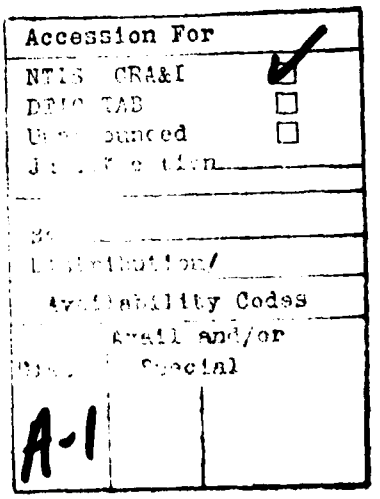

Table of Contents

List of Figures

List of Tables

Abstract

The measurement of the linewidths of the Hydrogen Fluoride Q-branch vibrational-rotational transitions was performed using coherent anti-Stokes Raman spectroscopy (CARS). A broadband CARS system was used to excite the first seven vibrational-rotational transitions in the Q-branch of HF. Low resolution spectra were recorded on an optical multichannel analyzer at pressures from 50 to 700 torr in 50 torr increments. At each pressure, 1000 measurements were averaged. A computer was programmed to best fit calculated spectra to experimental spectra by adjusting the linewidths. The linewidth of the Q(3) transition was estimated from infrared data then used as a reference in determining the linewidths of the other transition. All lines displayed pressure broadening in the pressure region investigated with relative magnitudes consistent with theory and available infrared data. Although the Q-branch lines of the observed spectra were partially blended, the CARS measurements and calculations permitted consistent linewidth measurements over the experimental pressure range. Accurate knowledge of the instrument slit function permits linewidth measurements without requiring a reference.

MEASUREMENT OF THE LINEWIDTHS OF HYDROGEN FLUORIDE Q-TRANSITIONS USING COHERENT ANTI-STOKES RAMAN SPECTROSCOPY

I. Introduction

Coherent anti-Stokes Raman spectroscopy (CARS) is an effective tool for remote diagnostics of gases. Parameters such as number density and temperature can be determined without introducing sensors into the medium under investigation. Much information is contained in the Raman transitions of gas molecules, so it is the goal of CARS to excite the transitions and produce an anti-Stokes signal that can be anaylzed to extract the desired information. Laser radiation provides the means for generating an anti-Stokes signal. Typically, two laser beams are focused to a point in the gas and the emerging anti-Stokes beam propagates away from the gas where it can be analyzed as conventiently as any ordinary coherent radiation.

Both CW and pulsed CARS systems have been built (1) (2) (3). The commercial availability of Q-switched lasers has enabled the development of CARS systems which can obtain spectra in sub-microsecond intervals. This capability permits the measurement of near-instantaneous gas parameters in highly dynamic environments. In CARS experiments, either a narrow excitation signal is used to excite one Raman transition or a broad-band excitation signal is used to excite a large number of transitions. The former narrow-band method can be used for high-

resolution spectroscopy but it must have the capability of precise frequency tuning. On the other hand, the broad-band method yields information about many Raman transitions simultaneously with lasers of fixed frequency.

Under proper conditions, the spectra obtained from a given CARS signal will not be affected by the behavior of molecules that do not have Raman transitions at the frequency of the transitions in the intentionally excited molecules. Cars is therefore suitable for the study of chemical reactions since one gas species can be investigated at a time. Combustion flames are routinely examined by tuning the CARS apparatus to the Raman transitions of nitrogen and recording the spectrum of the anti-Stokes radiation (3). Since the properties of the Raman transitions in N_2 at different temperatures are well documented, the spectrum can be used to determine information such as the temperature of the gas.

The objective of this thesis is measuring the linewidths of the Raman transitions of the Q-branch in hydrogen fluoride using CARS. Hydrogen fluoride is a product of the chemical reaction of hydrogen and fluorine when they are mixed for the purpose of providing the gain medium for high energy lasers. The Air Force is interested in HF lasers since their potential for propagating enormous amounts of energy makes them candidates for future weapons. During laser operation, making diagnostic meausurements of the HF produced in the reaction is difficult because ordinary sensors mounted in the combustion chamber cannot endure the high temperatures and the very corrosive HF. CARS is one possible diagnostic method since it does not require the placement of any material in the combustion chamber; it only requires windows through

which it can propagate laser radiation. However, if CARS is to be used for analyzing HF, then the properties of the Raman transitions must be understood as is true of the Raman transitions of N_2 in the earlier example.

The properties of the Raman transitions relevent to CARS are contained in the equation for the Raman susceptibility. The intensity of the anti-Stokes radiation at a given frequency is roughly proportional to the squared-modulus of the Raman susceptibility evaluated at the corresponding frequency of excitiation of the Raman transition. When the excitation energy is perfectly resonant with a transition, the Raman susceptibility is inversely proportional to the linewidth of the transition. For the case of broad-band CARS, where multiple Raman transitions are simultaneously excited, the relative intensities of the resolved anti-Stokes lines are determined by the relative linewidths and the densities of states of the transitions. In the earlier combustion example, the linewidths are known so other gas parameters can be determined. For the case of HF, the linewidths are not known to the best of our knowledge. Since linewidth knowledge is essential for HF CARS diagnostics, the first seven linewidths in the Q-branch are estimated in this project.

HF was also chosen for the project since the method of using broad-band CARS with a low resolution detector has not been established for measuring linewidths. Unlike most molecules, the linewidths of HF vary considerably with the rotational quantum number of the lower state of the transition. This peculiar property challenges the procedure since a range of linewidths are observed rather than similar linewidths in every observed transition.

TABLE III

Calculation of HF Linewidths at 1 Atmosphere (10)

HWHM cm^{-1}

R(J),P(J+1)	Temperature (K) 390	480
0	0.457	0.407
1	0.592	0.538
2	0.635	0.601
3	0.556	0.561
4	0.412	0.451
5	0.266	0.321
6	0.156	0.209

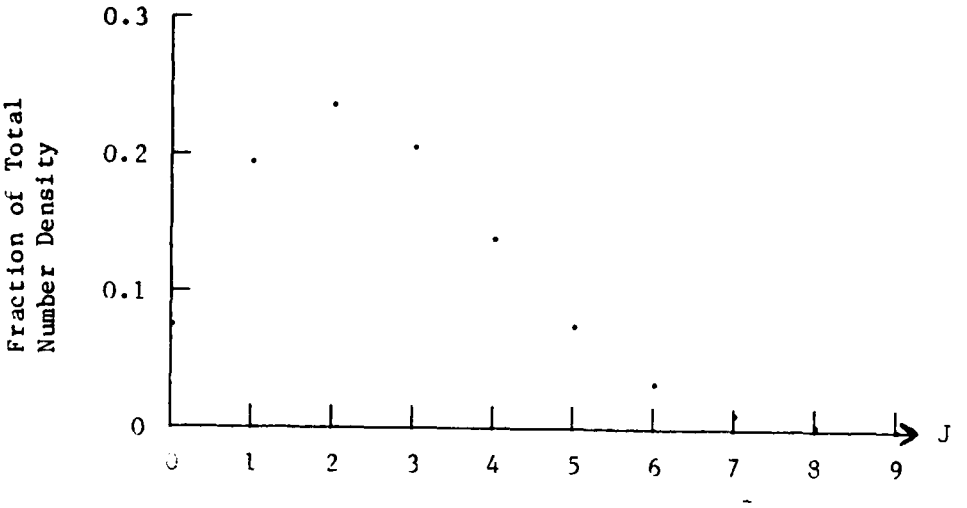

Fig. 3. Fractional Population Density in Rotational States of the Ground Vibrational State of HF at 373 K.

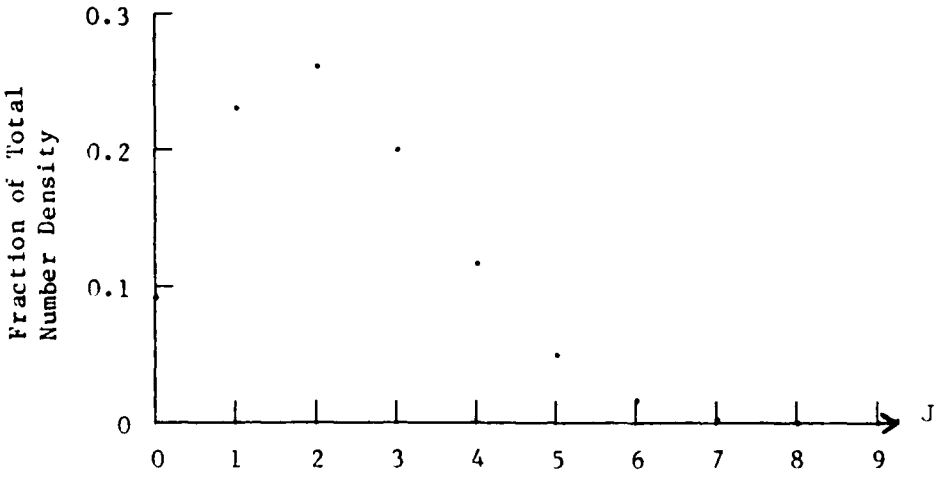

Fig. 4. Fractional Population Density in Rotational States of the Ground Vibrational State of HF at 300 K.

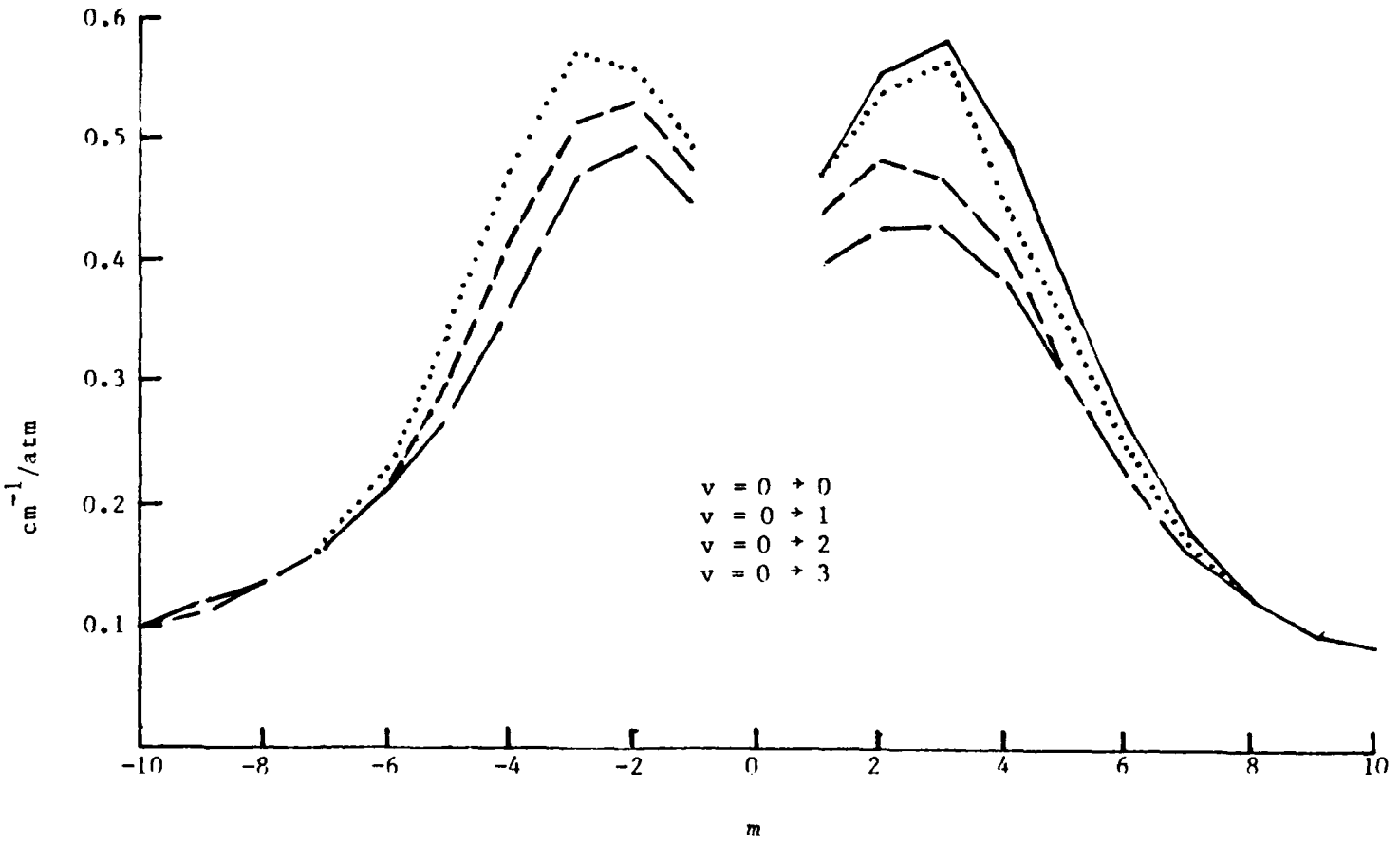

Fig. 2. Q-Branch Pressure-Broadening Coefficients Calculated for HF at 373 K (8). For R(J) transitions, m=J+1. For P(J) transitions, m=-J

$$\Gamma_J = [n\bar{v}/(2\pi C)] \sum \rho_j \alpha_j \qquad (16)$$

where J is the rotational quantum number of the lower state of a transition, $\bar{v}$ is the mean relative collision velocity, ρ_j is the density of perturbers, and α_j is the collision cross section for resonant interaction processes. It is reasonable to expect that a Q-transition formula has a similar form but different constants. For self-broadened lines, $\rho_j \approx N_J$ which is determined with Eqs (11-15). Each term in the sum is weighted by the density of states so the transitions corresponding to the most populous J levels are expected to be broadened most. Calculations at 373 K (Fig. 2) show that this qualitative estimation may have some validity, although a thorough knowledge of the cross section factor is needed to eliminate the possibility of coincidence. The population distribution for HF at 373 K is shown in Fig. 3.

For some gases, the temperature dependence of the linewidths in the pressure-broadened regime is primarily determined by the collision frequencies. Velocity and number density dictate the collision frequencies, so the velocity contributes a factor proportional to the square root of temperature while the number density contributes a factor inversely proportional to temperature. The net result is linewidths inversely proportional to the square root of temperature. For large temperature changes, the population of each J level will change significantly causing each linewidth to change in a more complicated manner than the simple inverse square root relation (Eq 16). Inspection of Table III reveals this peculiar effect in HF for temperatures of 390 K and 480 K. Linewidths of transitions with low J decrease with an increase in temperature, but transitions with higher J broaden over the

$$B_v = B_e - \alpha_e(v + 1/2) \tag{13}$$

The total number of molecules in a given energy state can be calculated from the Maxwell-Boltzmann distribution equation:

$$N_J = (N/Q_{vJ})(2J+1)\exp\{-[F_v(J) + G(v)]hc/kT\} \tag{14}$$

where F and G are the rotational and vibrational term values and Q_{vJ} is the state sum of all molecules in the sample:

$$Q_{vJ} = (2J+1)\exp\{-[F_v(J) + G(v)]hc/kT\} \tag{15}$$

The frequencies of the Raman transitions are determined by the term values. At room temperature the populations of levels with v>1 is negligible. The rotational quantum number of Q-branch transitions remains constant so for the most significant transitions, those ocurring between v=0 and v=1, $\Omega_J = F_1(J)+G(1)-F_0(J)-G(0)$ where Ω_J is the frequency of the Q(J) transition. Table II shows Ω_J for J=0 through 6.

Linewidth Dependence on Pressure, J, and Temperature.

The Raman transitions of HF are typically doppler broadened at low pressures while pressure broadening dominates at pressures above a few tenths of an atmosphere. Reference 8 shows one derivation of the linewidths of P-transitions and R-transitions using the Anderson theory of linebroadening (9):

TABLE I

Molecular Constants for HF (7)

$\omega e = 4138.32$

$\omega exe = 89.88$

$\omega eye = 0.98$

$Be = 20.939$

$\alpha e = 0.77$

$Dv \cong 22.0 \times 10^{-1}$ (for small v)

TABLE II

Calculated Frequencies of Q-Transitions of HF

J	Ω cm^{-1}
0	3961.57
1	3959.99
2	3956.85
3	3952.13
4	3945.84
5	3937.98
6	3928.54

difference between the two states of transition j, and Ω_j is the center frequency of the transition. If there is no nonresonant signal and if the Raman transitions are separated in frequency by more than their linewidths, the squared modulus of Eq (10) is a series of Lorenztian lineshapes with center frequencies and linewidths corresponding to the transitions. The linewidth measurement procedure of this project is possible since $|L_\Gamma|^2$, evaluated at perfect resonance of a particular transition, is proportional to the ratio of a_j and the linewidth. With broad-band excitation, many transitions are excited simultaneously so the linewidths can be partially determined from knowledge of the population densities and the relative intensities of the peaks in the experimental spectra.

Equation (10) contains two sets of variables if the nonresonant background is negligible. The linewidths are the unknowns to be found, so the population densities must be calculated from theory. Diatomic molecules such as HF behave as vibrating rotators. Energy term values corresponding to vibrational energy levels can be approximated by

$$G(v) = \omega_e(v + 1/2) - \omega_e x_e(v + 1/2)^2 + \omega_e y_e(v + 1/2)^3 \qquad (11)$$

where v is the quantum number of the energy level and the other variables are constants determined by spectroscopic analysis. Rotational term values are similarly modeled by equations containing experimentally determined constants (Table I):

$$F_v(J) = B_v J(J+1) - D_v J^2(J+1)^2 \qquad (12)$$

and

$$\chi^{(3)}(-\omega_{as};\ \omega_2,\ \omega_1,\ -\omega_s) = \chi_{NR} + \sum \frac{N/6\hbar\varepsilon_0}{\Omega_{fg} + \omega_s - \omega_1 - i\Gamma_{fg}}$$

$$\times\ [\overline{\rho(g)} - \overline{\rho(f)}]\overline{\alpha_{CARS}{}^{*}\alpha_R} \qquad (9)$$

where N is the number density of molecules, $\rho(g)$ is the fraction of molecules in the states g, Γ_{fg} and Ω_{fg} are the linewidth (HWHM) and frequency of a transition, $\overline{\alpha_{CARS}{}^{*}\alpha_R}$ is the orientation averaged product of matrix elements, and χ_{NR} is the nonresonant background contribution to the susceptibility. The experiments of this project were performed with room temperature HF which has most of the molecules in the ground vibrational state. As a result, Eq (9) is essentially the sum over the Q-branch transitions with significant population in the lower rotational levels. The state densities and transition frequencies for most diatomic molecules can be calculated from theory compiled by Herzberg (6). A weak frequency dependence typifies $\overline{\alpha_{CARS}{}^{*}\alpha_R}$ so it is essentially constant over the narrow range of frequencies normally spanned by the branch of Raman transitions with significantly populated states. The nonresonant background contribution should be negligible for single molecule species since only impurities can contribute transitions coincident with those of the gas under investigation.

The Raman susceptibility can be more conveniently represented by the spectrum function L which is used in the earlier equations:

$$L_\Gamma(\omega_d) = b + \sum_j a_j/(\omega_d - \omega_j - i\Gamma_j) \qquad (10)$$

where b represents the nonresonant contribution, a_j is the population

Stokes radiation that contains information about many transitions. The driving force can be produced with a broad pump beam spectrum, a broad Stokes beam spectrum, or both but the case shown here is that used in the experiment; L_1 and L_2 are narrow compared to L_s so Eq (4) reduces approximately to

$$L_d(\omega_d) \propto L_s(\omega_s). \tag{7}$$

If L_s is much broader than the frequency range of relevent Raman transitions represented in $|L_\Gamma|^2$, then Eq (6) reduces to

$$S_{as}(\omega_{as}) \propto \hat{I}_1\hat{I}_s\hat{I}_2 L_s(\omega_1{}^0 - \omega_{as} + \omega_2{}^0) \int |L_\Gamma(\omega_d)|^2 L_2(\omega_{as} - \omega_d)d\omega_d \tag{8}$$

where the superscript 0 indentifies the center frequency of a lineshape function. For typical cases, the laser lineshape is symmetric about a frequency as is a laser with a Gaussian lineshape. An exact definition of center is not necessary for the broad-band case developed here since L_s is very broad. If the results are sensitive to the definitions of the locations of the center frequencies of L_1 and L_2, then the broad-band approximation is not satisfied in the first place.

The CARS process is dependent on the nonlinear polarizability of the media being investigated. For the case of gases, the media is isotropic so the even order terms are zero because of inversion symmetry (5:256). The third order Raman susceptibility is derived from the third order polarizability and all higher terms are neglected:

$$S_d(\omega_d) \propto \hat{I}_1 \hat{I}_s L_d(\omega_d) \tag{3}$$

$$L_d(\omega_d) = \int L_1(\omega_d + \omega_s) L_s(\omega_s) d\omega_s \tag{4}$$

where S_d is the power spectral density of the driving force; $\hat{I}_1$ and $\hat{I}_s$ are the average intensities of the pump and Stokes lasers; and L_d, L_1, and L_s are the normalized intensity spectra which satisfy

$$S_1(\omega_1) = \hat{I}_1 L_1(\omega_1); \int L_1(\omega_1) d\omega_1 = 2. \tag{5}$$

For probe beams with general spectral profiles, a convolution is necessary to include all combinations of photons resulting in a photon at frequency ω_{as}. All integrations are combined to give the spectral profile of the anti-Stokes radiation from general laser profiles:

$$S_{as}(\omega_{as}) \propto \hat{I}_1 \hat{I}_s \hat{I}_2 \int |L_1(\omega_d)|^2 L_d(\omega_d) L_2(\omega_{as} - \omega_d) d\omega_d \tag{6}$$

where L_2 is the normalized spectrum of the probe beam. Eq (6) motivates the names of the lasers. $\hat{I}_1$ is mixed with $\hat{I}_s$ to "pump" a molecule to a higher state. $\hat{I}_2$ "probes" the result of the excitation process and conveys the information as $S(\omega_{as})$. A monochromatic probe beam ideally reproduces the results of the excitation in the anti-Stokes signal since $L_2(\omega) = \delta(\omega - \omega_2)$, but a typical lineshape blends the spectral lines of the Raman transitions in a manner analogous to the instrument slit function of a monochromator.

A broad-band CARS signal is generated by simultaneously exciting a band of Raman transitions so that the probe beam can mix to form anti-

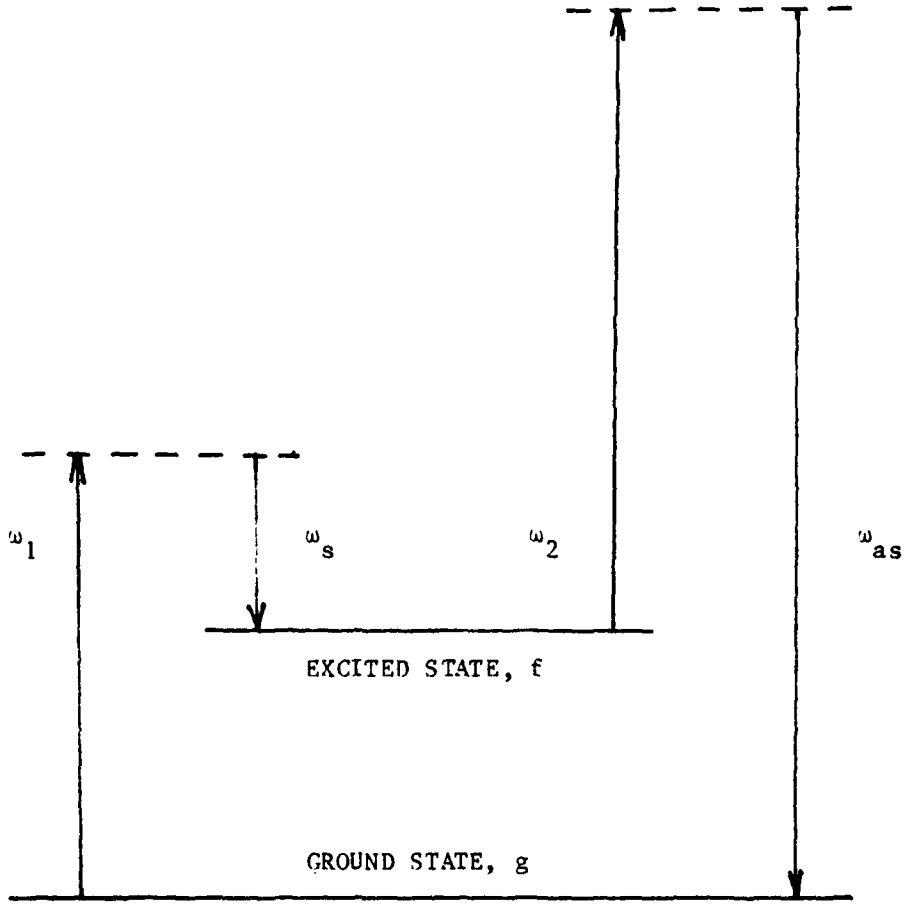

Fig. 1. CARS Photon Process. Dashed lines are virtual states.

derived (2) (4) (5). Fig. 1 shows the photon process that produces each photon of anti-Stokes radiation. A photon from a pump beam with frequency ω_1 mixes with a photon from a Stokes beam with frequency ω_s to excite a molecule from the ground state to a higher vibrational-rotational energy level. The probability of such an occurrence depends on how close the "driving force" frequency is to the frequency of the Raman transition; the Raman susceptibility governs this frequency dependent process. A photon from a probe beam with frequency ω_2 can excite the molecule to a virtual state from where it falls to the ground state. The frequency of the anti-Stokes radiation for monochromatic excitation is consequently

$$\omega_{as} = \omega_1 - \omega_s + \omega_2 \tag{1}$$

and the intensity is

$$I_{as}(\omega_{as}) \propto I_1 I_s I_2 |L_\Gamma(\omega_{as} - \omega_2)|^2 \tag{2}$$

where ω_1, ω_s, ω_2, ω_{as} are the frequencies of monochromatic pump, Stokes, probe, and anti-stokes beams; I_1, I_s, and I_2 are the intensities of the pump, Stokes, probe, and anti-Stokes beams; and $|L_\Gamma|^2$ represents the spectral profile of the squared-modulus of the Raman susceptibility.

For pump and Stokes beams with general power spectral densities, the excitation from the driving force is found by convolving the two spectral profiles to include all pairs of photons, one from each beam, that have frequencies with difference ω_d:

II. Theory

In this section, the equations for broad-band CARS are developed first and the Raman susceptibility theory is summarized. Then, linewidth dependence on pressure, rotational quantum number, and temperature is examined. Next, the calculation procedure required for the analysis of the experimental data is discussed and the effective slit function of the detection equipment is taken into account. The section ends with a discussion of the nonlinear least-squares curve fitting method used for fitting calculations to the experimental spectra.

Development of the Equations for Broad-band Cars

The following paragraphs develop the equations that describe the profile of the detected spectra of broad-band CARS signals. First, the equations for CARS signals generated by monochromatic laser beams are developed. Then the equations are expanded to accommodate lasers with general lineshapes. The equations for the special case of broad-band CARS is discussed next followed by the discussion of the Raman susceptibility. The CARS equations will finally be modified to include the broadening caused by the effective slit function of the detection equipment. Absolute intensity is not measured or calculated in this project. Only the normalized spectral profile of the detected spectra are used to find the pressure-broadening coefficients, so the equations are not intended to allow the determination of absolute intensities expected from known laser intensities.

The power spectral density of the anti-Stokes radiation has been

To determine the linewidths, CARS spectra are recorded for room temperature HF at 14 equally spaced pressures between 50 and 700 torr. Since the linewidths are the only unknown variables of the Raman susceptibility, they can be estimated by finding the values that will fit the observed spectra. This procedure is in direct contrast with the proposed CARS experiments with HF lasers where the linewidths will be known and used to find parameters such as temperature and pressure which are variable in a chemical reaction.

The CARS spectra are recorded on 65 channels of an optical multichannel analyzer. Nonlinear least-squared curve fitting routines are used to find the effective slit function of the detection equipment and to determine the linewidths that best fit each spectra. The linewidths are pressure-broadened at all of the experimental pressures, so the estimates of each of the linewidths should be linear with pressure. A linear least-squares regression analysis is used to find the pressure-broadening coefficient of each transition. In the procedure, the pressure-broadening coefficient of the Q(3) transition is estimated from infrared data obtained from earlier work and used as a reference for determining the other coefficients.

The experimental spectra contained information representing the first seven Q-branch transitions and all of the linewidths were found to be linear with pressure. The pressure-broadening coefficients varied with rotational quantum number in the same manner as the pressure-broadening coefficients of the P-branch and R-branch. The results in general show that broad-band CARS is satisfactory for measuring linewidths even when a low resolution detector is used.

same temperature range since the increase in temperature is accompanied by a population increase. Table III contains calculated results, but it is not known if they have been experimentally verified.

Calculation of CARS Spectra

The CARS equations are now applied to the experimental equipment and example calculations are made to demonstrate the types of data expected. This discussion includes the equations that calculate the broadening effect of the detection equipment.

Only two lasers are used to generate the CARS signal. A high power beam may serve as both the pump and probe beams if a Stokes beam can be chosen to provide an excitation band in the Q-branch. Also, probing the Q-branch with the high power laser must produce the anti-Stokes signal at a conveniently detectable frequency. The choice of a broad-band Stokes beam and a narrow band pump/probe beam keeps integration work to a minimum, as is shown in subsequent paragraphs.

The method of calculating an observed CARS spectrum begins with determining the populations of the states of HF using Eqs (11-15). It can be shown that at a temperature of 300K only the lowest vibrational state (v=0) has a significant population. Fig. 4 shows the fractional populations of the eight lowest J levels for v=0.

These populations, along with linewidth data for HF, can be used to calculate the Raman susceptibility in the frequency range of the Q-branch. Linewidths obtained from the results of this experiment were used to calculate $|L_\Gamma|^2$ from Eq (10) for HF at 50 torr and 700 torr, the pressure extremes of the experiment (Figs. 5,6). At 700 torr, the Q(0) and Q(1) transitions are partially blended.

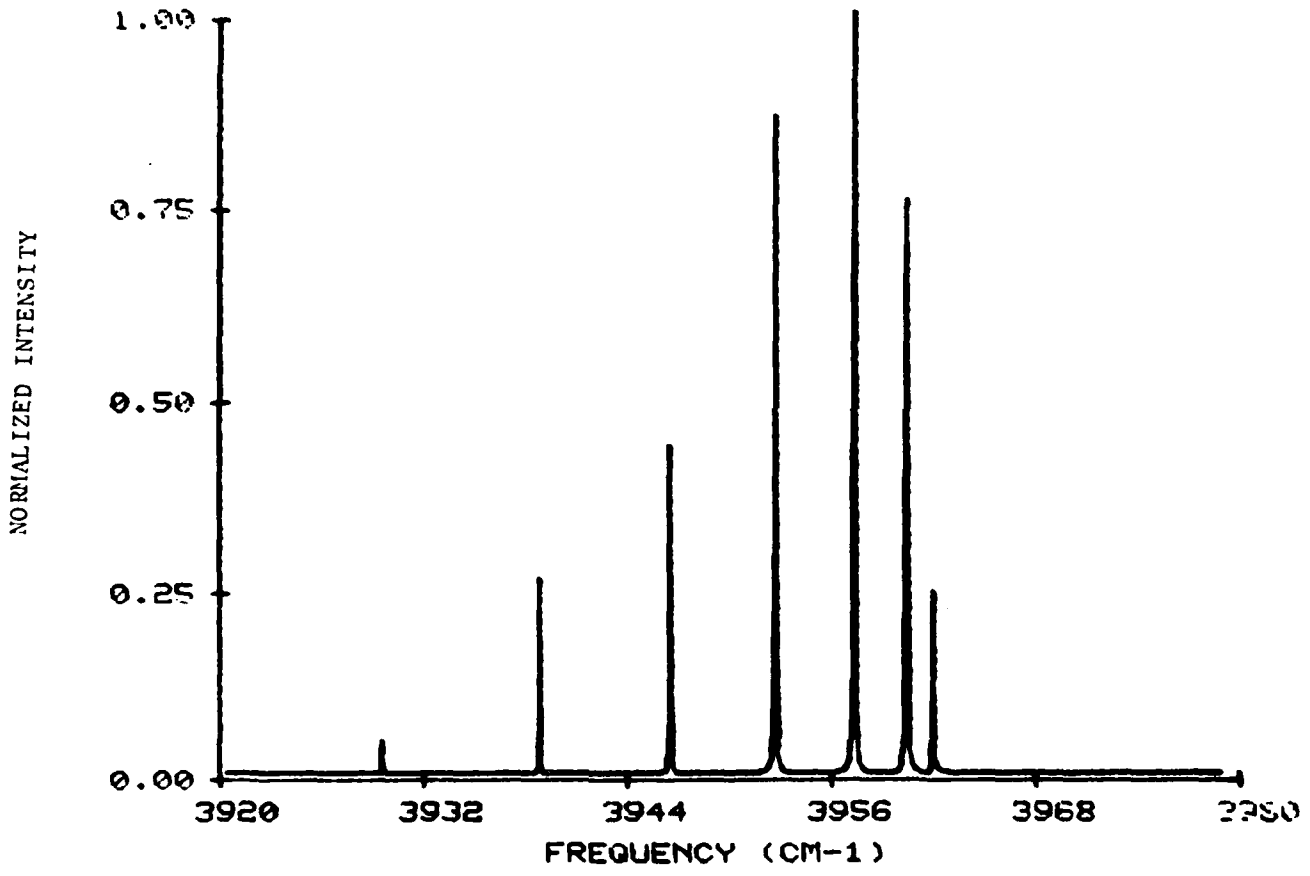

Fig. 5. Normalized $|\chi|^2$ of Q-Branch of HF at 50 Torr.

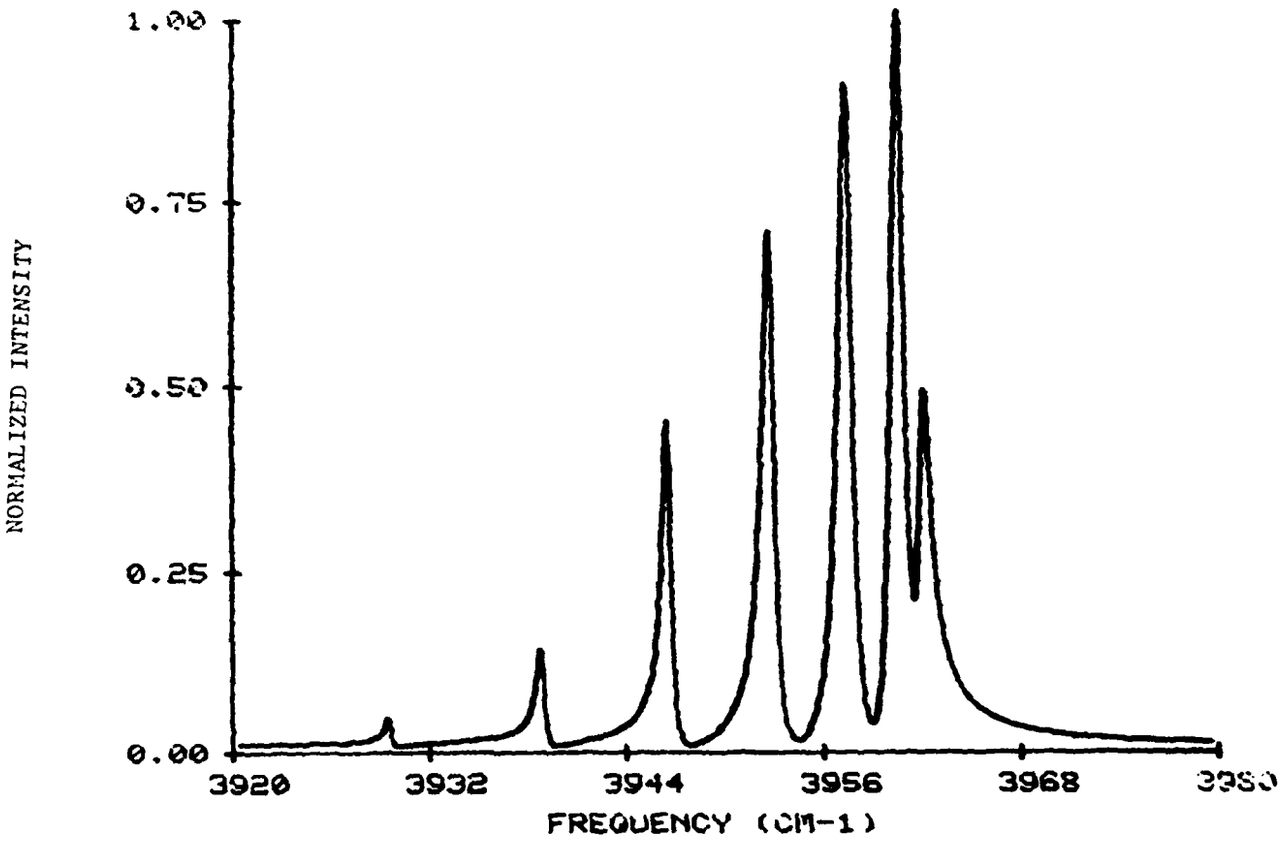

Fig. 6. Normalized $|\chi|^2$ of Q-Branch of HF at 700 Torr.

The broad-band CARS equation (Eq 8) is next used to include the broadening effect of the probe beam. Uniform excitation is assumed, in other words L_s is constant, but the excitation profile is measured in the experiment and included in the calculation; details are in the analysis section. The pump/probe beam laser has a Gaussian spectral profile with linewidth 0.5 cm^{-1} so $|L_\Gamma|^2$ is broadened considerably (Figs. 7,8). These graphs represent the spectral profile of the broad-band CARS signal, but the effective slit function of the detection equipment must be taken into account before a good prediction of the experimentally obtained spectra can be calculated.

For detecting the CARS signals, a monochromator is fitted with a diode array rapid scanning spectrometer (DARSS) detector. Essentially, the detector is 512 individual linear diodes which are mounted in the focal plane of the output lens of the monochromator. The equipment effectively broadens the system as a Lorenztian slit function does in a conventional monochromator. After experimentally determining the effective slit function, a CARS signal can be calculated by convolving the slit function with the actual CARS spectra:

$$S_{det}(\omega_{as}) \propto \int S_{as}(\omega_{as}) L_e(\omega - \omega_{as}) d\omega \qquad (17)$$

where L_e is the effective slit function of the detection equipment. Figs. 9 and 10 show the final calculation of the detected spectra at 50 and 700 torr. Transitions Q(0) and Q(1) are no longer resolved and the normalized profiles are similar even though the Raman transitions have linewidths that are different by over an order of magnitude.

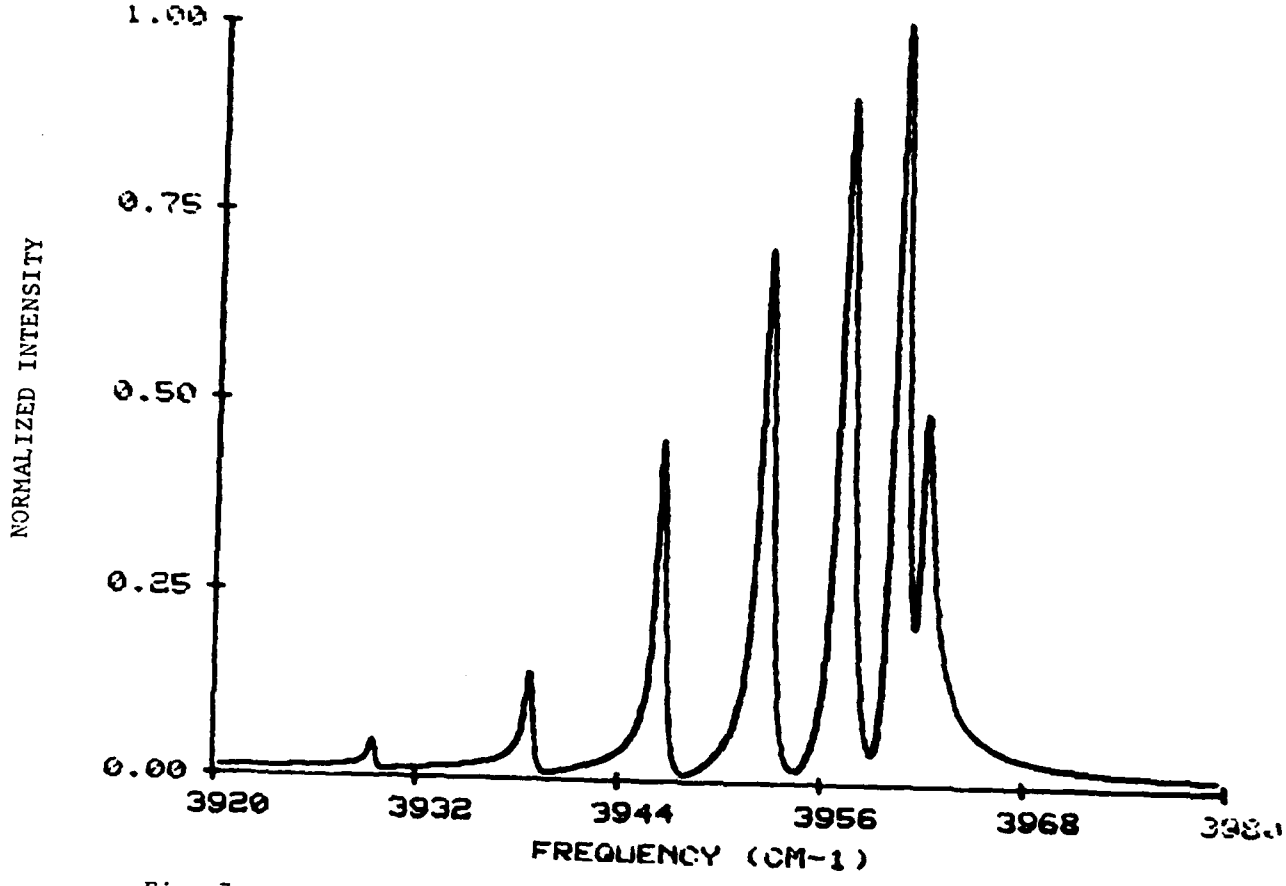

Fig. 7. Result of Probe Beam Broadening in CARS of HF at 50 Torr.

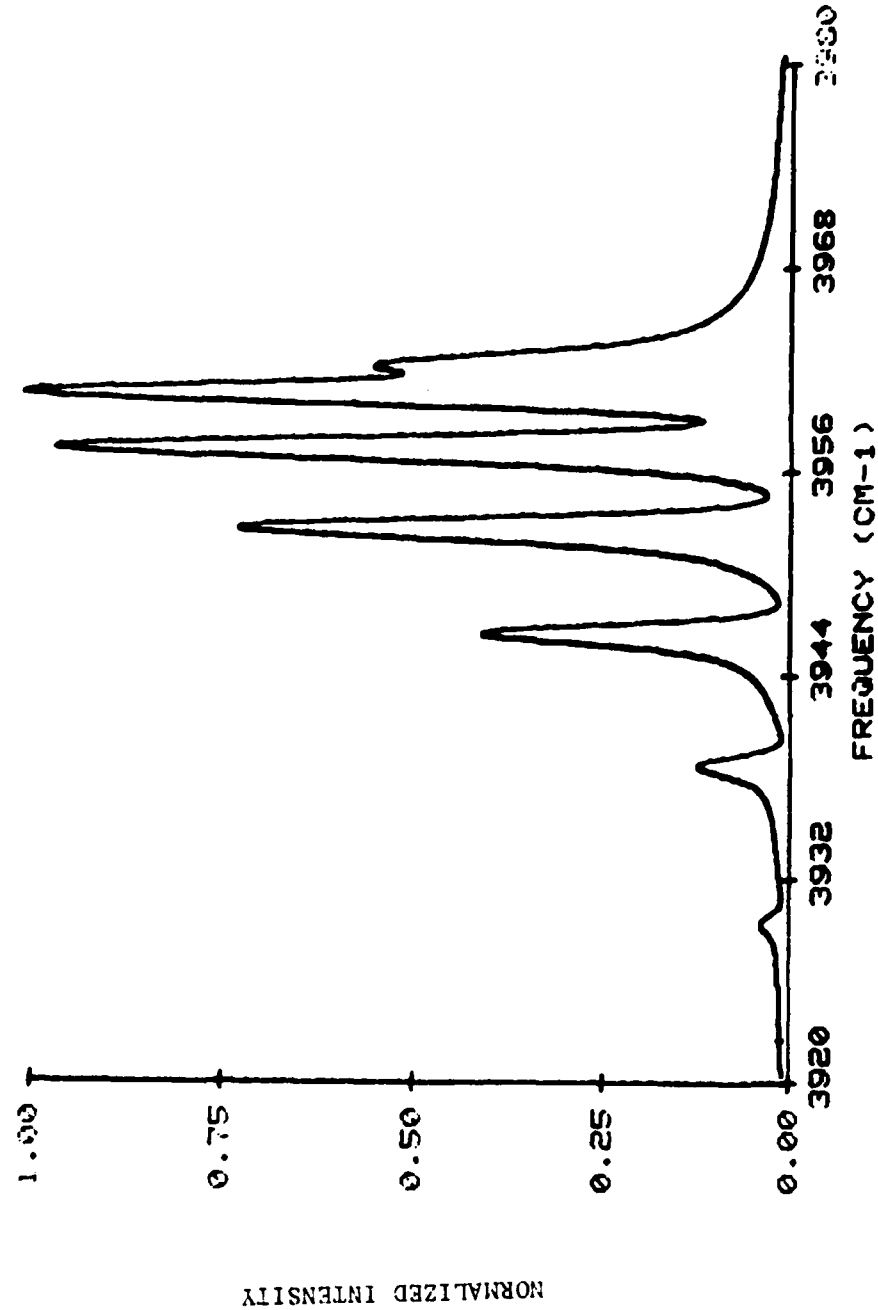

Fig. 8. Result of Probe Beam Broadening in CARS of HF at 700 Torr.

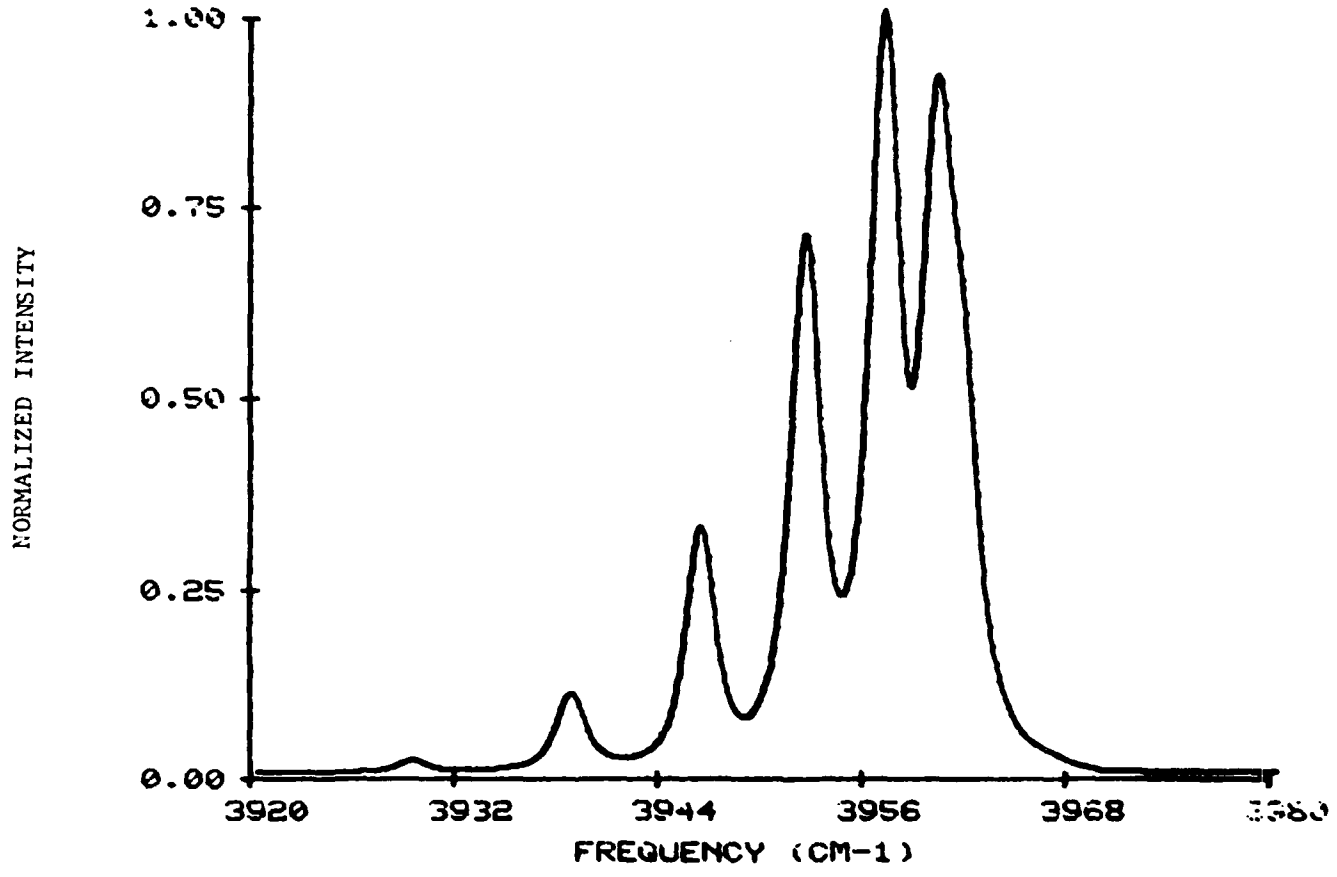

Fig. 9. Result of Instrument Broadening in CARS of HF at 50 Torr.

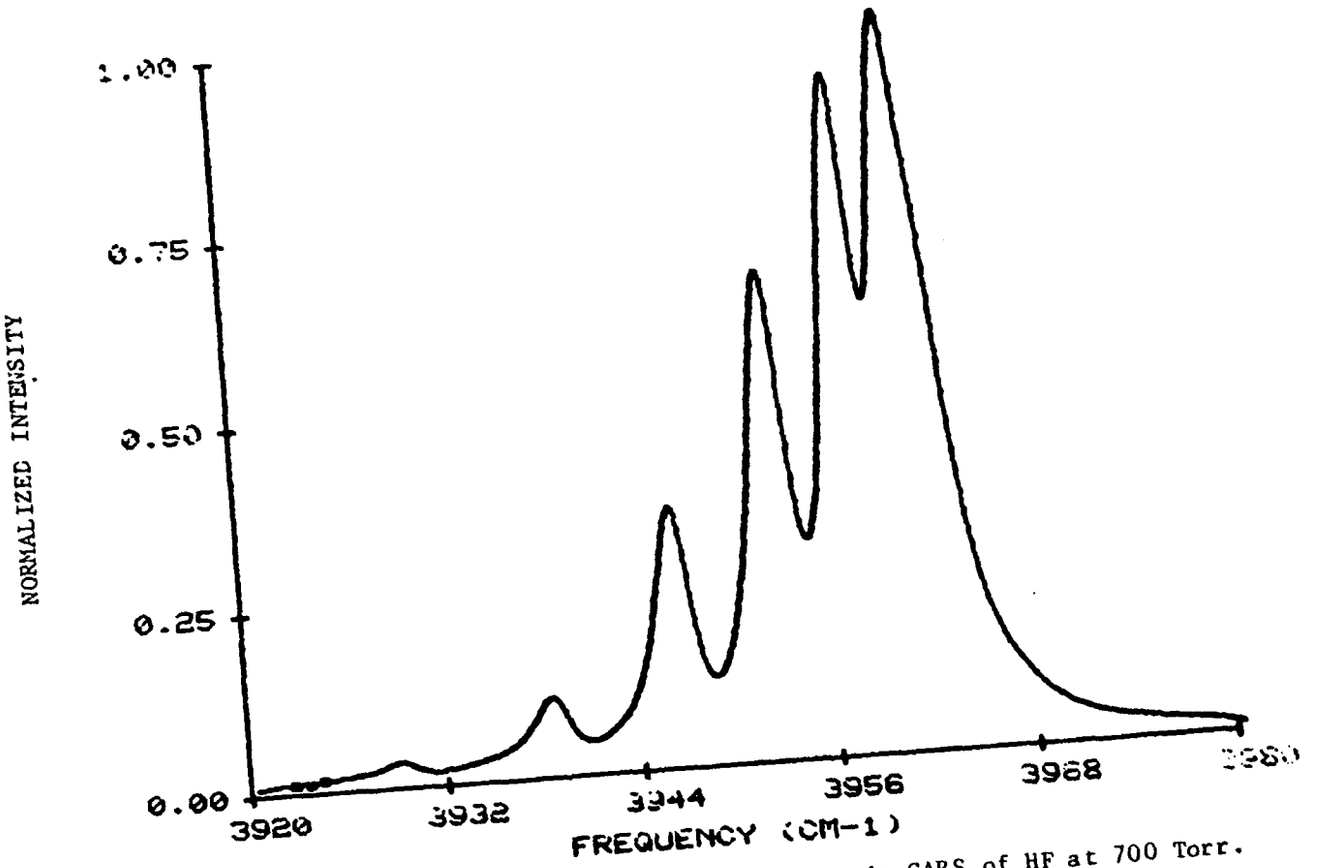

Fig. 10. Result of Instrument Broadening in CARS of HF at 700 Torr.

Non-linear Least Squares Curve Fitting Routine

A nonlinear least-squares fitting procedure is used to fit the calculations to the observed spectra (11:120-122). Several combinations of independent and dependent variables are used to represent eight variables. The variables are the breadth of the slit function, Γ_e (HWHM), and the linewidths of the Raman transitions, Γ_J (HWHM), for J=0 through 7. Details of the configurations are explained in the analysis, but the outline is given here.

First, Γ_e is found by treating Γ_3 as an independent varible whose value is determined from infrared data. Γ_e and the other six linewidths are treated as dependent variables and one of the experimental spectra is best fit by the routine. Second, all experimental spectra are fit while Γ_J for J=0,1,2,4,5,6 are the only dependent variables. Γ_3 is calculated from infrared data for each experimental spectrum. Third, all seven of the linewidths of the Raman transitions are treated as dependent variables and each experimental spectra is fit again.

The general equation for updating dependent variables is

$$\underline{\Gamma}_{n+1} = \underline{\Gamma}_n + \Delta\underline{\Gamma}_n \tag{18}$$

where $\underline{\Gamma}$ is a vector of up to seven elements which includes the desired dependent variables. $\Delta\underline{\Gamma}$ is computed with the following equation before each iteration:

$$\Delta\underline{\Gamma} = (J^T J)^{-1} J^T \underline{E} \tag{19}$$

where J is the Jacobian matrix with elements

$$J_{ij} = \frac{\delta I_i}{\delta \Gamma_j}. \tag{20}$$

I_i is the intensity of the calculated spectra at the frequency corresponding to a relevant detector channel. Γ_j is the dependent variable in element j of the vector. Each element of the matrix in Eq (20) is approximated by calculating the change in calculated intensity due to a ten percent change in the dependent variable. E is the vector of errors in intensity between the experimental data and the calculated spectra of the previous iteration:

$$E_i = D_i - I_i \tag{21}$$

where D_i is the intensity measured by detector channel i.

The uncertainty of each dependent variable is determined from the variance matrix:

$$V(\alpha) = (J^T J)^{-1} \alpha^2 \tag{22}$$

α^2 is the variance of the entire distribution which is estimated by:

$$\chi^2 = s^2 = [1/(m-n)] \sum_{i=1}^{m} (D_i - I_i)^2. \tag{23}$$

where n is the number of dependent variables and m is the number of channels that are being fit. Diagonal element i in V is the variance of Γ_i so the uncertainties will be reported in the analysis as the square roots of the diagonal elements (ie, the standard deviations).

III. EXPERIMENT

This section contains a brief description of the equipment, experimental procedure, and results. The system was aligned and tested over a period of about a week, but automated data collection permitted all of the data to be acquired and stored during one afternoon.

Optical System

The equipment schematic diagram is shown in Fig. 11. A Q-switched Quanta-Ray Nd:YAG laser with an amplifier stage is frequency-doubled then filtered through a prism harmonic separator. The resulting 532 nm beam is split into four equal intensity beams. Three of the beams are used to pump a three stage dye laser while the remaining beam is focused in the sample cell (along with the dye beam) to generate the CARS signal.

The dye laser beam is generated from an oscillator stage and two amplifier stages. Each stage is optically pumped by one of the equal intensity portions of the 532 nm beam. A single mechanical pump circulates the dye fluid in series through all three stages. Fig. 12 shows a picture of the three dye laser stages and the hardware that separates the frequency doubled Nd:YAG beam.

A collinear focusing arrangement is incorporated by first collimating the dye beam with a simple telescope then combining it through a dichroic mirror with one of the four 532 nm beams. The combined beams are focused through a 30 cm lens into a gas cell fitted with saphire windows that are impervious to the highly corrosive HF gas.

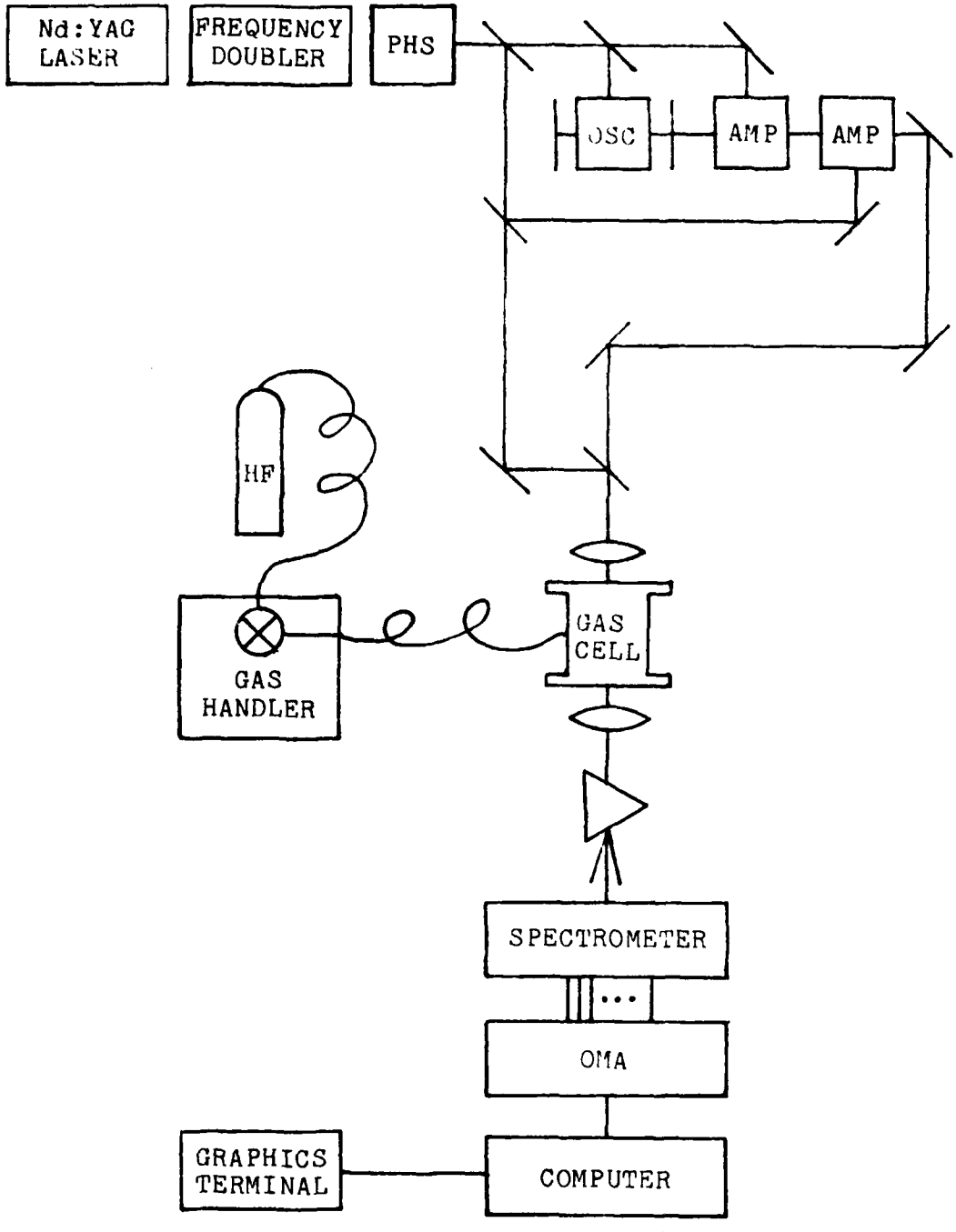

Fig. 11. Schematic Diagram of Equipment

Fig. 12. Three Stage Dye Laser and Optical Pumping Hardware.

A gas handling system was employed to transfer the gas to the cell through a combination of stainless steel tubing and polyethylene hoses. Pressure is monitored with a capacitance manometer built into the gas handling system.

The two beams and the generated CARS signal exiting the gas cell are collimated with a second 30 cm lens. Separating the CARS signal from the dye beam and 532 nm beam is achieved with a Pellin-Borca prism and an aperture. The signal is then focused into a SPEX 3/4 m monochromator. Fig. 13 shows the dichroic mirror and the cell arrangement with focusing lenses.

The momochromator was fitted with a 512 channel diode array rapid scanning spectrometer (DARSS) detector head compatible with a Tracor-Northern Model TN-1710 optical multi-channel analyzer (OMA). A gated multi-channel plate intensifier is incorporated in the head along with an analog-to-digital converter. Meausurements can be taken during the laser pulse then converted and read by the OMA before the next pulse occurs. A 632 groove/mm grating with a blaze angle of 49 degrees produces dispersion equivalent to 0.875 cm^{-1}/channel of the detector. The individual diodes are separated by 50 microns.

CARS measurements may be acquired by the OMA and immediately sent to a Modcomp MODACS III sixteen bit minicomputer where the data is stored on tape for future analysis. The system is capable of producing and recording CARS data at a ten Hertz rate, so it was possible to record in one afternoon one thousand pulses of CARS data at 14 different sample pressures.

consistently at 1,2,3,4, and 5 atmospheres by measuring the linewidths at those pressures and dividing by the pressure. Pressure-broadening coefficients are calculated similarly in this analysis when references report linewidths rather than pressure-broadening coefficients.

The following paragraphs show how the infrared data was used to calculate a_3 in the Q-branch. First, assumptions are made of the relationship between the linewidths in the P-branch, R-branch and Q-branch. Then, the results of the previous experiments are examined and one is chosen for calculating a good estimate of a_3.

Assumptions of Linewidth Behavior. To estimate a_3, it is assumed that Γ_3 is between the the linewidths of the P(3) and R(3) transitions. The assumption is plausible since the three transitions have a common lower rotational state while the energy of the upper state of the Q(3) transition is between those of the R(3) and P(3) transitions. Linewidths of transitions are partially determined by the lifetimes of the corresponding rotational states and the lifetimes typically decrease with an increase in energy. This theory predicts that the linewidths of the P(3), Q(3), and R(3) transitions are successively narrower since the energies of the upper states are successively higher. For the case of transitions with common upper state J=3, the linewidths of the P(4), Q(3), and R(2) transitions are successively broader since the energies of the lower states are successively lower. In this analysis, it is assumed that the linewidth of the Q(3) transition is equal to the mean of the transitions with common upper or lower states. In the pressure-broadening region, the linewidths are directly proportional to pressure. Therefore, the previous linewidth assumptions apply to the pressure-broadening coefficients as well. For example, a_3 of the Q-branch can be

calculated and observed spectra, but it must be shown that the final values for the linewidths are physically meaningful rather than merely mathematically satisfying. The results of the comparison are encouraging since the pressure-broadening coefficients obtained using the two methods are almost identical with the exception of a_0.

For further verification of the analytical results, the pressure-broadening coefficients of the Q-branch are compared to those of the P-branch and R-branch. All three branches are similarly dependent upon the lower rotational state of the transition. This result is encouraging although rigorous theory has not been found to support it or prove otherwise.

Finally, the effect of slit function uncertainty on the results of the second NLLS routine is examined. The y-intercepts of the linewidth vs. pressure graphs are nearly zero when the NLLS fitting routine uses the slit function chosen to yield the a_3 estimated from the literature; pressure broadening theory supports such behavior. Over-estimations of the slit function breadth will cause negative intercepts while under-estimations produce positive intercepts. Since the y-intercepts are sensitive to effective slit function modelling, the assumed a_3 and the corresponding slit function are apparently good estimates.

Estimation of a_3 from Infrared Data

Since it has never been measured, the pressure-broadening coefficient of the Q(3) transition is estimated from infrared data available in the literature (12) (13) (14). Specifically, P-branch and R-branch data are used to deduce a_3. Reference 12 shows that the pressure-broadening coefficient of the R(2) transition is determined

experimental parameters. The final values for Γ_0 are apparently sensitive to the errors in the assumption of the linewidths of the Q(3) transitions, so the data is further analyzed with a second NLLS fitting routine.

The fourth part of the analysis explains a second NLLS fitting routine that varies Γ_J of all seven of the transitions so that the variables are free to compensate for incorrect assumptions of Γ_3 inherent in the first NLLS fitting routine. The breadth of the effective slit function is chosen by trial and error to yield the value of a_3 determined from the literature. Convergence to the final values is slower and less definitive than when the first routine is used. Graphs of Γ_J vs. pressure show that all of the lines have random qualities, yet they can be adequately represented by a straight line determined from linear regression calculations. This second NLLS fitting routine provides a more satisfying estimate of a_0 since the graph of Γ_0 vs. pressure has a much better linear fit than the graph obtained with the first routine.

The fifth part of the analysis begins with a comparison of the pressure-broadening coefficients estimated with each of the two NLLS fitting routines. The credibility of the second routine is questionable since it must distinguish subtle changes in the breadth of peaks in the final spectra even when there are large percentage changes in the Raman linewidths. A good fit can be achieved with a range of sets of Γ_J since any set near the actual solution can provide a spectrum with peaks that match the magnitudes of the observed spectrum; the small errors introduced by slightly erroneous breadths are not as important as the magnitudes. The routine will minimize the small residuals between

recorded in the laboratory, and the Q(0) and Q(1) transitions are not resolved.

In the third part, the pressure-broadening coefficients are estimated by utilizing the first of two non-linear least squares (NLLS) fitting routines used in the analysis. The spectrum recorded at each pressure is fit to a calculated spectrum using the effective slit function estimated from the spectra recorded at the lowest HF pressure. At each pressure, Γ_3 is calculated from the a_3 that was determined in the first step of the analysis. The independent variables in the fitting routine are Γ_3 and the breadth of the effective slit function while the dependent variables are Γ_J for J=0,1,2,4,5,6. For a given spectrum, the linewidths of each transition compared to Γ_3 ultimately determine the magnitude of the peaks in the observed spectra relative to the magnitude corresponding to the Q(3) transition. Consequently, representing Γ_3 as an independent variable permits the curve fitting routine to converge rapidly and consistently to a final solution. After fitting the spectra recorded at each of the fourteen experimental pressures, the linewidths of each of the transitions are known as a function of pressure. The pressure-broadening coefficients are determined by fitting the linewidth functions with linear regression routines; the coefficients are equal to the slopes of the regression lines.

The first NLLS curve fitting analysis yields Γ_J linear with pressure for all observed transitions except the Q(0) transition. Due to the unresolved Q(0) spectra, greater uncertainty is expected, but the poor linear fit is believed to be caused by fixing Γ_3 to calculated values that cannot vary to compensate for random fluctuations of

IV. Analysis

The goal of the analysis is estimating the pressure-broadening coefficients (a_J) of the first seven vibrational-rotational transitions of HF. First, all of the Raman linewidths at each experimental pressure are obtained from the data then the pressure-broadening coefficients are calculated from the slopes of the linewidths vs. pressure. Perhaps the most important concept is the dependency of the magnitudes of the peaks in the observed spectra on the linewidths (Γ_J) of the corresponding Raman transitions. At a given pressure, the Raman linewidths will partially determine both the magnitudes and the breadths of the peaks of the observed spectrum. However, the range of Raman linewidths encountered in the experiment is small compared to the resolution of the experimental process so the analytical procedure depends mostly on the information contained by the magnitudes of the peaks.

The analysis is presented in five parts. First, a_3 is estimated from P-branch and R-branch data that is available in the literature. Later in the analysis, this estimated value of a_3 is used as an aid for determining the other pressure-broadening coefficients. In each experimental spectrum the frequency range corresponding to the Q(3) transition is fairly well resolved and has high intensity, so a_3 is likely to be determined with the least uncertainty.

In the second part, graphs of the experimental data are briefly examined to show that the resolution of the system is not adequate for graphical estimates of the Raman linewidths. Observed breadths of the peaks in each spectrum differ only mildly over the pressure range

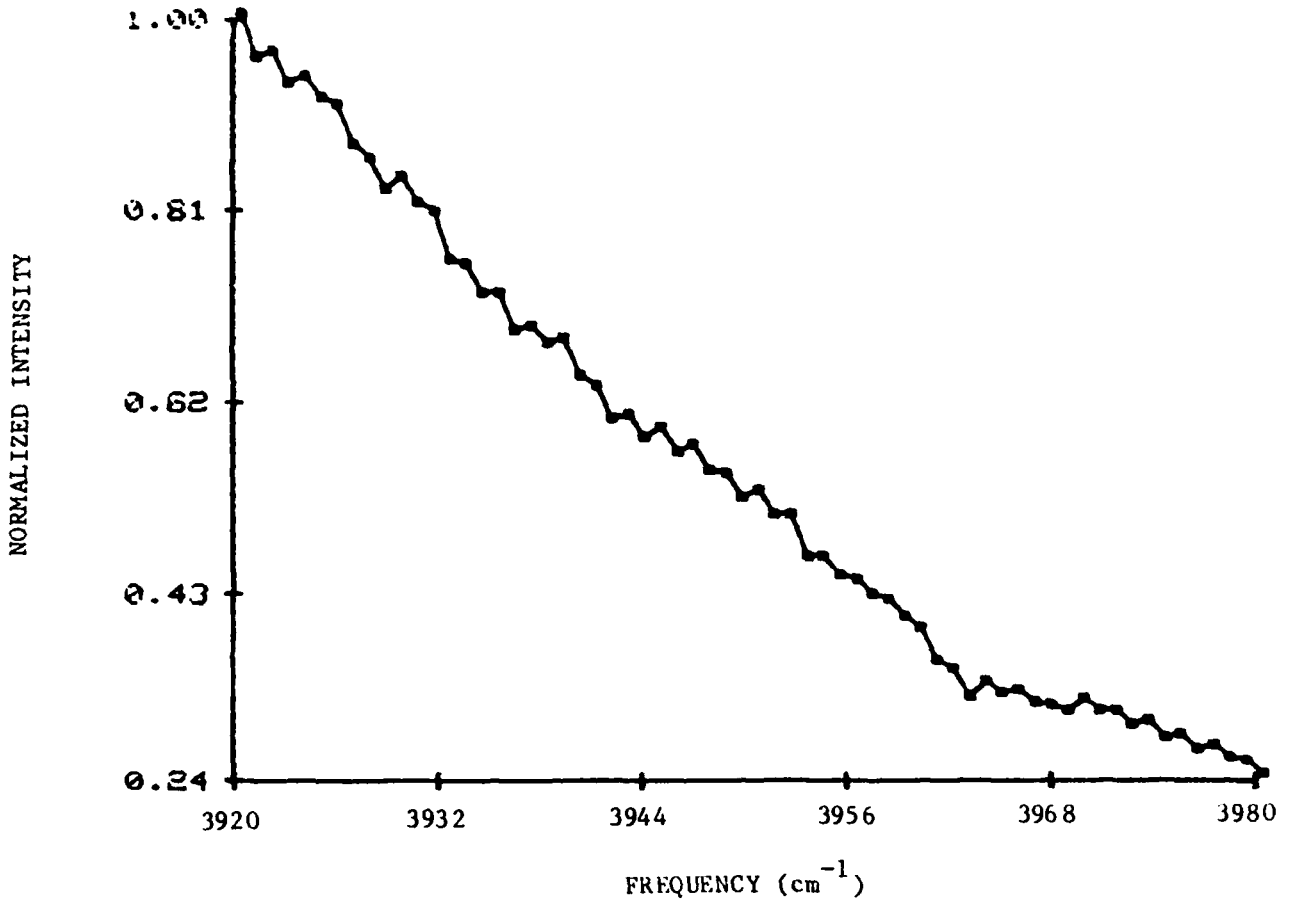

Fig. 19. CARS Driving Force Spectrum.

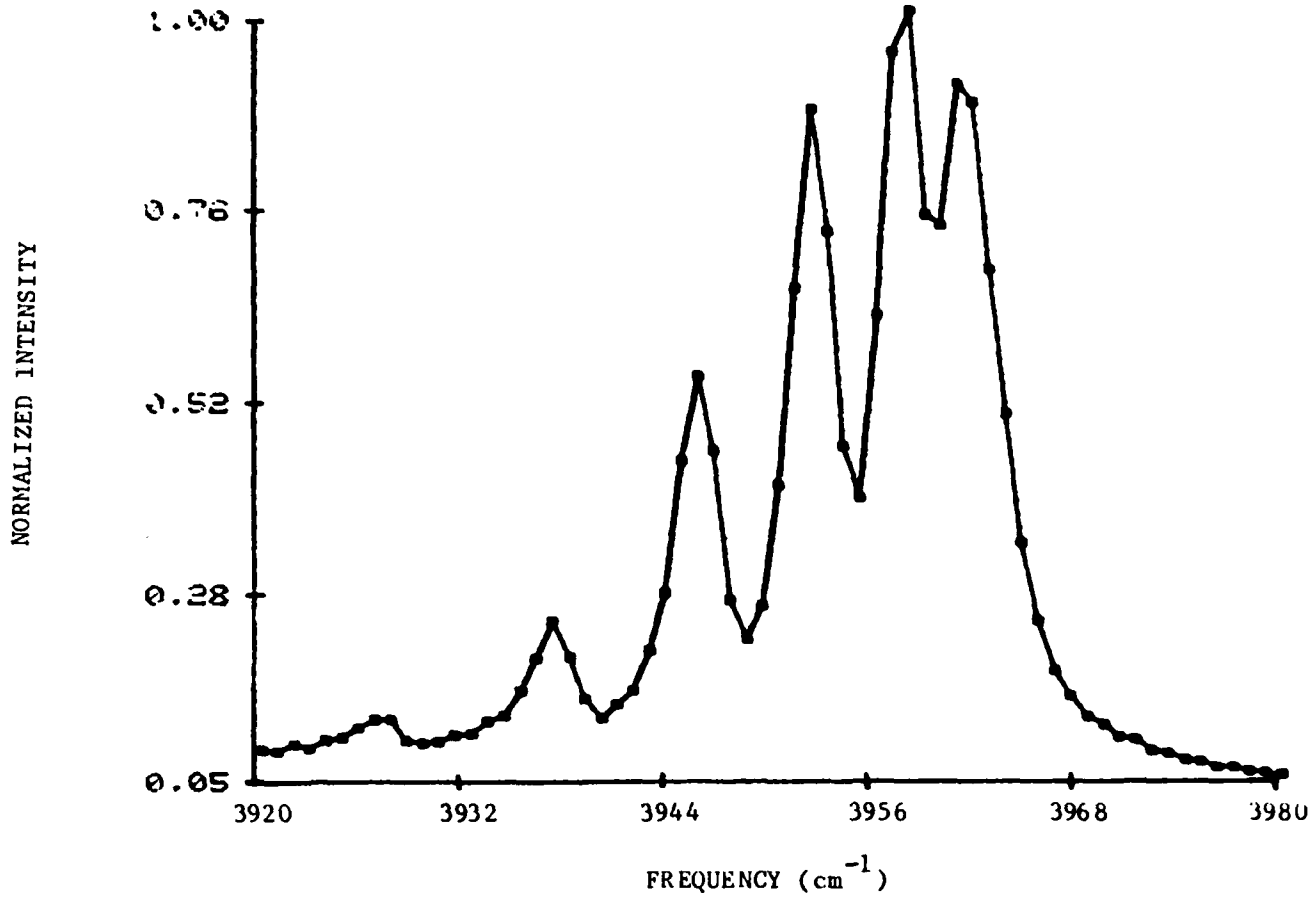

Fig. 18. Experimental Spectrum of 700 Torr HF (65 Channels). Frequency Shown Corresponds to Raman Spectrum.

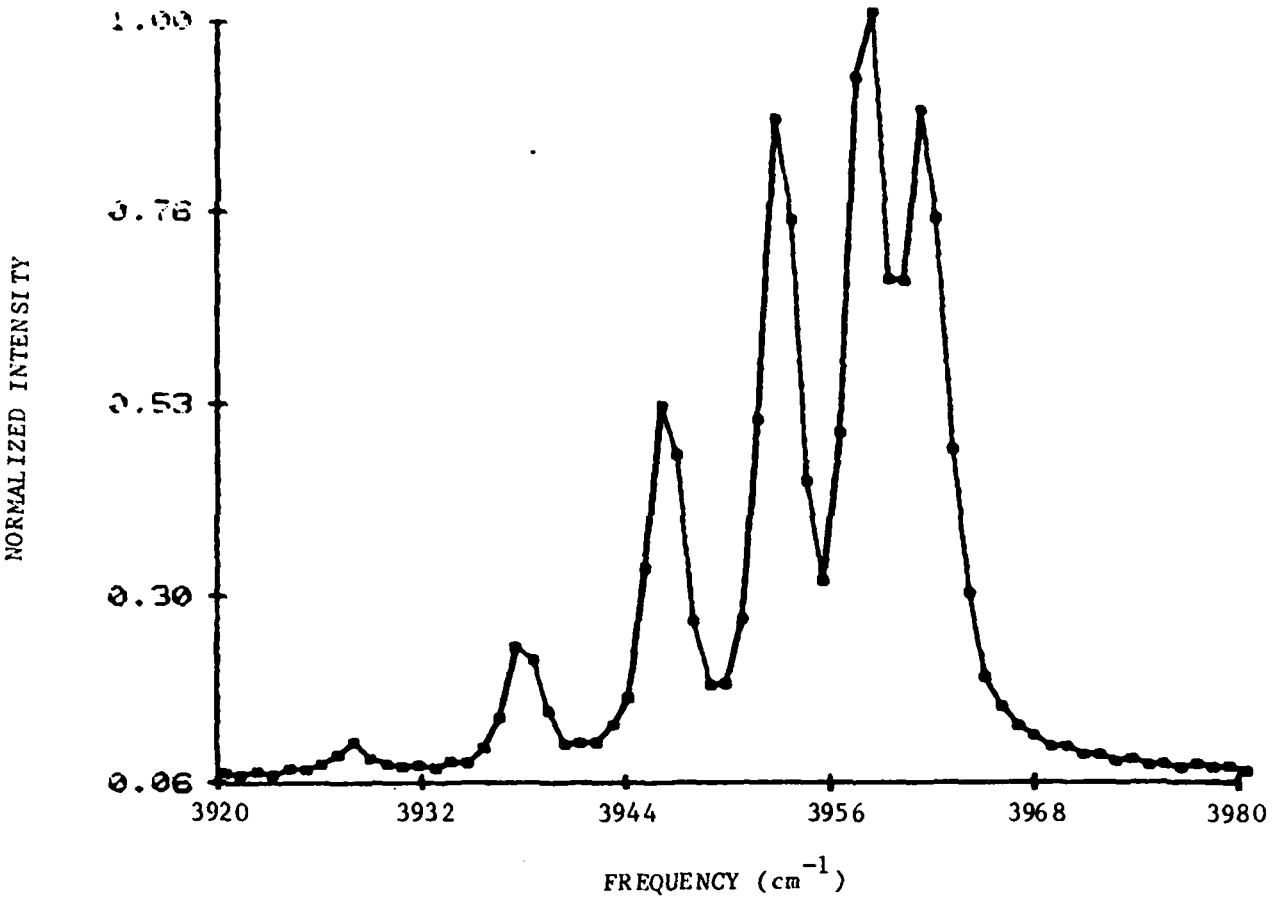

Fig. 17. Experimental Spectrum of 50 Torr HF (65 Channels). Frequency Scale Corresponds to Raman Spectrum.

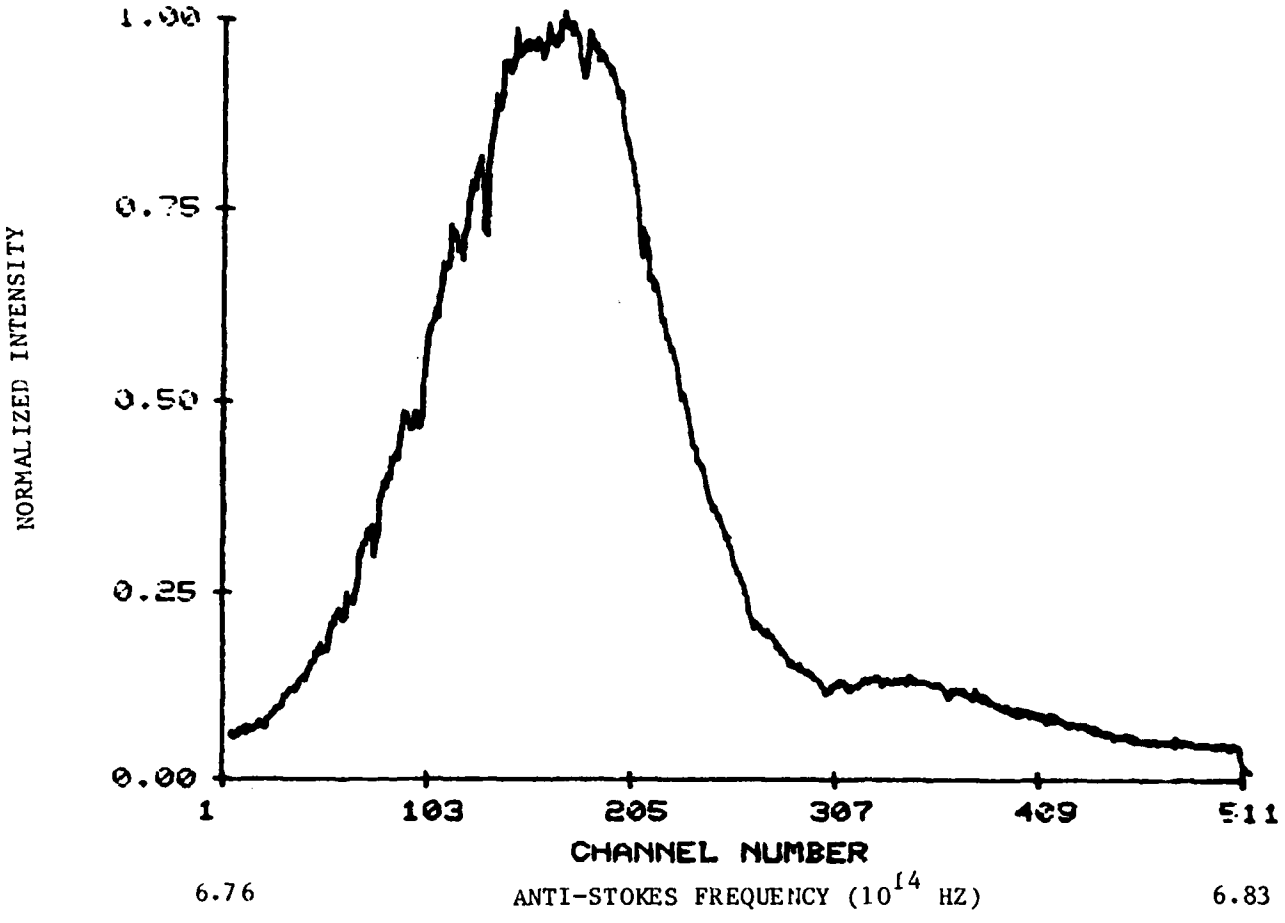

Fig. 16. CARS Driving Force Spectrum (512 Channels).

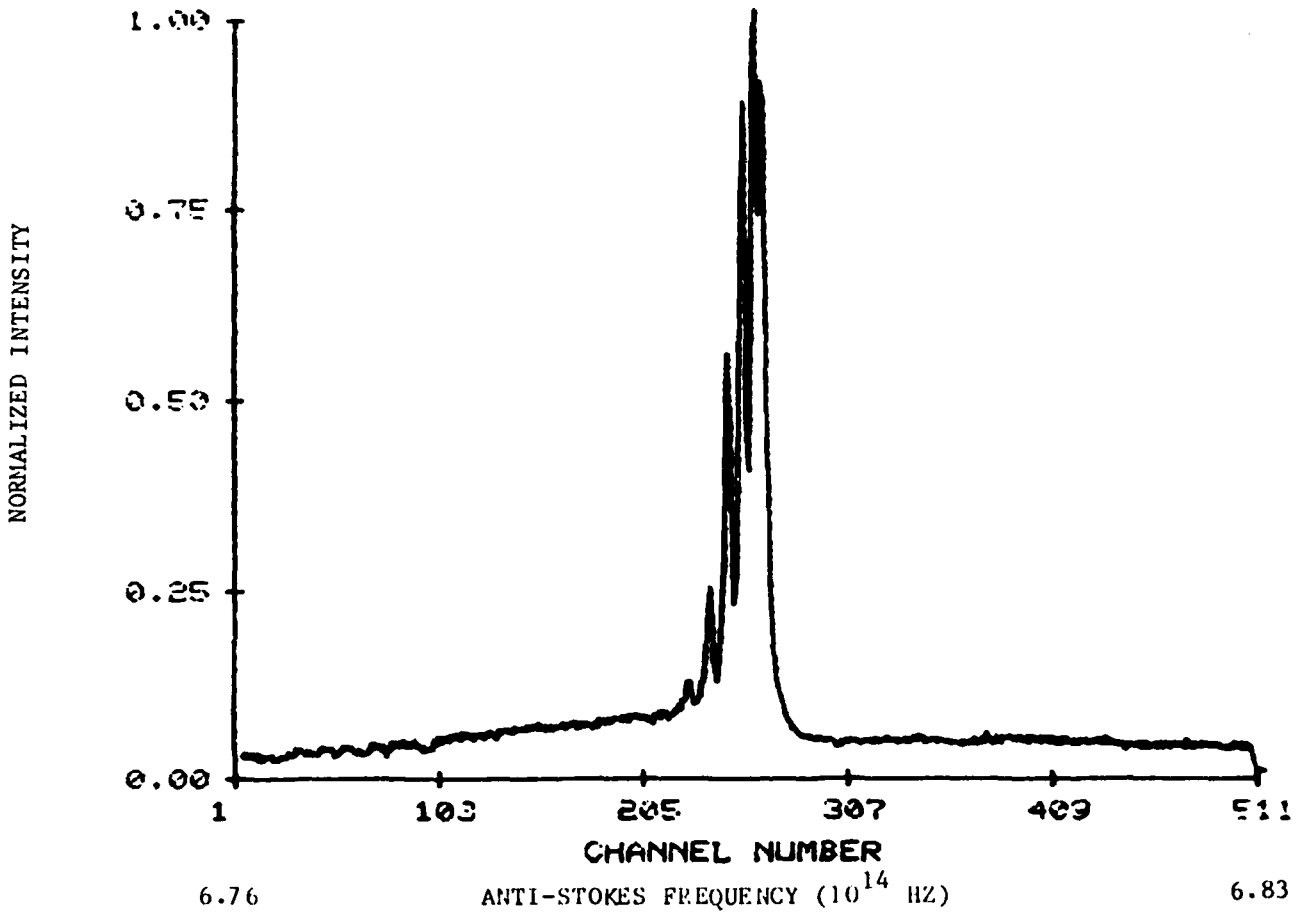

Fig. 15. Experimental Spectrum of 700 Torr HF (512 Channels).

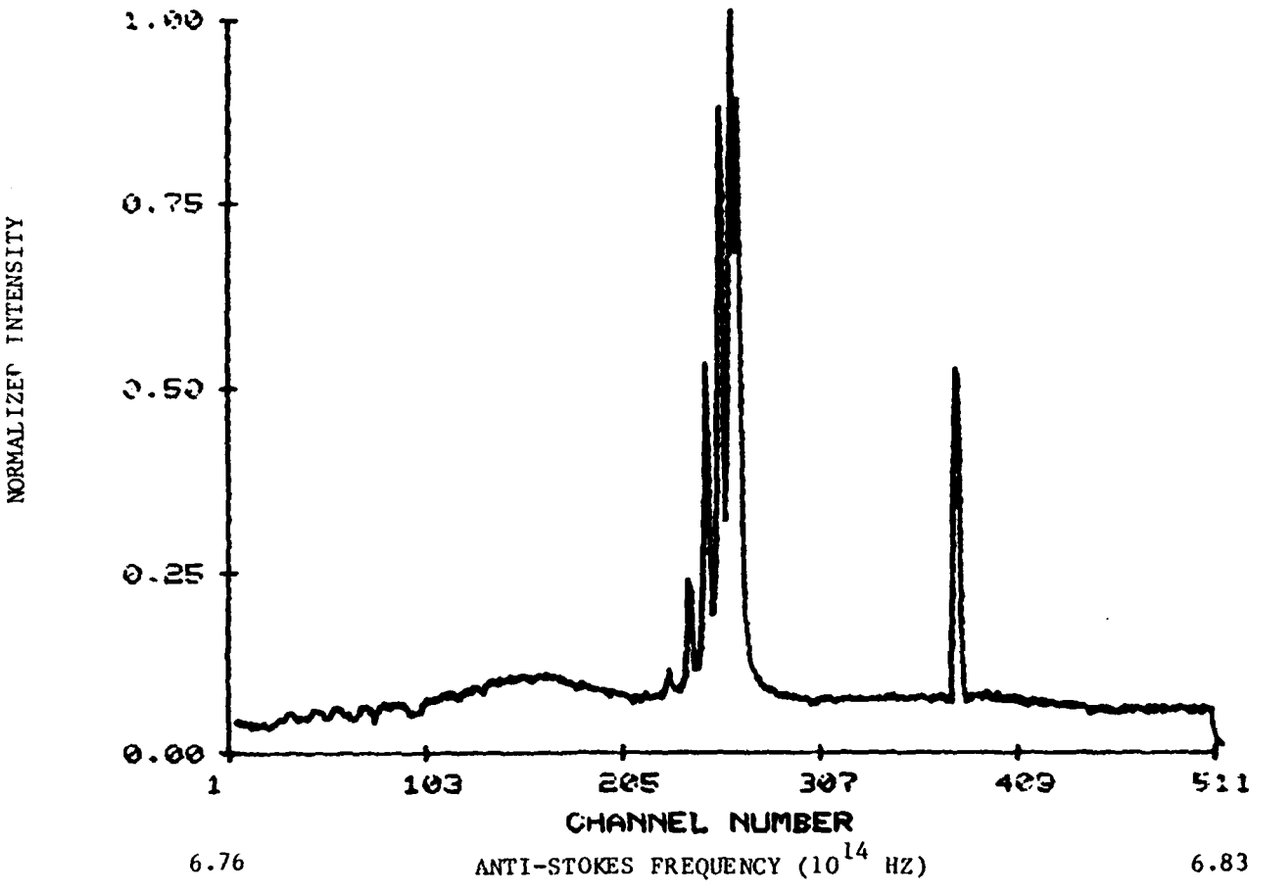

Fig. 14. Experimental Spectrum of 50 Torr HF (512 Channels).

nonresonant component was generated with a peak at about 3800 cm^{-1}. Figs. 14 and 15 display all 512 channels of raw data at 50 and 700 torr and Fig. 16 shows the spectral profile of the dye laser to illustrate the correspondence between the dye laser profile and the non-resonant signal. The high intensity beams caused the gas to break down at high pressures, so the focusing lens was skewed to enlarge the focal point.

Figs. 17 and 18 show the spectra from the 50 and 700 torr HF to illustrate the results at the linewidth extremes. The averaged and background corrected dye laser profile is graphed in Fig. 19. Only channels 218 through 282 are shown since no other resonant CARS data outside of this range was observed. The nonlinear least-squares curve fitting routines of the next section will fit these 65 channels with calculated spectra.

RESULTS

The experimental data stored on tape consisted of CARS intensity and background intensity measured at each of the 512 detector channels. Background data was recorded by blocking the dye beam to eliminate the CARS signal then measuring the intensity due to the 532 nm beam scattered inside the monochromator. The DARSS detector is constructed with two separate amplifiers which are interfaced to alternate diodes in the array. Uneven noises are normally present, so the background subtraction process is also intended to improve the correlation between the two amplifiers. The spectral profile of the dye laser was also recorded by generating a non-resonant CARS signal in propane gas. The profile will be used in the analysis since the dye laser in general does not provide uniform excitation of the Q-branch.

One thousand pulses of CARS data and two hundred pulses of background data were recorded at approximately 50 torr increments between 50 and 700 torr inclusive. At each pressure, the CARS and background data were individually averaged then the background was subtracted from the CARS intensity recorded by each channel. The dye laser signal generated in propane was averaged similarly and the average background intensity was subtracted.

An unexpected level of nonresonant signal was observed especially at the higher pressure. It was believed that impurities may have contaminated the gas. The problem may have gone unnoticed if a dye were available that could be tuned closer to the Q-branch. Even though oxazine 720 is the most appropriate dye, the peak could not be concentration tuned closer than 150 cm^{-1} to the Q(6) transition. High power was required to adequately excite the lines, so a strong

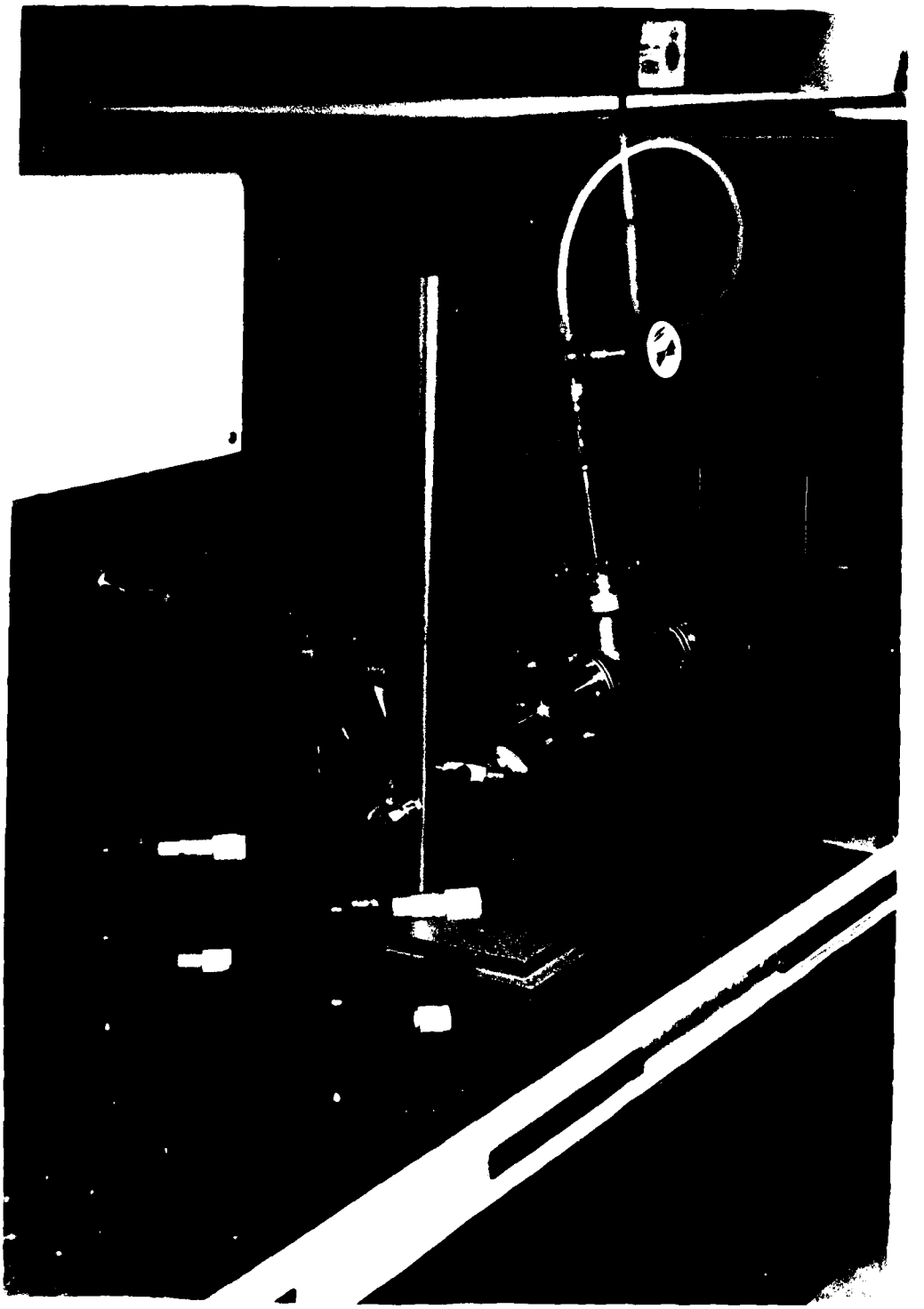

Fig. 13. Gas Cell and Hardware for Focusing Laser Beams.

calculated by averaging the pressure-broadening coefficients of the P(3) and R(3) transitions.

Tables IV and V show the results of different experiments at 390 K and 373 K. In both cases the pressure-broadening coefficient of the R(3) transition is smaller than that of the P(3) transition, and the pressure-broadening coefficient of the R(2) transition is larger than that of the P(4) transition. Also, both cases show that the average of the pressure-broadening coefficients of the P(3) and R(3) transitions is remarkably close to the average of the pressure-broadening coefficients of the P(4) and R(2) transitions. Since the results are nearly equal, a_3 is calculated later from the average of the pressure-broadening coefficients of the P(3), R(3), P(4), and R(2) transitions. These results show that the lifetime arguments apparently are applicable to HF. However, it will be shown next that simple temperature theory does not predict the differences between the linewidths of identical transitions reported at different temperatures.

Typical vibrational-rotational transitions have linewidths that are proportional to $T^{-1/2}$ where T is the temperature in Kelvin. Chapter II summarizes this approximation which considers only the changes in the collisional velocity and number density that occur with a change in temperature. The molecular transitions of HF do not appear to behave as predictably. Reference 10 contains the results of theoretical calculations at two different temperatures, 390 K and 480 K (10). The results were presented in Table III. The calculations do not distinghish between P(J) and R(J+1) transitions and the available experimental data shows that the linewidths of such transitions are fairly equal (12) (13). This observation is also supported by lifetime

TABLE IV

Estimation of Q(3) Pressure-Broadening Coefficient from IR Data* of HF at 390 K

Units: 10^{-3} cm^{-1}/torr HWHM

Transition	Coefficient	Transition	Coefficient
R(3)	0.530	R(2)	0.620
P(3)	0.668	P(4)	0.569
Mean	0.599	Mean	0.595

*Data taken from (12).

TABLE V

Estimation of Q(3) Pressure-Broadening Coefficient from IR Data* of HF at 373 K

Units: 10^{-3} cm^{-1}/torr HWHM

Transition	Coefficient	Transition	Coefficient
R(3)	0.587	R(2)	0.707
P(3)	0.725	P(4)	0.596
Mean	0.656	Mean	0.651

*Data calculated from linewidths given in (13).

arguments; the energy of the lower state of a P(J) transition is higher than that of the lower state of an R(J+1) transition, but the energy of the upper state of the P(J) transition is lower than that of the lower state of the R(J+1) transition. The effect of one energy difference apparently cancels the other and the resulting lifetimes yield transitions with similar linewidths. At the two temperatures, the linewidths of the R(0) and P(1) transitions are approximately proportional to $T^{-1/2}$, but the narrowing effect decreases with rotational quantum number. Transitions beyond R(3) and P(4) are shown to broaden with temperature. Perhaps the increase in the share of the total population density that occurs in the higher rotational states has a broadening effect caused by an increase in effective perturbers. This conjecture is based on the assumption that only molecules with nearly equal energies will interact and cause broadening. If the calculations are accurate, then the mean of the linewidths of R(3) and P(3) remain fairly constant with an increase in temperature since the linewidth of P(3) decreases while R(3) increases. It is not believed that these calculations have enough merit for precise calculations, but they do suggest that the linewidths of the P(3), Q(3), and R(3) transitions are not affected by temperature as severly as the factor $T^{-1/2}$ indicates.

Determining the Best Infrared Data. Three references were scrutinized before one of them was selected for estimating a_3. More data was available (Fig. 2), but the pressure-broadening coefficients were only reported graphically. Two of the references have already been introduced in Tables IV and V; they provide both P-branch and R-branch data for temperatures of 373 K and 390 K. The third reference (14) summarizes only R-branch measurements at 295 K. The results of all

three experiments are examined to find a good estimate of the pressure-broadening coefficients of the R(3) and P(3) transitions. Since room temperature HF was measured in the CARS experiment, the data for 295 K HF appears to be the most suitable for determining a_3. However, the report has discrepencies between the graphs and tabular data of the pressure-broadening coefficients. Also, the pressure-broadening coefficient reported for the R(3) transition is larger than reported by all of the other references. Transitions are expected to broaden with a decrease in temperature, but the results of the previous analysis of the theoretical calculations show that the lower temperature does not justify such large pressure-broadening coefficients.

The theoretical calculations are used to compare the pressure-broadening coefficients of the R(3) transitions reported at the three temperatures. These calculations indicate that the pressure-broadening coefficients scale with temperature by a factor less severe than $T^{-1/2}$, so $T^{-1/2}$ is accepted as the limit. Using this limit as the scaling factor, all of the data is translated to 300 K from the temperatures at which the experimental measurements were made. The results of scaling the pressure-broadening coefficients from the data reported at 295 K, 373 K, and 393 K, are respectively 8.7 X 10^{-4} cm^{-1}/torr, 8.1 X 10^{-4} cm^{-1}/torr, and 6.0 X $10^{-4}cm^{-1}$/torr. These results are not very consistent and the two closest values are believed to be further apart than indicated since the limit of the scale factor was used. In other words, the calculation of the 373 K data gives an upper bound result while the 295 K data remains almost constant; a less severe scale factor would yield results that differ more. Since the data reported are so widely varied, the final determination of the R(3) and P(3) pressure-

broadening coefficients are made after considering the three procedures used for the measurements.

All three of the earlier experiments measured the linewidths with absorbtion techniques, but the measurement at 295 K was obtained with an approach different than that of the other two experiments. The 295 K HF was scanned by a narrow-band tunable laser with a linewidth of about 100 KHz. Absorbtion spectra were recorded and the linewidths were determined graphically. To determine the pressure-broading coefficients, spectra were recorded at approximately 1000 torr, then the linewidths were divided by the pressure. Unfortunately, only R-branch data were reported and the article does not define the notation that represents the linewidths. The graphical and tabular data appear to be contradictory, so the notation cannot be deduced. Although impressive equipment was used, the confusing report is less reliable than the other papers. Consequently, the very high pressure-broadening coefficients are disregarded.

The experiments which measured 373 K and 390 K HF were carried out with similar absorbtion techniques. A broad-band source illuminated the gas and a narrow-band detection system recorded graphical spectra. The effect of instrumental broadening was carefully analyzed so that good estimates of the actual linewidths could be made. The substantial difference between the two results is puzzling, especially since the temperature difference was only 17 K.

To choose the data for the calculation of a_3, the results of the previous analysis of the temperature dependence are used. In other words, it is believed that the pressure-broadening coefficients at 300 K are broader than those reported at 373 K and 390 K but not by as much as

the factor of $T^{-1/2}$ indicates. The pressure-broadening coefficients measured in the 373 K HF are accepted as adequate estimates without making temperature conversions to 300 K. This is intended to be a compromise between the two sets of data since the accepted values would fall between the larger values obtained by scaling the data with temperature. The final estimate of a_3 is calculated with the averaging method shown earlier; the pressure-broadening coefficients of the P(3), R(3), P(4) and R(2) transitions are averaged: $a_3 = 6.54 \times 10^{-4}$ cm^{-1}/torr. The NNLS fitting procedures used later in the analysis show that this value has merit, but it cannot be determined more accurately.

Graphical Analysis of Experimental Spectra

This second part of the analysis shows that the resolution of the experimental spectra is not sufficient for the measurement of the Raman linewidths. Before the spectra are analyzed, corrections are made to the baselines to eliminate contributions from sources other than the resonant CARS signal. Then, to facilitate computations, the spectra are corrected so that they represent the CARS signal that would have been measured if the Q-branch had been excited uniformly by the radiation from the pump and Stokes lasers. Both of these corrections are made in all parts of the analysis.

Correcting the Baselines of the Experimental Spectra. The graphs of the raw data (Figs. 17,18) indicate that the detected signals have a higher baseline at the low frequency end of the spectra. At the frequency extremes, the intensity would be negligible if only CARS signals due to the Raman transitions were present. This bias in the signal is probably due to nonresonant CARS radiation excited in

impurities by the same radiation that excites the Raman transitions. Figs. 14 and 15 clearly show a broad peak below the frequency range of the Raman transitions. This peak aligns with the peak of the excitation spectra (Fig. 16) that was recorded by generating a CARS signal in the propane gas. Ordinary noise in the detection system also contributes to the baseline as can be seen by the constant baseline at the high frequency end of the spectrum.

The computation of the squared modulus of the Raman susceptibility is complicated by these undesireable nonresonant components since χ_{nr} in Eq (9) is not zero. It is not possible to accurately estimate χ_{nr}, so it is assumed that the cross terms generated by squaring $\chi_r + \chi_{nr}$ are negligible. (χ_r refers to the resonant component.) The excitation spectra in the vicinity of the Raman transitions is almost linear with frequency (Fig. 19), so the combined effect of the nonresonant CARS contribution and the noise is a linear bias with non-zero slope. The integrity of the data in the vicinity of the Q(6) transition is most compromised by the approximation, but the other lines are of sufficient magnitude that their shapes probably are not seriously affected by the nonresonant signals.

The baselines of the spectra are corrected by subtracting a constant slope line that produces experimental spectra that fit calculated spectra. Calculations show that the intensity of CARS at the selected extreme detector channels should be nearly zero (calculation details are discussed in the next part of the analysis.) The three channels at each end of the spectra are averaged then the correction line is formed that will reduce the intensity of the middle channel of each triad by the corresponding average. All other channels are reduced

by the magnitude of the correction line at that frequency.

Correcting for Nonuniform Excitation of the Q-Branch. In all of the analysis parts, examination of the data is enhanced by assuming uniform excitation of the Q-branch because data can be compared to calculations without including the excitation spectra in the calculations. Consequently, the data must be corrected to represent spectra that would have been recorded if the Q-branch were uniformly excited. Properties such as linewidths and relative intensities of the peaks can then be directly observed from the graphs.

Eq (8) represents the power spectral density of a CARS signal generated by a Stokes beam with a broad power spectral density and a pump beam with a narrow power spectral density. This equation applies to the experiment since the excitation profile is very broad and the spectral profile of the pump beam has an approximate Gaussian lineshape with a breadth of 0.5 cm^{-1} HWHM. To correct the data, the baselines are first corrected then each channel of every experimental HF spectra is divided by the magnitude of the corresponding channel of the spectra of the excitation signal. No corrections were made to the baseline of the spectra of the excitation signal. Figs. 20 and 21 show the results obtained by correcting the spectra of the 50 and 700 torr HF. The decrease in the magnitudes of the peaks at low frequencies is due to the high intensity of the excitation signal at low frequencies. When the corrections are made, the magnitudes of the peaks at low frequencies are decreased relative to the peaks at higher frequencies because the power spectral density of a uniform excitation signal would not be greater at low frequencies as is the experimental signal.

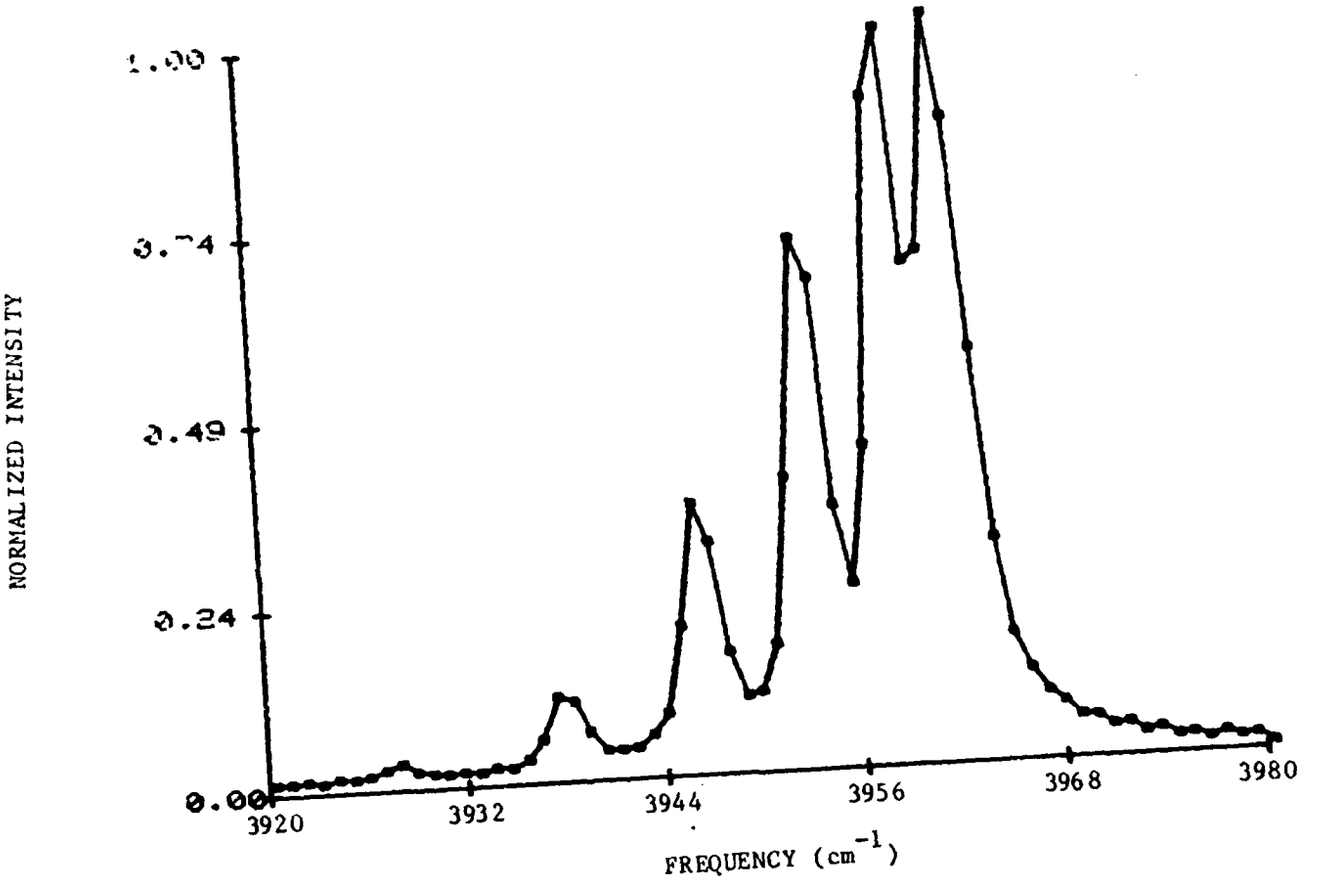

Fig. 20. Experimental Spectrum of 50 Torr HF Corrected for Uniform Excitation of Q-Branch.

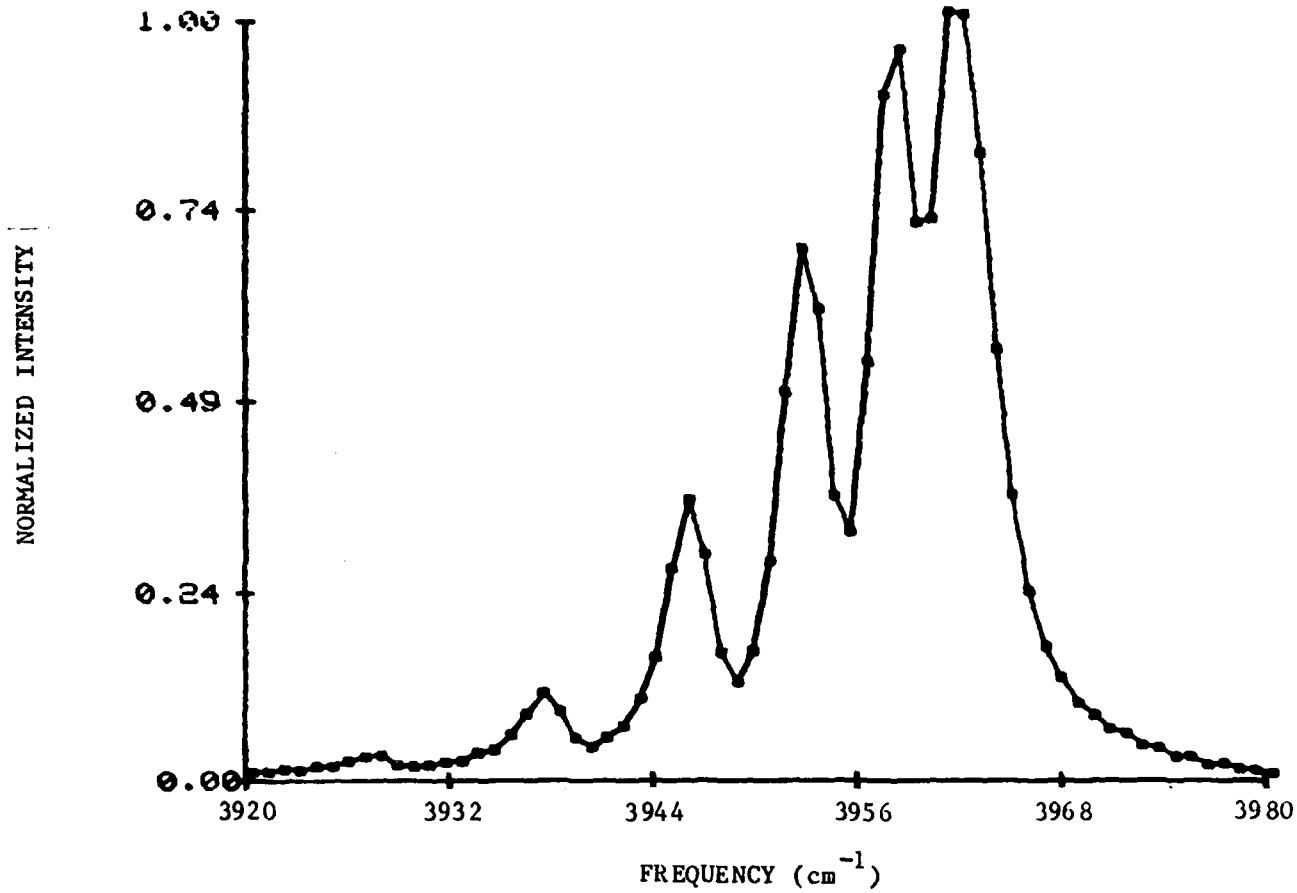

Fig. 21. Experimental Spectrum of 700 Torr HF Corrected for Uniform Excitation of Q-Branch.

Estimating a_3 Graphically. The previous few sections have shown how the experimental spectra are corrected so that they represent the detection of broad-band CARS signals with uniform excitation of the Q-branch. Eq (8) is modified for uniform excitation by setting $L_s(\omega_s)$ equal to an arbitrary constant. This form shows that the CARS signals are convolutions of the squared modulus of the Raman susceptibility and the probe beam spectral density. The experimental spectra are found by convolving the CARS signal with the effective slit function of the detector using Eq (17). The profile of the probe beam and the slit funtion were the same during all experiments, but the Raman susceptibilty varies with pressure due to the pressure dependence of the densities of states and of the Raman linewidths. Pressure changes within the experimental range do not affect the relative magnitudes of the densities of states, so the profiles of the graphs should only show *differences caused by the changes in* the linewidths of the Raman transitions.

If the resolution of the measurement process were much higher, it would be possible to measure the difference in the breadth of the data peaks at different pressures. Deconvolution techniques could then be used to deduce the change in the Raman linewidths so that the pressure-broadening coefficients could be calculated. However, superimposing the 50 torr and 700 torr spectra (Fig. 22) shows that the change in the breadths of the data peaks is small compared to the broadening caused by the probe beam and the effective slit function. Also, the Q(0) and Q(1) transitions are not resolved at any pressure. Accurately estimating the pressure-broadening coefficients by measuring the breadths of the experimental spectra is therefore not possible.

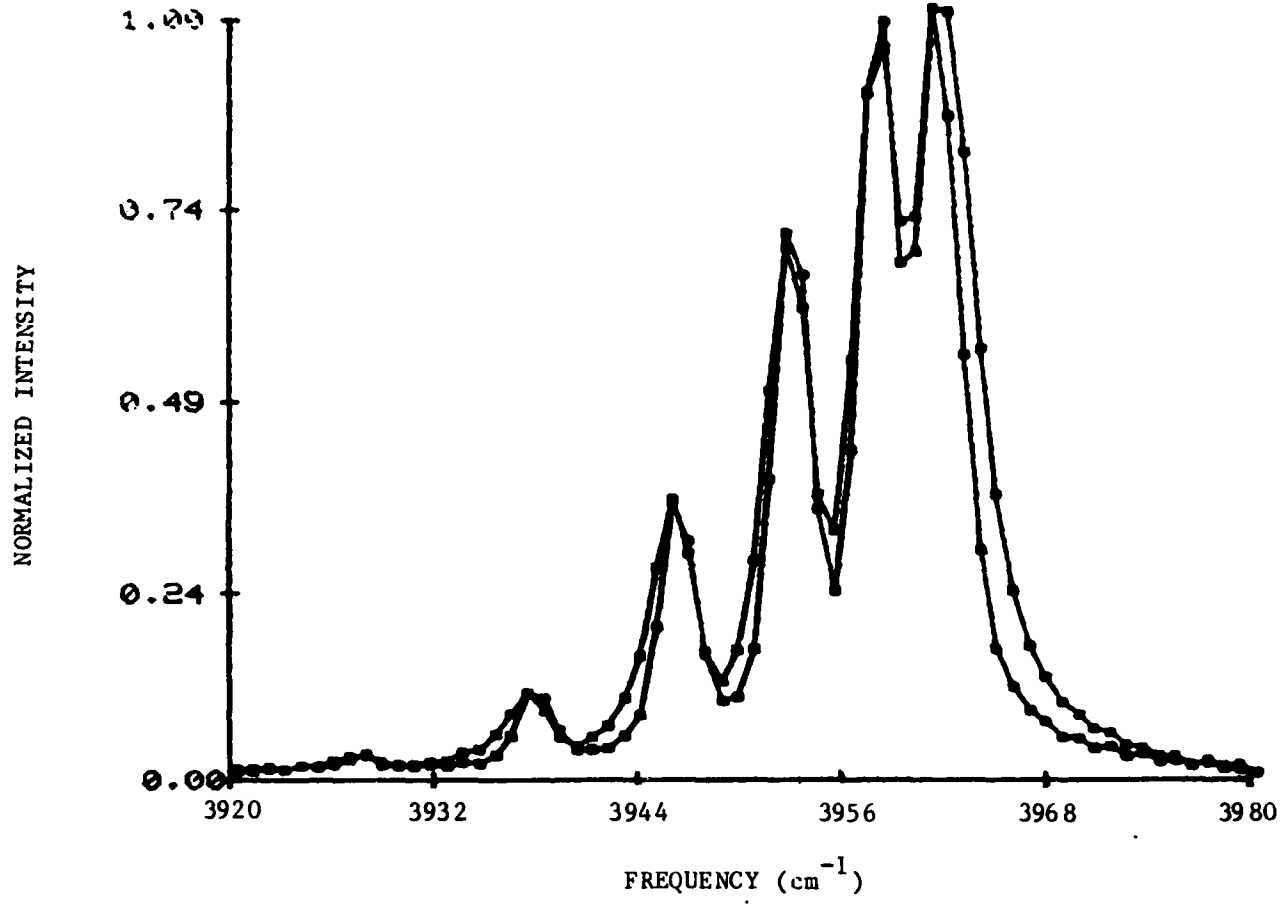

Fig. 22. Superimposed Spectra of 50 Torr and 700 Torr HF. The maximum intensity of each spectrum was normalized to 1.

Since a_3 was estimated from previous experiments and the Q(3) transition is well resolved in the experimental spectra, a rough estimate of a_3 is made from the graph in Fig. 22. For this purpose, it is assumed that the observed breadth change in the portion of the spectra corresponding to the Q(3) transition is equal to the change in Γ_3. (If the effective slit function and the spectral profile of the probe beam were both Lorenztian, the assumption would be true.) Measuring the difference between the breadths and dividing by the difference in pressure yields the crude estimate for a_3. The result is $a_3 = 4 \times 10^{-3}$ cm^{-1}/torr. The result estimated from the literature was 6.54×10^{-3} cm^{-1}/torr. Considering the low resolution and the many approximations, the two answers are close.

It is important to recognize at this point why it is worth the trouble to pursue more extensive curve fitting analyses when it appears that the resolution is inadequate for measuring the small changes in linewidths. If only one transition were observed at the resolution of this system, meticulous curve fitting would not be much more valuable than graphically measuring the change in the breadth of the spectra. There would be only about a half-dozen points to describe the spectra so curve fitting would rely on unrealistically accurate representations of the spectral profile of the probe beam and the effective slit function. However, the actual experimental data contains seven transitions whose relative linewidths determine the relative maxima of the peaks as well as their breadths. The curve fitting calculations performed in the next two parts of the analysis essentially extract both the information contained by the magnitudes and the information contained by the breadths. Another important point is the fact that the calculations are

not claimed to achieve unusually accurate linewidth estimates at any of the fourteen pressures. They do yield good estimates at each pressure so that linear regression analyses of the linewidths at all fourteen pressures can determine the pressure-broadening coefficients of each transition. In summary, the success of the calculations that follow are due to the fact that seven sets of breadth and magnitude information are simultaneously taken from each of fourteen experimental spectra, and the information in all of the spectra is used to determine the pressure-broadening coefficients.

NLLS Fit with Γ_3 an Independent Variable

In this part of the analysis, a NNLS fitting routine and a linear regression routine are used to find a_J for J=0,1,2,4,5,6. Using the estimate of a_3 obtained from the infrared data, Γ_3 is calculated at each of the experimental pressures. The effective slit function of the detector is found by fitting the slit function to the CARS spectrum of HF at 50 torr. Next, the calculated values of Γ_3 and the effective slit function are used to best fit the other six linewidths to the spectra obtained at each pressure. Finally, the pressure-broadening coefficients of each transition are estimated by calculating the slope of the linear least squares regression line that passes through the graph of the linewidth of each transition vs. pressure. The following paragraphs outline the details of the calculations and present the results of the procedure.

Calculation Procedure. Cars spectra are repeatedly calculated by the NLLS fitting routines. The experimental spectra that are fit to the routines are corrected, as described in the previous part of the

can practically be determined by inspection due to the excellent linear results, but the graph of Γ_6 has considerable deviations most probably due to its low signal to noise ratio.

Γ_0 is linear up to about 400 torr, but increases in slope at higher pressures. It was found that the cause of this discrepency is likely to be a result of fixing Γ_3 to a value calculated from the value for a_3 estimated from infrared data. The procedure unfortunately assumes Γ_3 is correct and does not allow the varibles representing the linewidths to fluctuate with random experimental parameters. Overestimates of Γ_3 cause overestimates of the linewidths of the other transitions. For highly resolved transitions, the problem is not critical since errors in Γ_3 cause similar errors in the other linewidths. This explains why the graphs of most of the linewidths are extremely linear even though it is doubtful that the actual gas samples were prepared so precisely; Γ_3 was forced to be linear so the other linewidths must be linear in order to create proper relative magnitudes. However, the unresolved Q(0) and Q(1) transitions are more seriously affected by overestimates of Γ_3 since excessive blending is caused. The Q(1) transition involves over twice the population density of the Q(0) transition (Fig. 4), so the intensity of the experimental spectra in the region corresponding to the Q(0) transition is calculated to be artificially high. Consequently, the fitting routine increases Γ_0 for the purpose of decreasing the contribution of the Q(0) transition to the intensity; a large linewidth in the denominator of the Raman susceptibility effectively reduces the peak intensity.

Table VI shows the pressure-broadening coefficients calculated from the linear regression analysis of Γ_J vs. pressure. The result for a_3 is

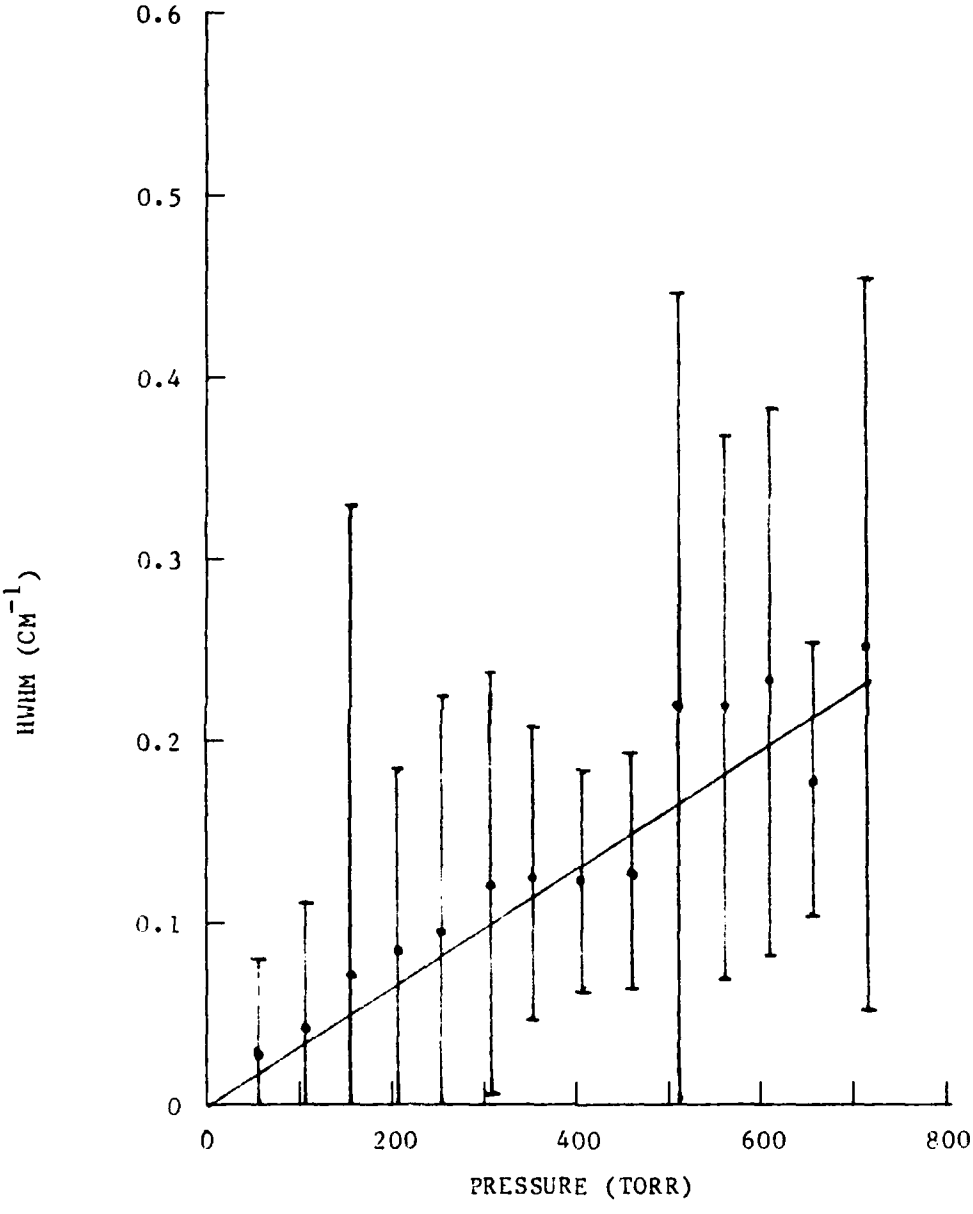

g) Γ_6 vs Pressure.

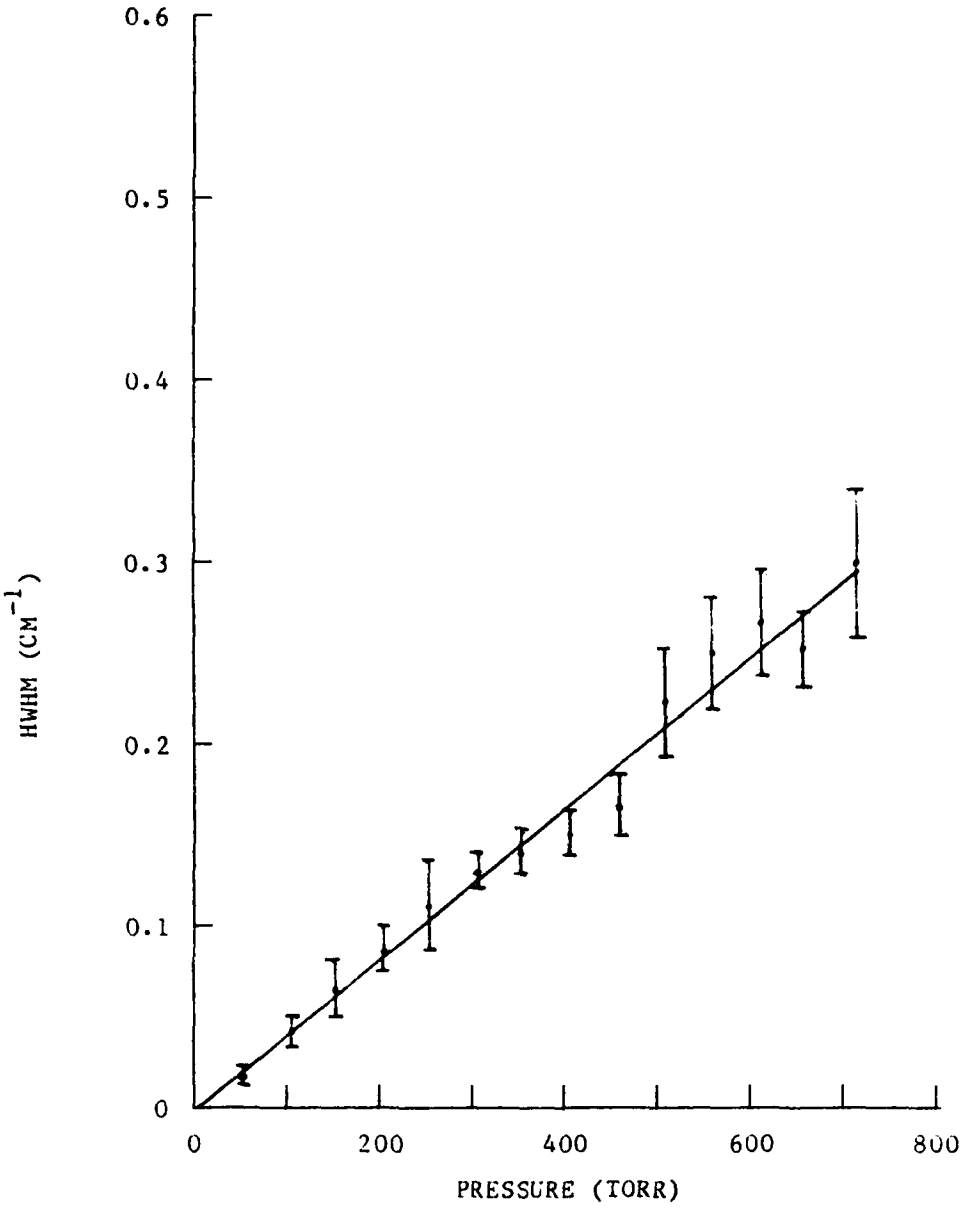

f) Γ_5 vs Pressure.

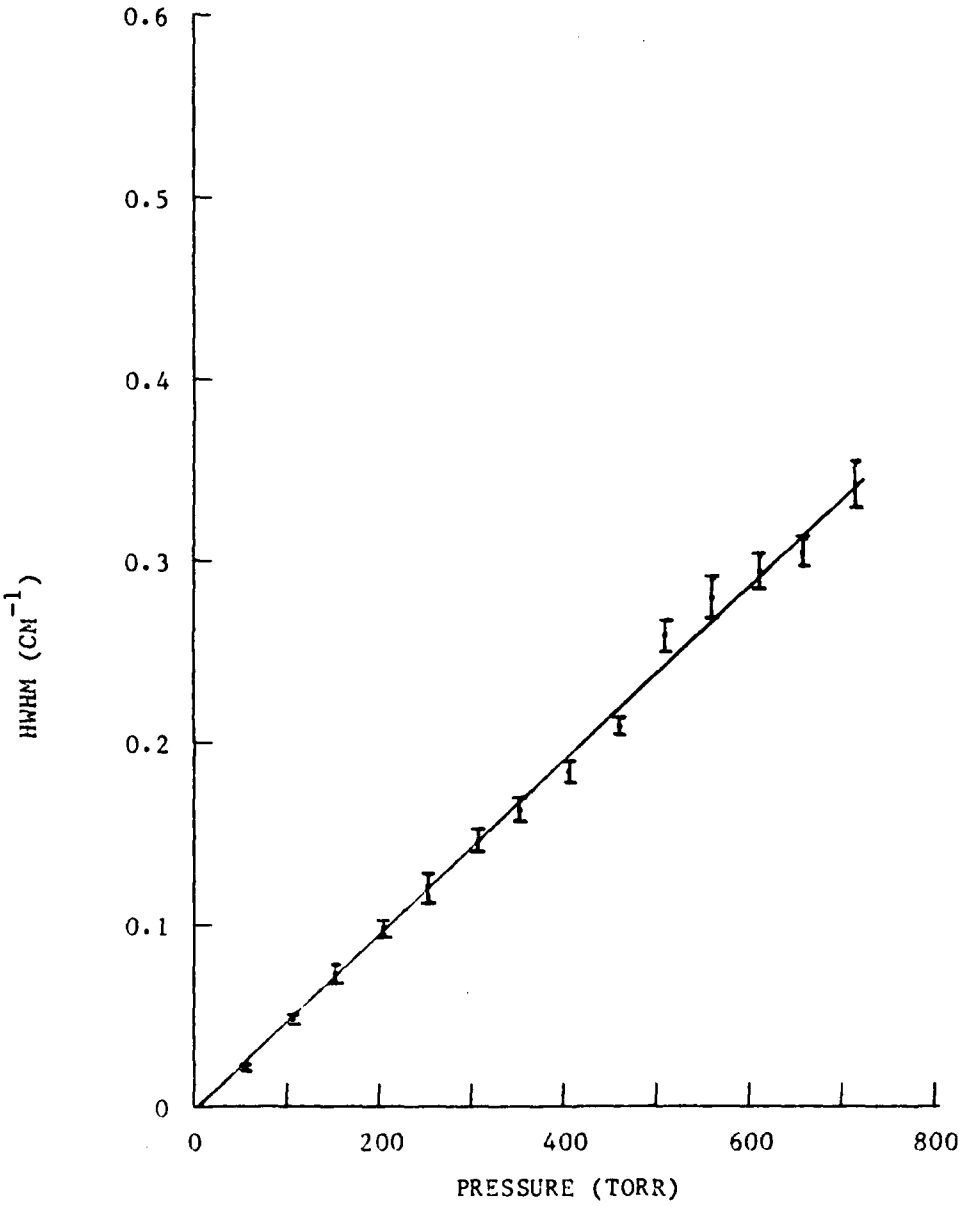

e) Γ_4 vs Pressure.

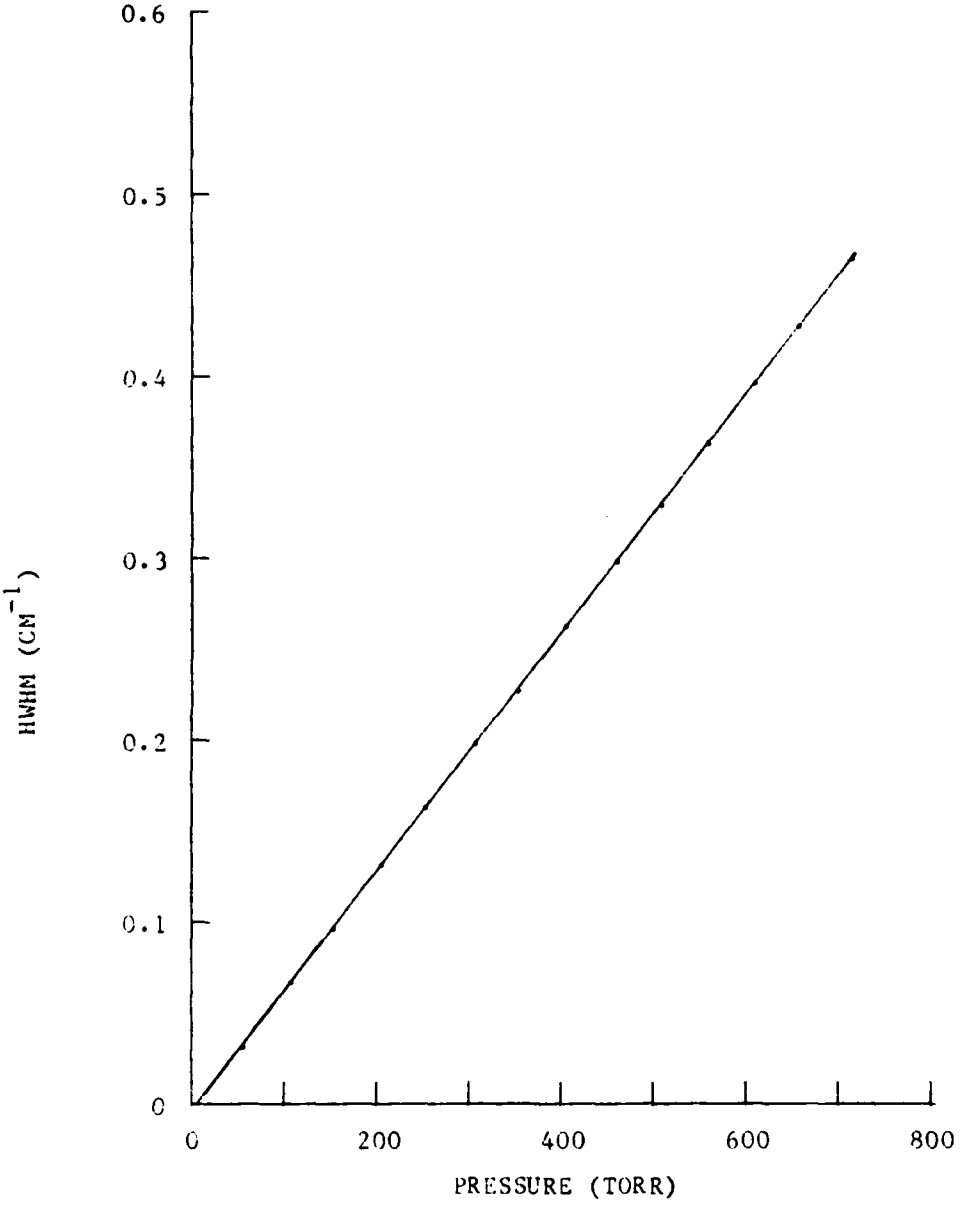

d) Γ_3 vs Pressure.
(reference linewidths)

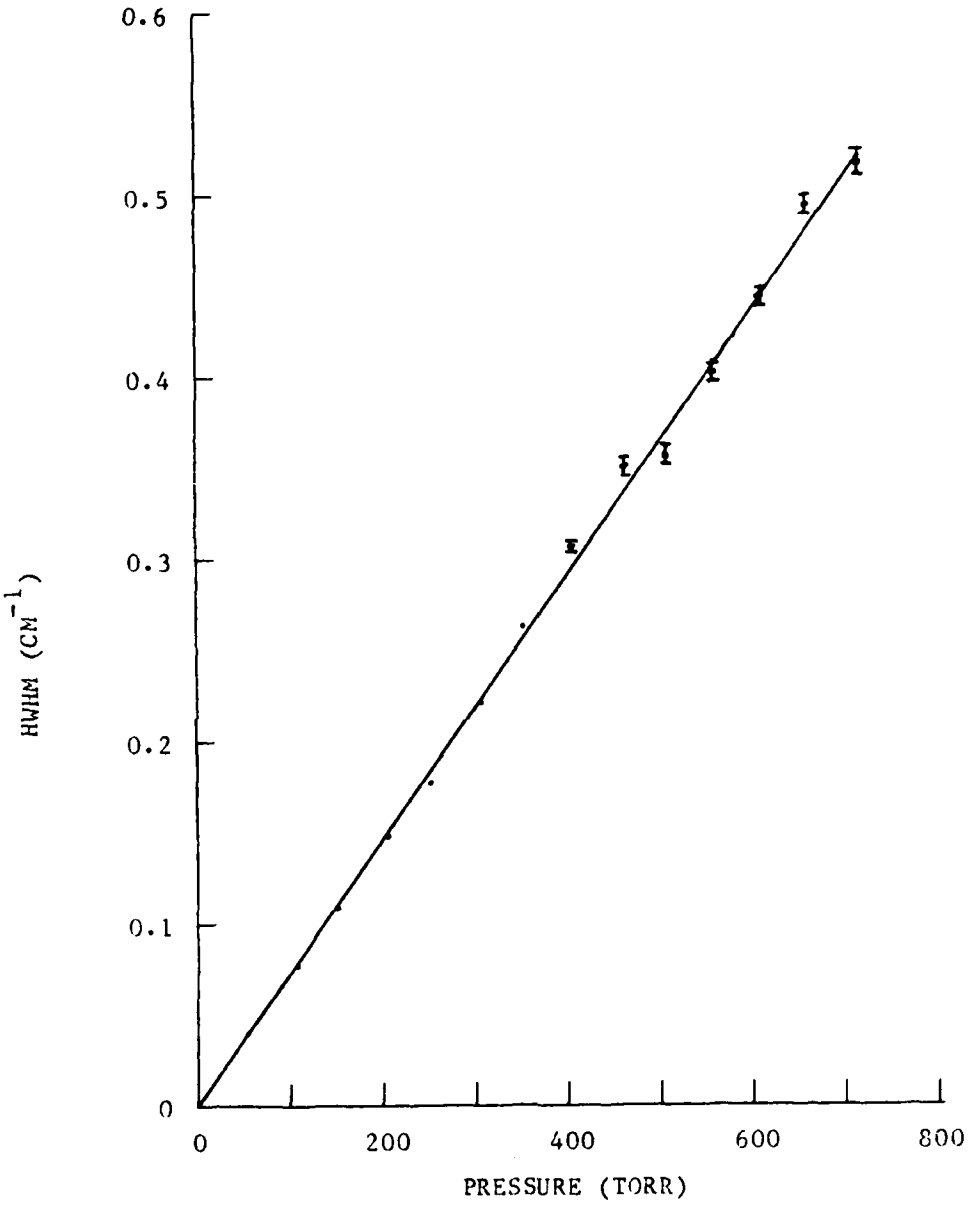

c) Γ_2 vs Pressure.

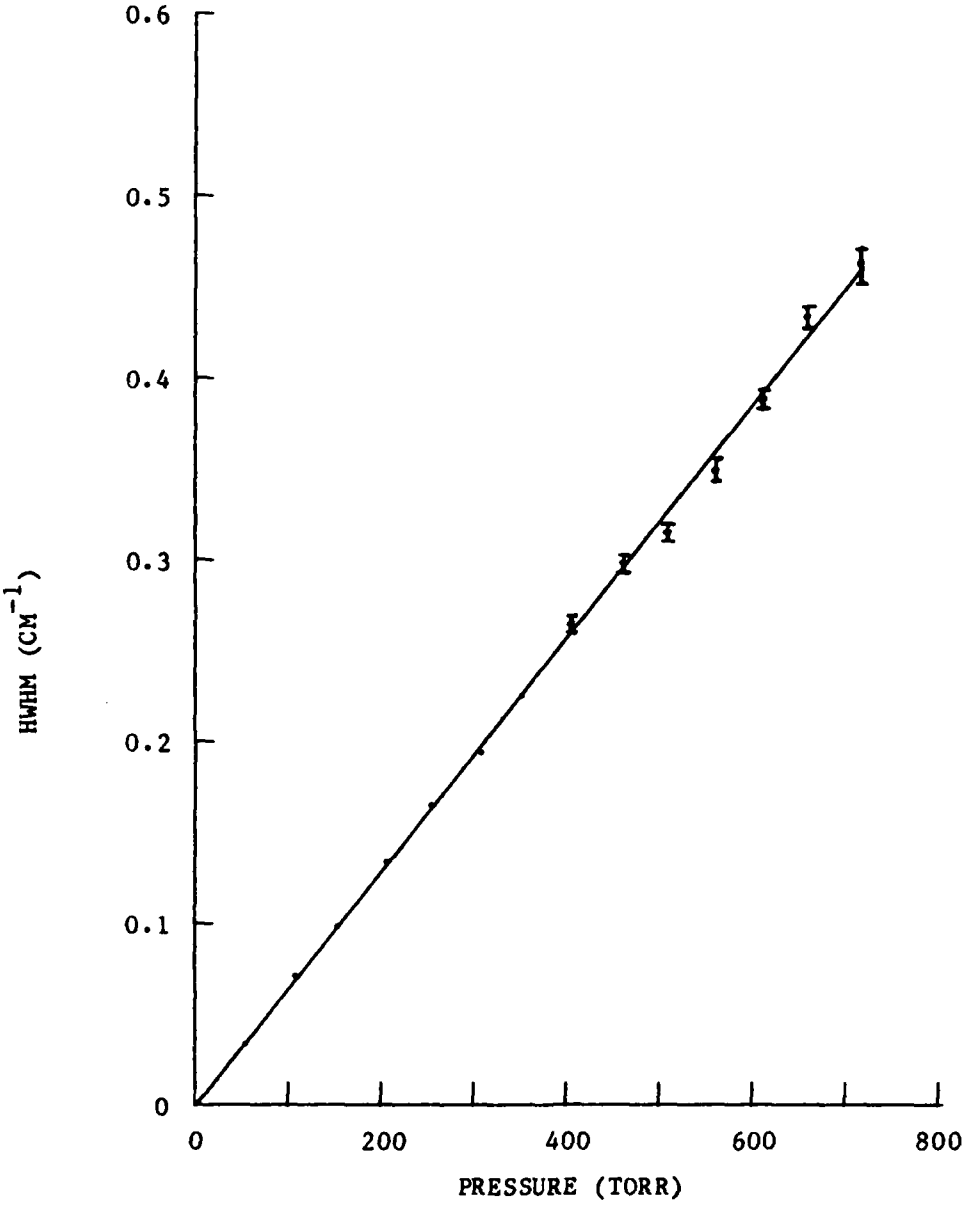

b) Γ_1 vs Pressure.

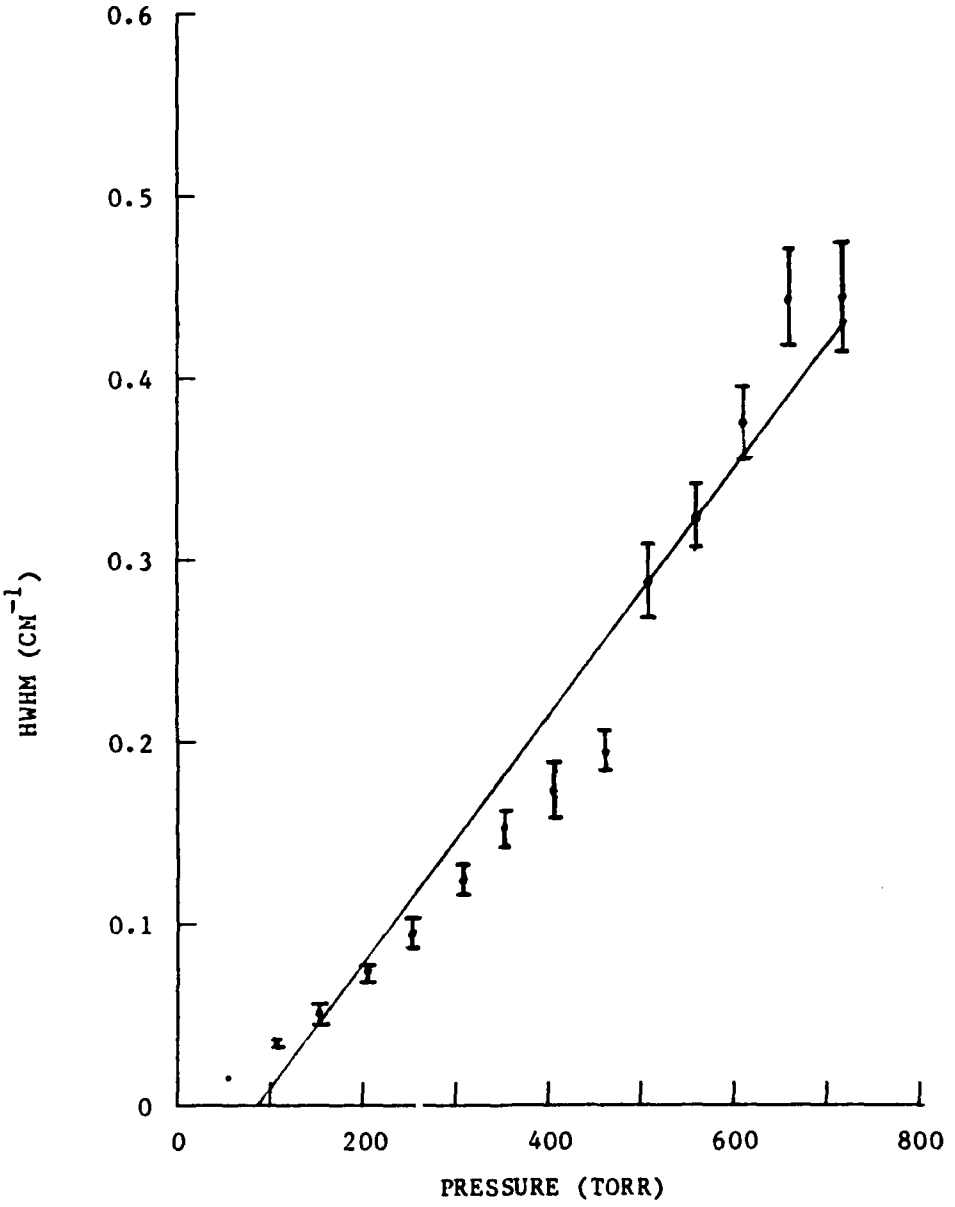

Fig. 25. Γ_J vs. Pressure from the Results of NLLS Fitting Procedure Using Γ_3 as a Reference Linewidth. Error bars correspond to ± 1 standard deviation (See Section II). Errors less than .003 cm^{-1} are not marked.

a) Γ_0 vs Pressure.

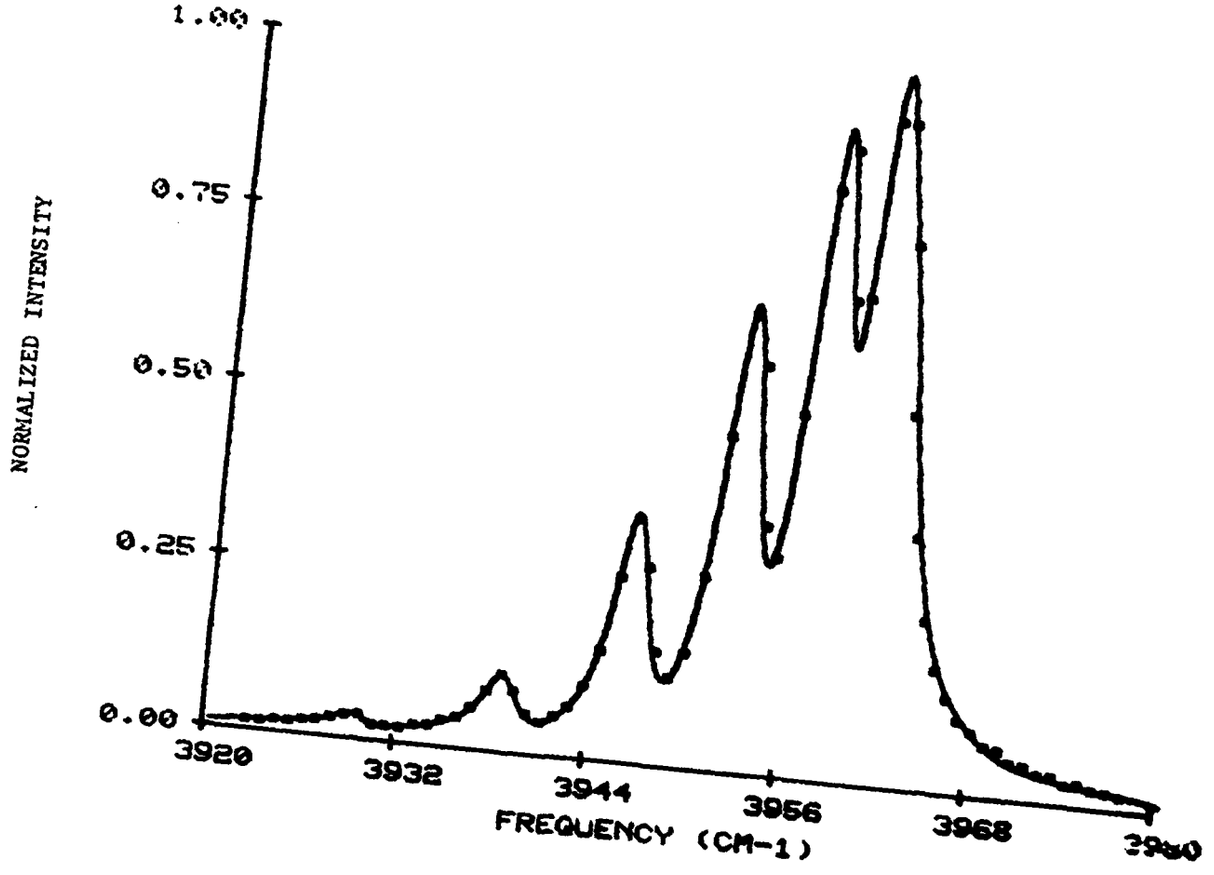

Fig. 24. Nonlinear Least-Squares Fit of CARS Spectrum of 700 Torr HF.

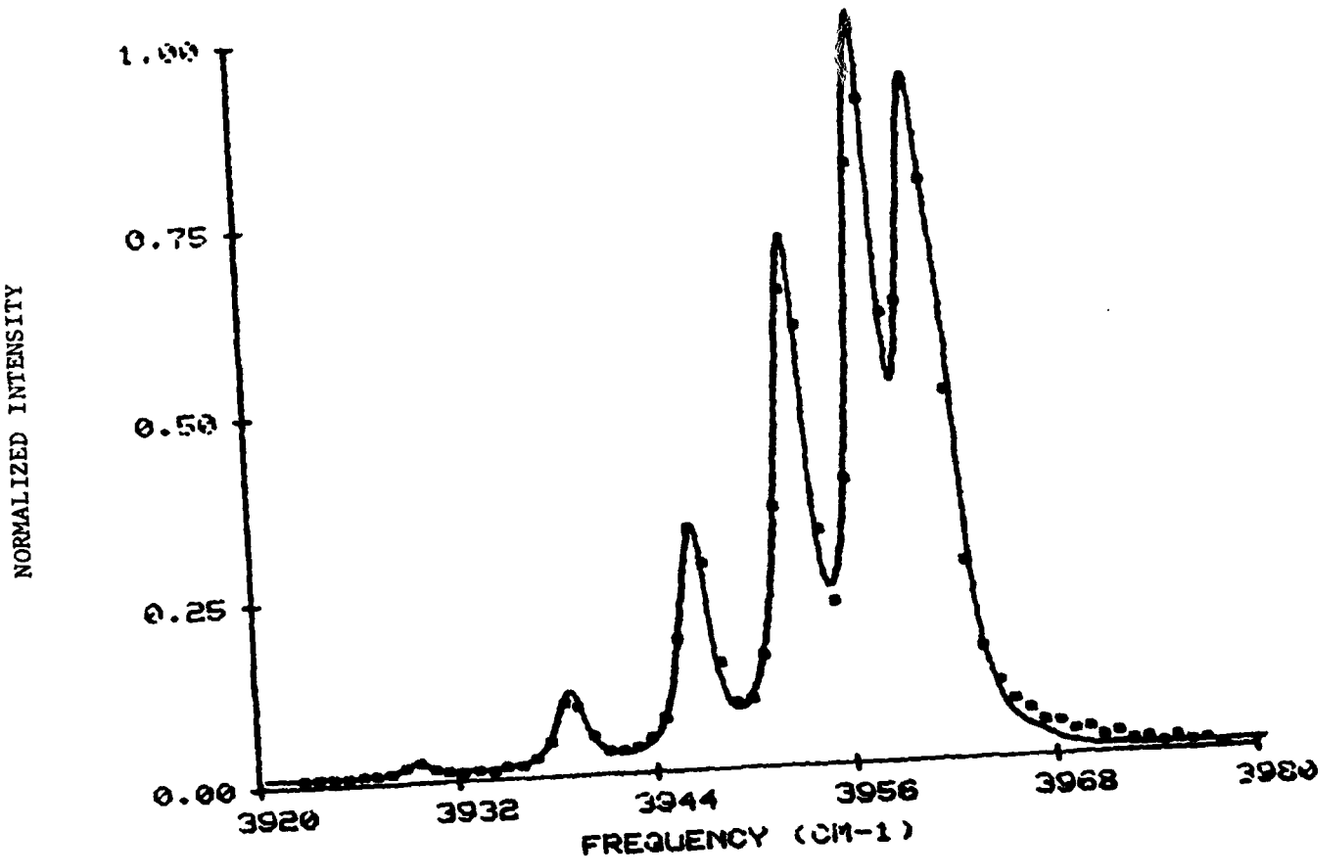

Fig. 23. Nonlinear Least-Squares Fit of CARS Spectrum of 50 Torr HF.

determined from the infrared data. Each experimental spectrum was fit in order to find the pressure dependence of the linewidths. To determine the sensitivity of the results to errors in Γ_e, several spectra were fit with Γ_e equal to .8 cm^{-1} and .76 cm^{-1}. The results for the linewidths were essentially the same in all three cases. This insensitivity is due to the fact that Γ_3 is fixed and the relative intensities of the individual peaks in the spectra are determined by the linewidths of the corresponding Raman transitions relative to Γ_3. It was shown earlier that the values of Γ_J in the denominator of the Raman susceptibility determine the magnitudes of the peaks, so fixing Γ_3 essentially fixes the magnitude of the portion of the CARS spectra corresponding to the Q(3) transition. In the NNLS fitting procedure, the other linewidths must vary to produce calculated spectra that will have peaks that have magnitudes correctly related to the magnitude of the Q(3) line. An erroneous value for Γ_e causes larger residuals between the experimental and calculated spectra, but the variables still converge to nearly the same linewidths since the relative magnitudes of the peaks can only be matched with a certain set of linewidths. If Γ_3 is not an independent variable, as is true in a later part of the analysis, the results are critically sensitive to errors in Γ_e.

Figs. 23 and 24 show the results of fitting the spectra of HF at 50 torr and 700 torr. The baseline deviation at low pressures indicates that the effective slit function probably has higher wings than a true Lorentzian. Fig. 25 shows the graphs of the linewidths of the transitions as a function of pressure. Included in each graph is the line computed from the linear least-squares regression analysis. The pressure-broadening coefficients of the Q(1) through Q(5) transitions

iterations are typically needed. A more complicated approach, such as fitting the baseline with least squares computations, does not seem worthwhile since the results do not appear to be sensitive to small changes in the baselines.

Results of the First NLLS Fitting Procedure. The effective slit function of the detection equipment is determined from the spectrum of HF at 50 torr. The linewidths of the Raman transitions at this pressure are so narrow that the profile of the resolved peaks in the experimental spectra are primarily determined by the effective slit function and the spectral profile of the pump beam. The relative amplitudes of the peaks are affected by the linewidths, but the spectral profile of the resolved peaks are not. To show the narrow linewidths of the transitions, Γ_3 is calculated from the value of a_3 determined from the infrared data. The linewidth is only 0.034 cm^{-1} HWHM while the breadth of the peaks in the experimental spectra are several cm^{-1}.

It was discovered through trial and error that the effective slit function is accurately represented by a Lorentzian lineshape. To find the correct breadth of the effective slit function, Γ_e, the NLLS fitting routine was configured to treat Γ_3 as an idependent variable and treat as dependent variables Γ_e and the linewidths of the other six transitions. The routines converged slowly and oscillated about the final solution, but the smallest sum of the squares of the residuals between the trial spectra and the experimental spectra occured when Γ_e was 0.785 cm^{-1}.

The NLLS fitting routine was next modified to represent both Γ_3 and Γ_e as independent variables. At each experimental pressure, Γ_e was fixed at 0.785 cm^{-1} and Γ_3 was calculated from the value of a_3

determined in this manner was 0.875 (1/cm) per channel and proved a reliable constant for all of the data since no adjustments were made to the spectrometer during the experiment.

A form of area normalization is used to match the amplitude of the data to the calculations. The detection equipment has insufficient resolution for determining the maximum amplitude or the frequency of the peaks in the experimental spectra. Consequently, normalizing by peak intensity could not be adequately accomplished. The area of calculated spectra were approximated by adding the intensities at only the frequencies that correspond to a detector channel. Adding the experimental intensities and dividing by the sums of the calculations provide the normalization constants.

In order to carry out the amplitude normalization and frequency scaling procedures, slight corrections are made to the baselines of the experimental spectra. The intensities at the frequency extremes of the raw data were set to zero during the process that converted the raw data to spectra that represent a uniformly excited Q-branch. However, the calculations show that a slight positive intensity is predicted at the extremes. To rectify the slight discrepency, a correction is performed in a manner similar to the method used to correct the raw data. The magnitude of a correction line is subtracted so that the average of the group of three channels at each end of the spectra passes through the magnitude of the calculated spectra at the frequency of the middle channel. Since area normalization slightly affects the baseline, the area normalization and baseline corrections are alternately performed until the calculated and experimental spectra have equal area and equivalent baselines. The correction is so slight that only two

analysis, so that Eq (8) can be used with L_s=1. Numerical integration is used to evaluate the the equation. The four step procedure for calculating a trial spectrum is a modification of that used by Goss when calculating CARS spectra of nitrogen in turbulent flames (3). First, the densities of states of the first seven rotational levels in the two lowest vibrational states are found using Eqs (11-15). The gas temperature was low enough that almost all of the molecules are in the lowest vibrational state, but the next higher level is calculated for insurance. Second, the squared modulus of the Raman susceptibility is computed after evaluating Eq (10). Third, the CARS spectra is calculated by performing an integration over the spectral profile of the probe beam Eq (8). The probe beam is modelled as a Gaussian lineshape with a breadth of 0.5 cm^{-1}. Finally, the spectra produced by the detection equipment is determined by convolving the CARS spectra with the effective slit function using Eq (17). A substantial amount of computer memory and computation time are required to make these calculations. Appendix shows the details of the calculations and the techniques used to make the problem manageable.

Before the experimental data is fit to the calculated spectra, the frequency and amplitude are scaled to match the calculations. Frequency calibration sources were not used in the experiment and no attempt is made to calculate the absolute intensity of the CARS signal; only the spectral profile is calculated. The frequency scaling was determined by simultaneously graphing the calculations and data on the Tektronix graphics terminal. The linear dispersion of the data and the position of the spectra were adjusted manually until all data appeared to fit calculations closely. The dispersion of the detection equipment

TABLE VI

Pressure-Broadening Coefficients Obtained with First NLLS Procedure

J	a_J (cm^{-1}/torr)	Y-intercept (cm^{-1})
0	0.6914×10^{-3}	-0.0625
1	0.6414 "	0.00294
2	0.7346 "	0.00140
3	0.6540 "	0.00000
4	0.4832 "	-0.00015
5	0.4192 "	-0.00057
6	0.3260 "	0.01481

Breadth of instrument slit function = .785 cm^{-1}

TABLE VII

Pressure-Broadening Coefficients Obtained with Second NLLS Procedure

J	a_J (cm^{-1}/torr)	Y-intercept (cm^{-1})
0	0.5646×10^{-3}	-0.0307
1	0.6376 "	0.0045
2	0.7310 "	0.00305
3	0.6481 "	0.00055
4	0.4796 "	0.00050
5	0.4102 "	0.00105
6	0.2888 "	0.03

Breadth of instrument slit function = .767 cm^{-1}

questionable since the linear fit is not very good. The next part of the analysis uses a modified version of the NLLS fitting routine which yields better results for a_3 and the same results for the other coefficients.

NLLS Fit with Γ_3 a Dependent Variable

The value of a_0 obtained with the previous NLLS fitting procedure is questionable since Γ_0 has a poor linear fit. Representing Γ_3 as an independent variable is suspected to be the cause of the problem. In this fourth part of the analysis, all seven Γ_J are represented with dependent variables while Γ_e is represented with an independent variable as it is in the previous procedure. A different method is used to determine Γ_e, then the calculations are fit to each of the fourteen experimental spectra. The values of a_J for J=0 through 6 are then calculated with linear regression routines as before.

The NLLS fitting routine converges to results that depend on Γ_e. An overestimated Γ_e causes the routine to converge to smaller values of Γ_J since the total contribution of Γ_e, Γ_J, and the breadth of the spectral profile of the pump beam must best fit the breadths of the peaks in the experimental spectra. Since the results are sensitive to errors in Γ_e, it was estimated with a different method. In the previous procedure, Γ_e was estimated by fitting the effective slit function to the spectra of HF at 50 torr. The method has the shortcoming of assuming that a single spectra of low resolution has so few errors that other spectra are not needed for verification. An acceptable value is obtained since the results of the previous procedure are not sensitive to small errors in Γ_e. The new method uses all of the spectra to

determine the Γ_e rather than relying on only the spectra of HF at 50 torr. To determine Γ_e, the entire analysis procedure is performed with trial values of Γ_e. The accepted breadth is that which produces a_3 equal to the pressure-broading coefficient estimated from the infrared data. ($a_3 = 6.54 \times 10^{-4}$ cm^{-1}/torr) Trial values were used until it was found that an effective slit function with breadth 0.767 cm^{-1} HWHM yields $a_3 = 6.48 \times 10^{-4}$ cm^{-1}/torr. The value for Γ_e determined earlier, 0.785 cm^{-1}, yields $a_3 = 6.25 \times 10^{-4}$ cm^{-1}/torr. A 2.3% change in Γ_e causes a 3.5% change in a_3.

This second NLLS fitting procedure converges to linewidths that, as in the earlier procedure, yield magnitudes of the peaks which match the experimental spectra. However, the breadths of the experimental peaks are also fit since all Γ_J are dependent variables. The values for Γ_J may vary considerably because they are not bound by the independent Γ_3 as before. In other words, this second procedure provides a complete fit of the experimental spectra while the first procedure essentially only fits the magnitudes of the peaks. The routine converges more slowly than the routine with independent Γ_3 since it has the added degree of freedom.

The graphs of Γ_J vs. pressure are shown in Fig. 26 and the values for a_J are listed in Table VII. Γ_0 has a better linear fit than obtained with the earlier prodedure except for the linewidth at 650 torr. It is not known why the solution is so large at that point. All trial slit functions produced the same result. When a_0 was calculated, the point was ignored. The graph of Γ_3 illustrates the problem of treating it as an independent variable. The graph shows that the best fit is achieved with values of Γ_3 that are not on the straight line

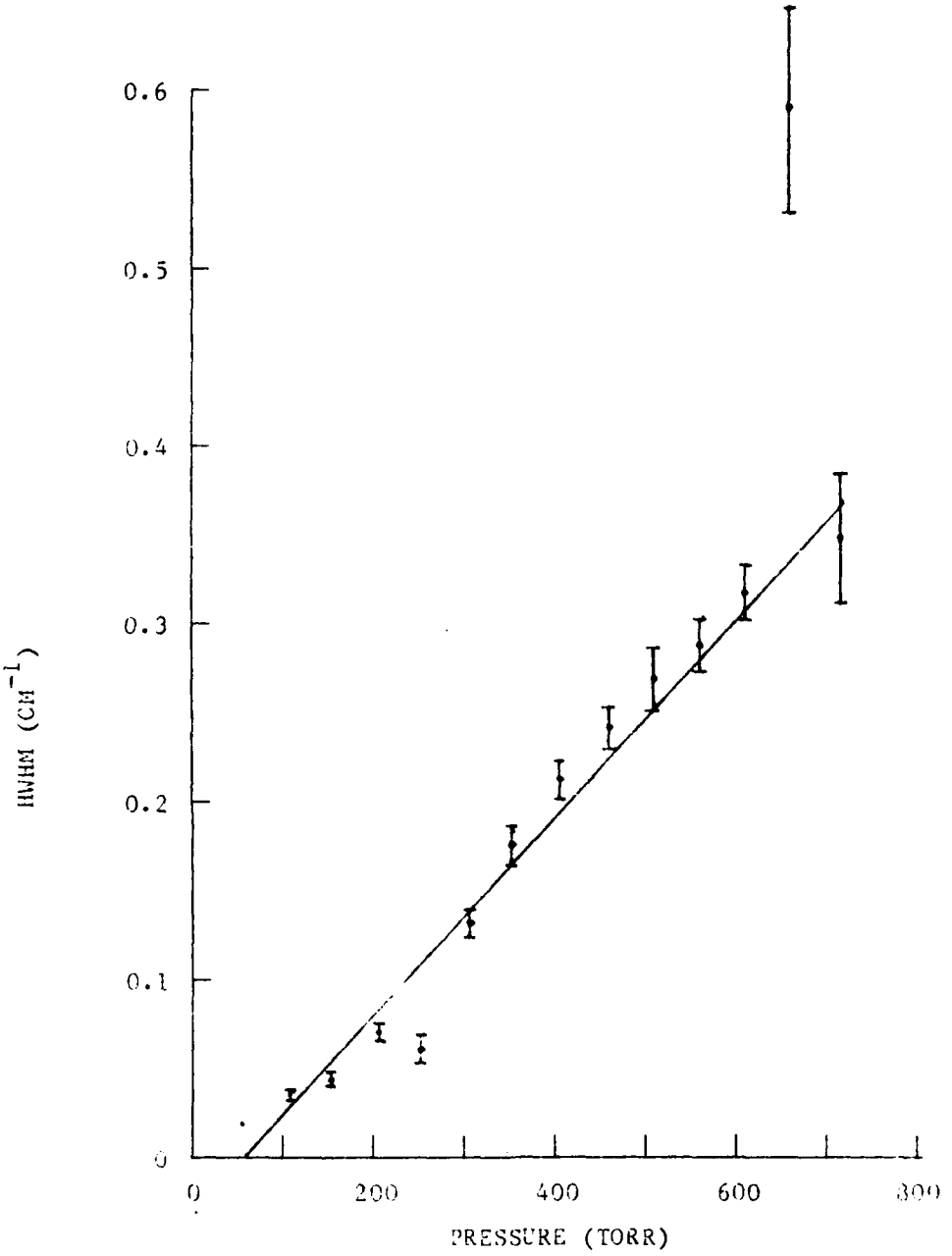

Fig. 26. Γ_J vs Pressure from the Results of NLLS Fitting Procedure Using No Reference Linewidth. Error bars correspond to $\pm$ 1 standard deviation (See Section II). Errors less than .003 cm^{-1} are not marked.

a) Γ_0 vs Pressure.

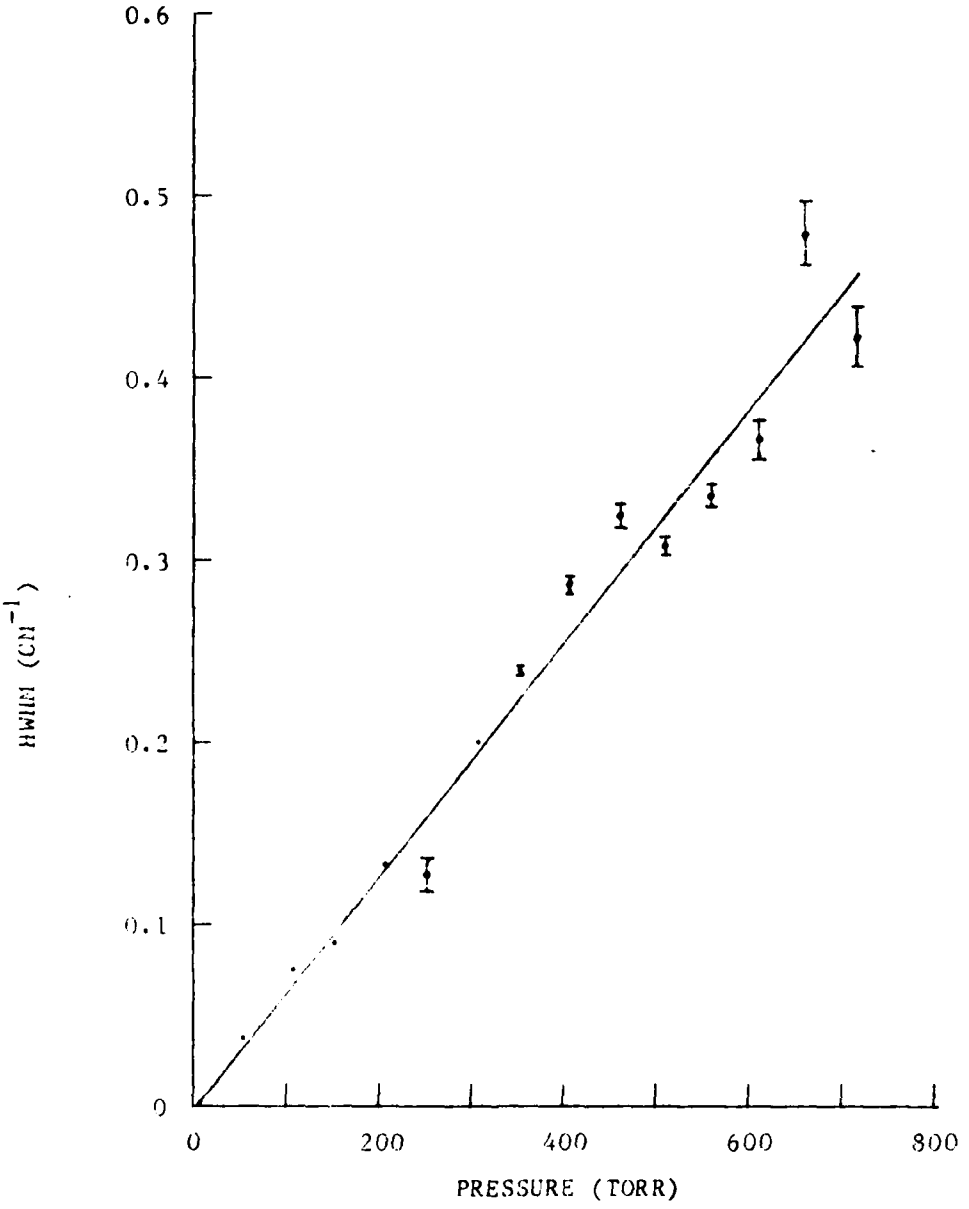

b) Γ_1 vs Pressure.

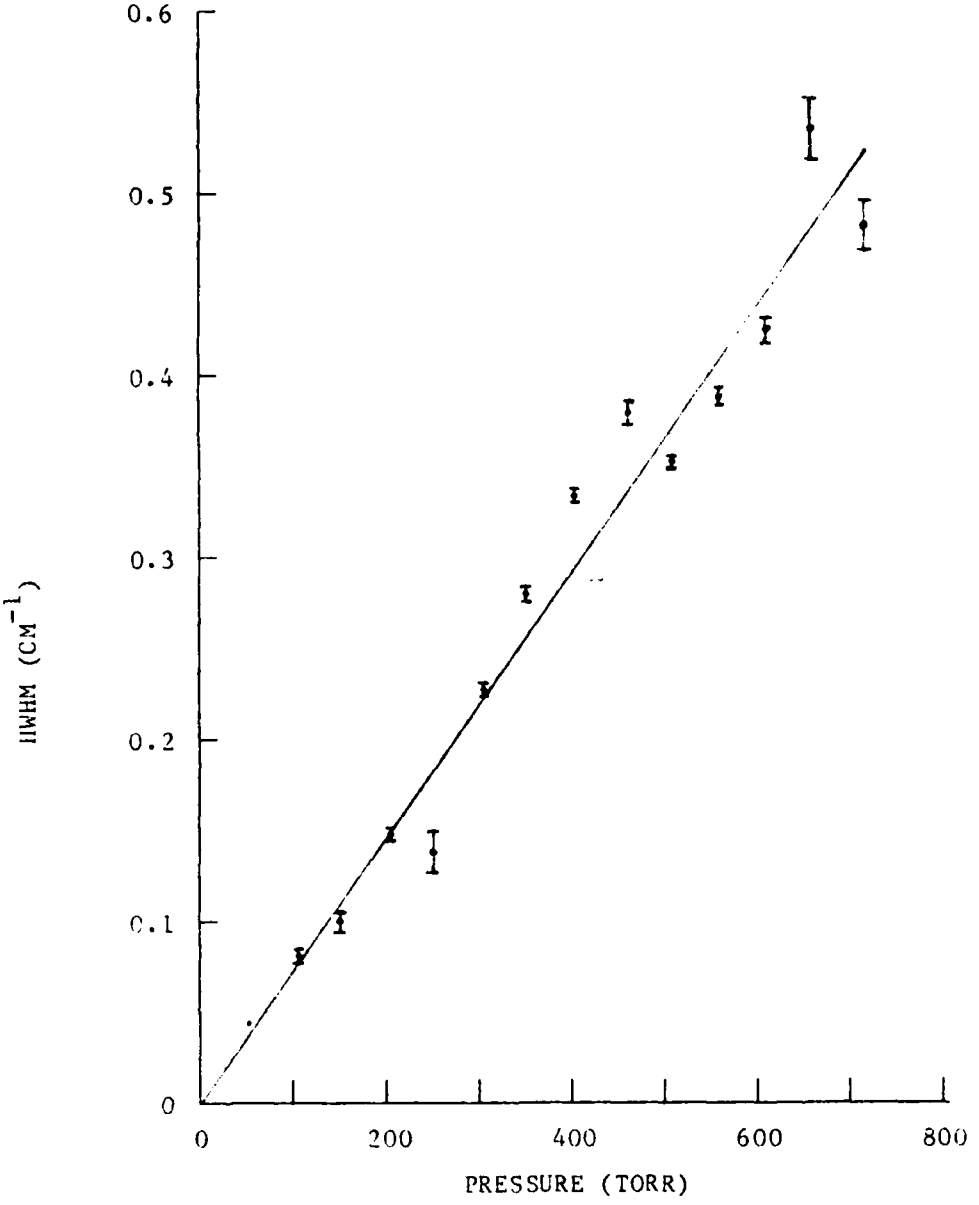

c) Γ_2 vs Pressure.

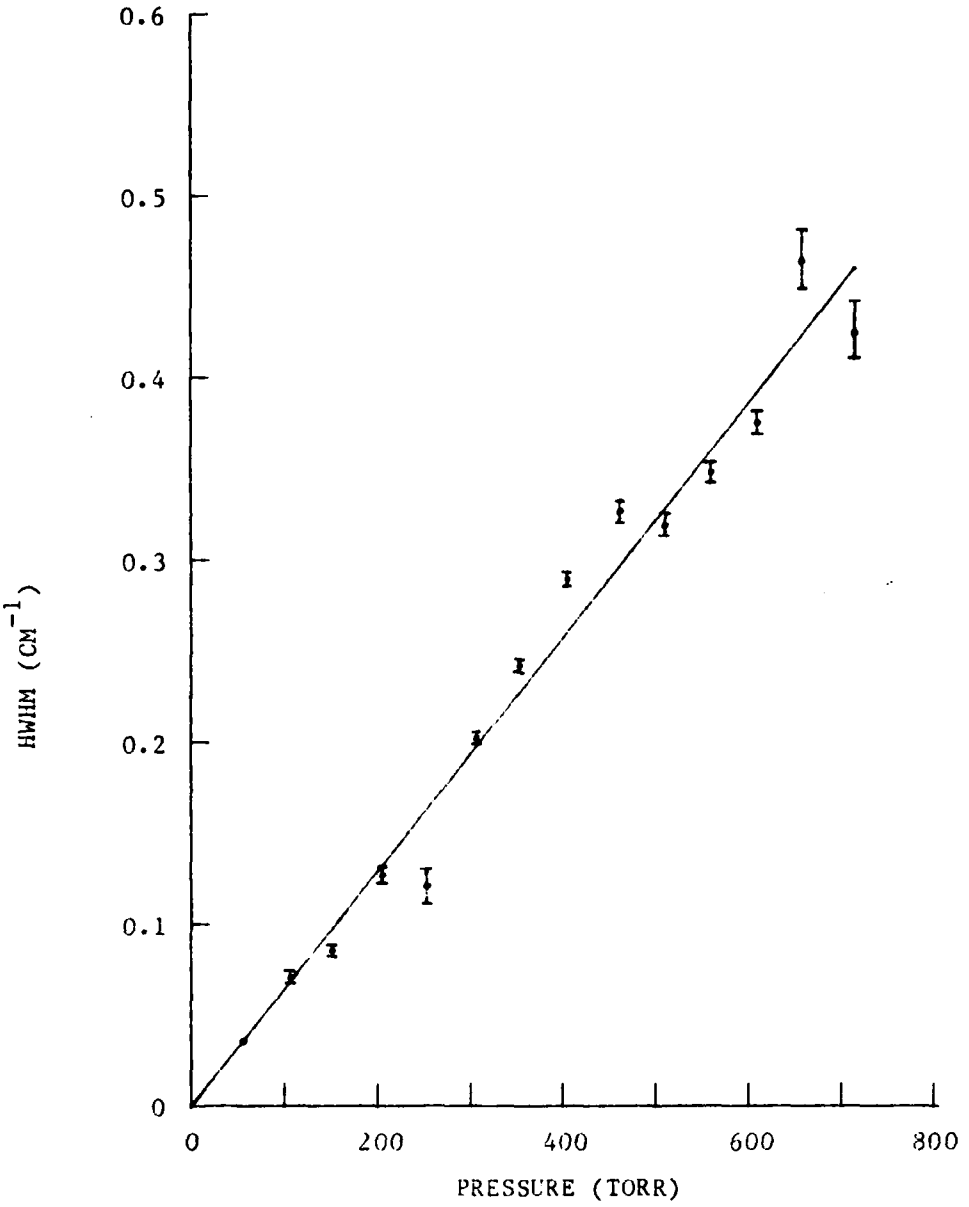

d) Γ_3 vs Pressure.

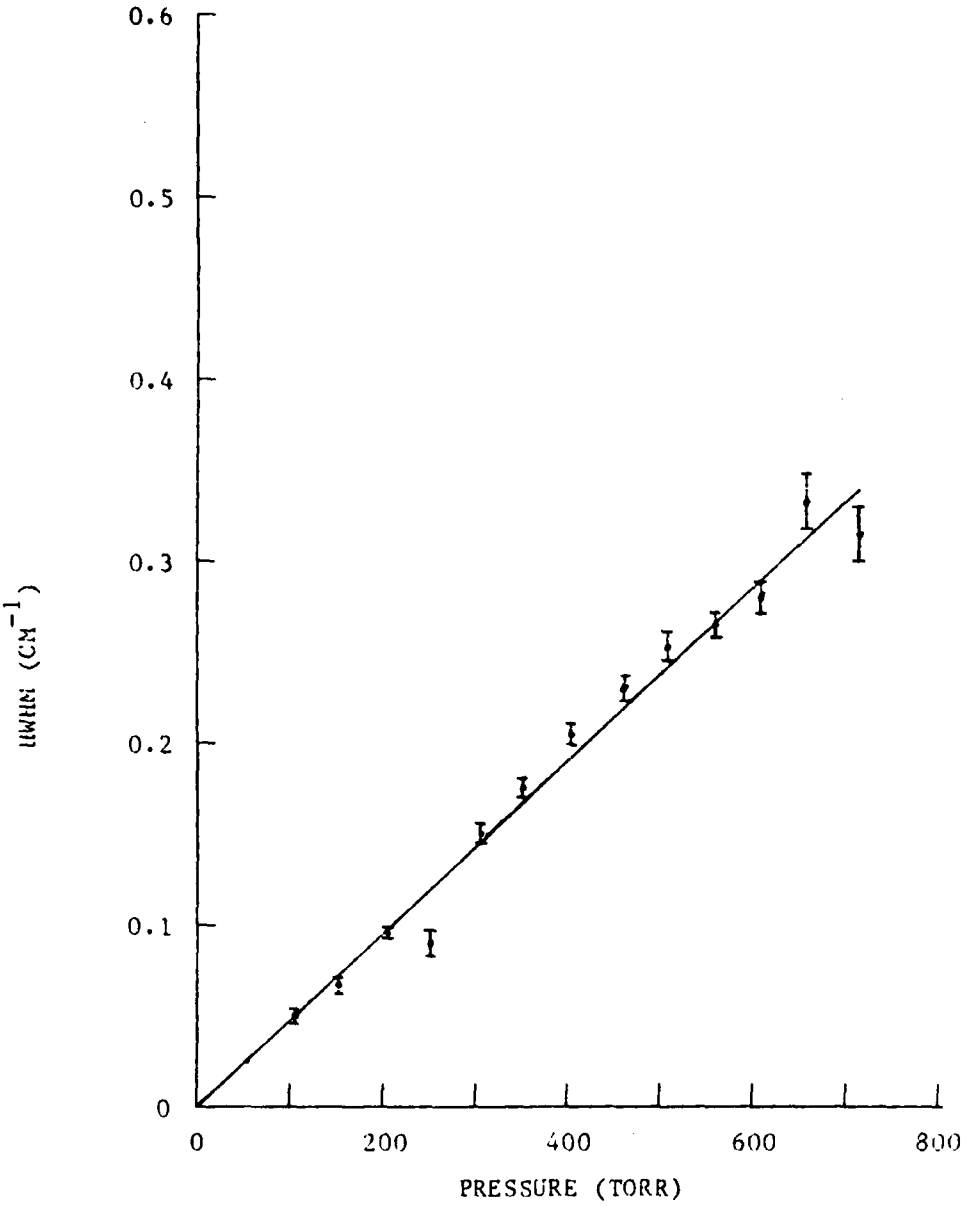

e) Γ_4 vs Pressure.

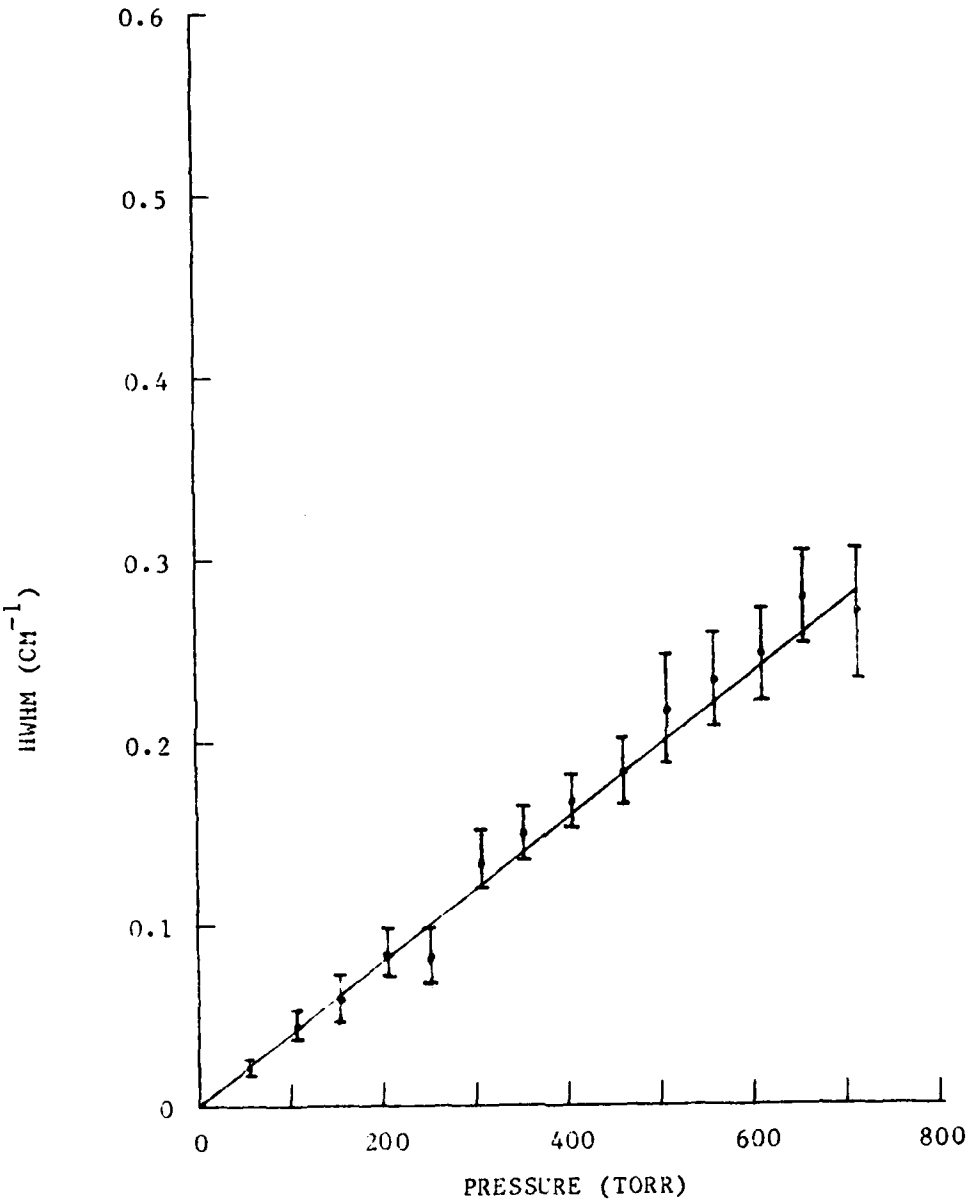

f) Γ_5 vs Pressure.

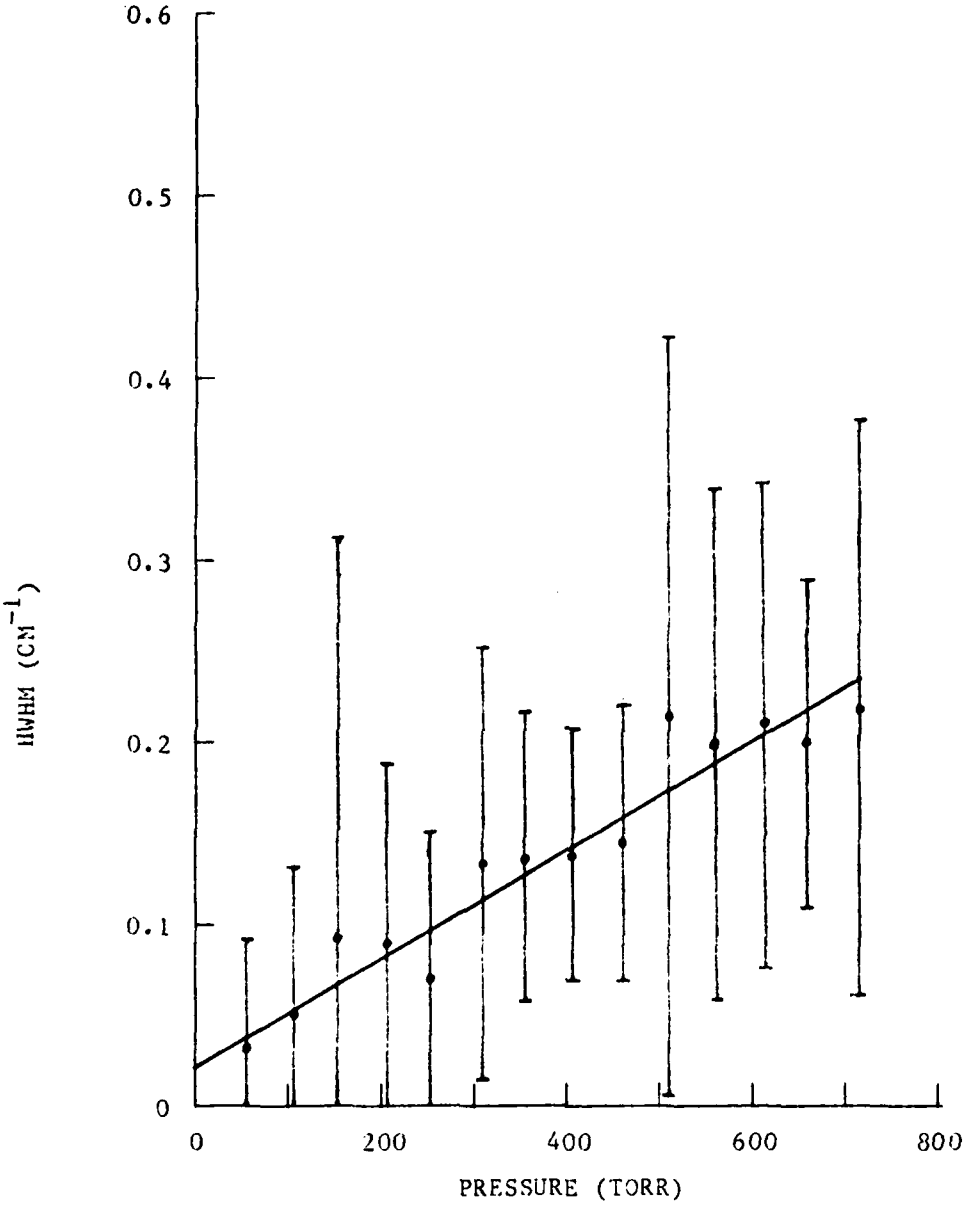

g) Γ_6 vs Pressure.

assumed in the earlier analysis. In the final part of the analysis, the validity of this second NLLS fitting procedure is tested by comparing the results with the first procedure and investigating the y-intercepts of the graphs of Γ_J vs. pressure.

Discussion of the Analysis Results

Two different procedures were used to find the pressure-broadening coefficients of the first seven Raman transitions given a_3. Both procedures require using NLLS fitting routines to estimate the linewidths of the transitions from each experimental spectra. However, the NLLS fitting routines were conceived for different reasons. The first routine is intended to exploit the knowledge of the linewidth of one transition so that the other linewidths can be found. At each pressure, Γ_3 was fixed to a known value and the NLLS fitting routine was programmed to find the other linewidths that would best fit the experimental spectra. On the other hand, the second routine is intended to exploit the knowledge of the pressure-broadening coefficient of one transition. Γ_e is chosen so that the solutions of Γ_3 at all pressures have a linear least-squares fit vs. pressure with a slope equal to the known value of a_3. The two methods are conceptually very different, but the results are not.

The pressure-broadening coefficients obtained from both procedures are graphed in Fig. 27. Even though the two procedures were different, the same solutions were obtained for all but the Q(0) and Q(6) transitions. The first procedure essentially extracts the linewidths from the information contained in the magnitudes of the peaks of each spectra. It is believed that accurate results can be obtained with

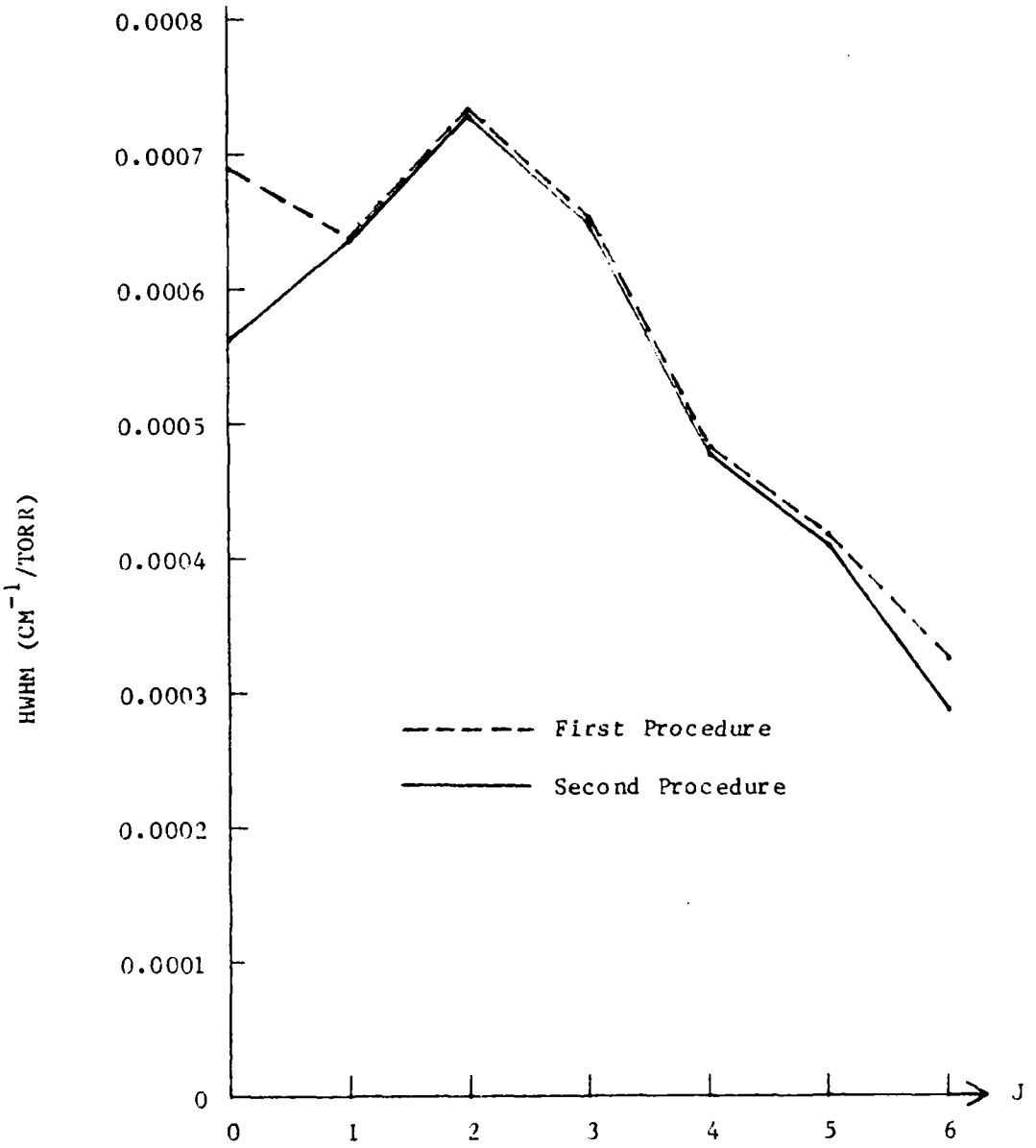

Fig. 27. Comparison of Pressure-Broadening Coefficients Obtained from Both NLLS Fitting Procedures.

accurate knowledge of Γ_3 because only a specific set of linewidths, with Γ_3 one member, can fit the magnitudes of the peaks in the experimental spectra. The insensitivity to small errors in Γ_e instills confidence in the procedure, but the result obtained for a_0 is questionable.

On the other hand, it was initially believed that the second procedure is unreliable since the final values for Γ_J at each pressure depend on the ability of the routine to distinguish small changes in the final spectra even with large percentage changes in the variables representing Γ_J. A fit with small residuals can be obtained with a wide range of Γ_J; a good fit is attained with any reasonable set of linewidths that yield the correct relative magnitudes of the peaks in the final spectra. The NLLS fitting routine minimized the residuals but they were so small that the validity of the process relies on the accuracy of all of the lineshape models used in the experiment. The fact that most of the results of the second procedure agree with those of the first indicates that the procedure is much more reliable that expected. Since it yields graphs of Γ_0 with a better linear fit than the first procedure, the second procedure probably gives the best estimate of a_0. The discrepency between the results of a_6 is probably due to the low intesity of the signal corresponding to that transition.

The estimate of a_3 was made from infrared data under the assumption that lifetime properties cause it to be between the pressure-broadening coefficients of the P(3) and R(3) transitions. Fig. 28 shows the graph of the pressure-broadening coefficients of the P-branch, Q-branch, and R-branch. The values for a_J are expected to be between the pressure-broadening coefficients of the P(J) and R(J) transitions. All a_J either

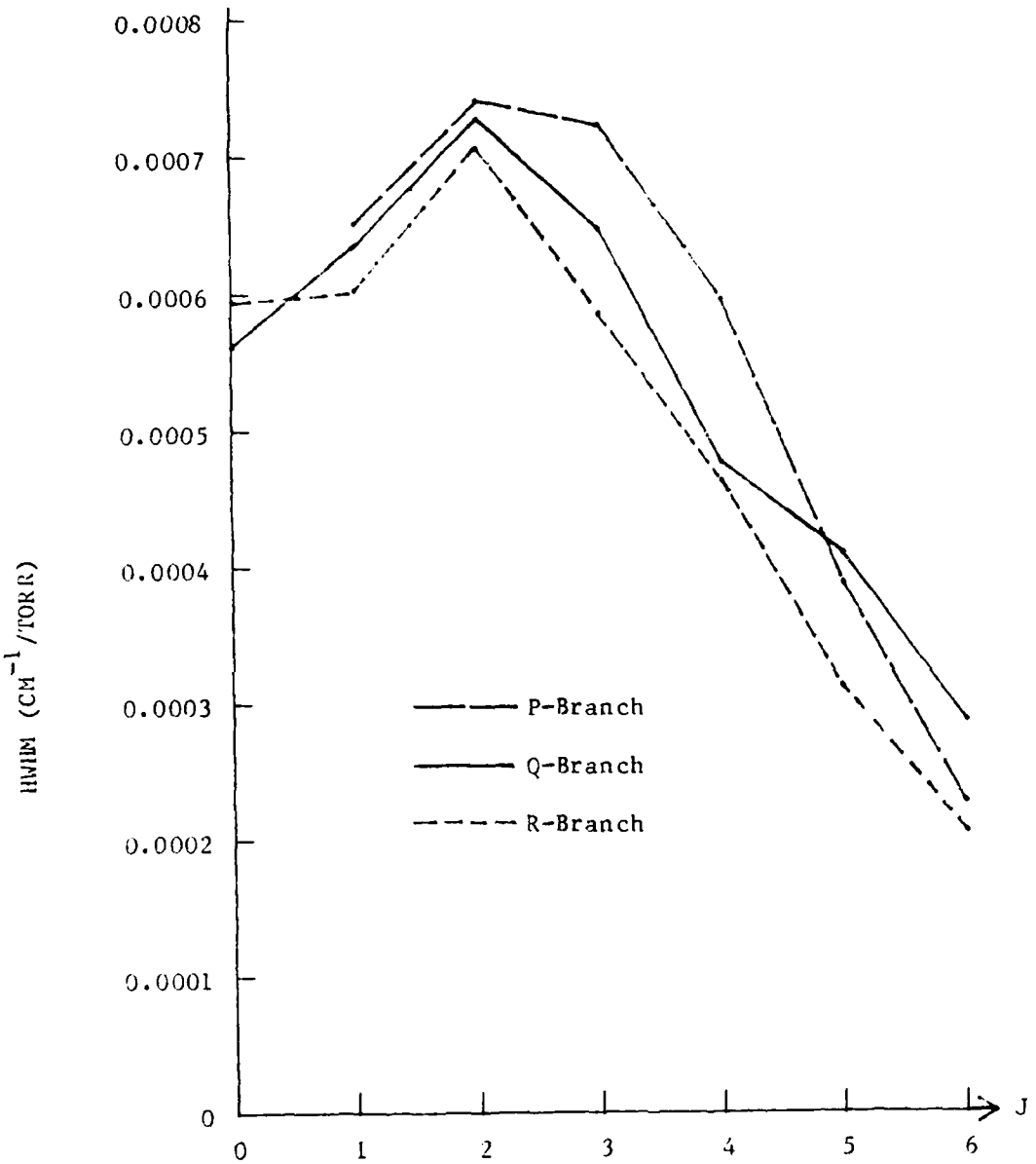

Fig. 28. Comparison of Pressure-Broadening Coefficients of the P-Branch, Q-Branch, and R-Branch of HF.

AD-A151 703 MEASUREMENT OF THE LINEWIDTHS OF HYDROGEN FLUORIDE Q-TRANSITIONS USING CO.. (U) AIR FORCE INST OF TECH WRIGHT-PATTERSON AFB OH SCHOOL OF ENGI.. R A CLEIS

2/2

UNCLASSIFIED DEC 83 AFIT/GEO/PH/83D-2 F/G 7/4 NL

END

FILMED

DTIC

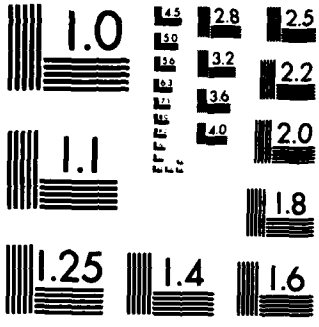

MICROCOPY RESOLUTION TEST CHART
NATIONAL BUREAU OF STANDARDS-1963-A

exhibit such behavior or at least have values close to the other pressure-broadening coefficients. Experimental and analytical errors contribute to the differences and the assumption is too simple to be accurate for all a_J. No consideration is given to the population densities of the states involved in the transitions even though the populations affect the pressure-broadening coefficients as well as the lifetimes of the states.

The validity of the second procedure can further be tested by investigating the y-intercepts of the regression lines computed for Γ_J vs. pressure. Although pressure-broadening does not occur at low pressures, the extrapolation of the regression lines should pass through the origin. The y-intercepts of the Q(1) through Q(5) transitions are near the origin, and the y-intercept of the Q(0) and Q(6) transitions are good considering the former is not resolved and the latter produced low intensity signals during the experiment (Table VIII). Since the only independent variable in the NLLS fitting routine was Γ_e, the sensitivity of the y-intercepts to Γ_e is analyzed.

The pressure-broadening coefficients and y-intercepts were determined, using the routines of the second procedure, with Γ_e equal to 0.7 cm^{-1} and 0.9 cm^{-1}. Table VIII displays the y-intercepts of each result as well as the y-intercepts obtained with the best estimate of Γ_e that was determined earlier. The overestimate causes negative intercepts and the underestimate causes positive intercepts. The negative intercepts obtained with Γ_e = 0.9 cm^{-1} HWHM are not very large since the fitting routine does not permit negative solutions to the linewidths. When Γ_e is overestimated, the solutions of all Γ_J become smaller, but the values of Γ_J at the lowest pressures can only approach

TABLE VIII

Values of Y-Intercepts of Linewidth Graphs from NLLS Fit Using Three Different Instrument Slit Functions

Units: cm^{-1} HWHM

	Breadth of Slit Function (cm^{-1} HWHM)		
Γ_J	0.7	0.767	0.9
0	-0.0528	-0.0307	-0.0023
1	0.1460	0.0045	-0.0060
2	0.0223	0.0036	-0.0120
3	0.0173	0.0006	-0.0118
4	0.0131	0.0050	-0.0074
5	0.0109	0.0011	-0.0040
6	0.0451	0.0300	-0.0193

zero. The effect not only keeps the solutions at low pressures artificially high; the solutions at the higher pressures are affected since the relative magnitudes of the peaks in the experimental spectra are determined by the relative magnitudes of Γ_J. Underestimates of Γ_e, on the other hand, cause the y-intercepts to rise more rapidly since the solutions to the linewidths can increase without bound.

The previous paragraph has shown that the y-intercepts are sensitive to errors in Γ_e, so the intercepts contain some information. The value of a_3 determined from the infrared data is probably a good estimate since the corresponding value for Γ_e yields y-intercepts near the origin.

The pressure-broadening coefficients that were obtained in the analysis of the y-intercepts are shown in Fig. 29. Errors in Γ_e cause approximately the same absolute error for each a_J except a_0. The graph practically can be used to estimate all of the a_J if any one of them is known. Six values of Γ_e between 0.7 cm^{-1} and 0.9 cm^{-1} were used to evaluate a_J, but they are not included in the graph for clarity reasons. All of the graphs were parrallel, so plotting a parallel graph through a known a_J should enable good estimates of the other six pressure broadening coefficients.

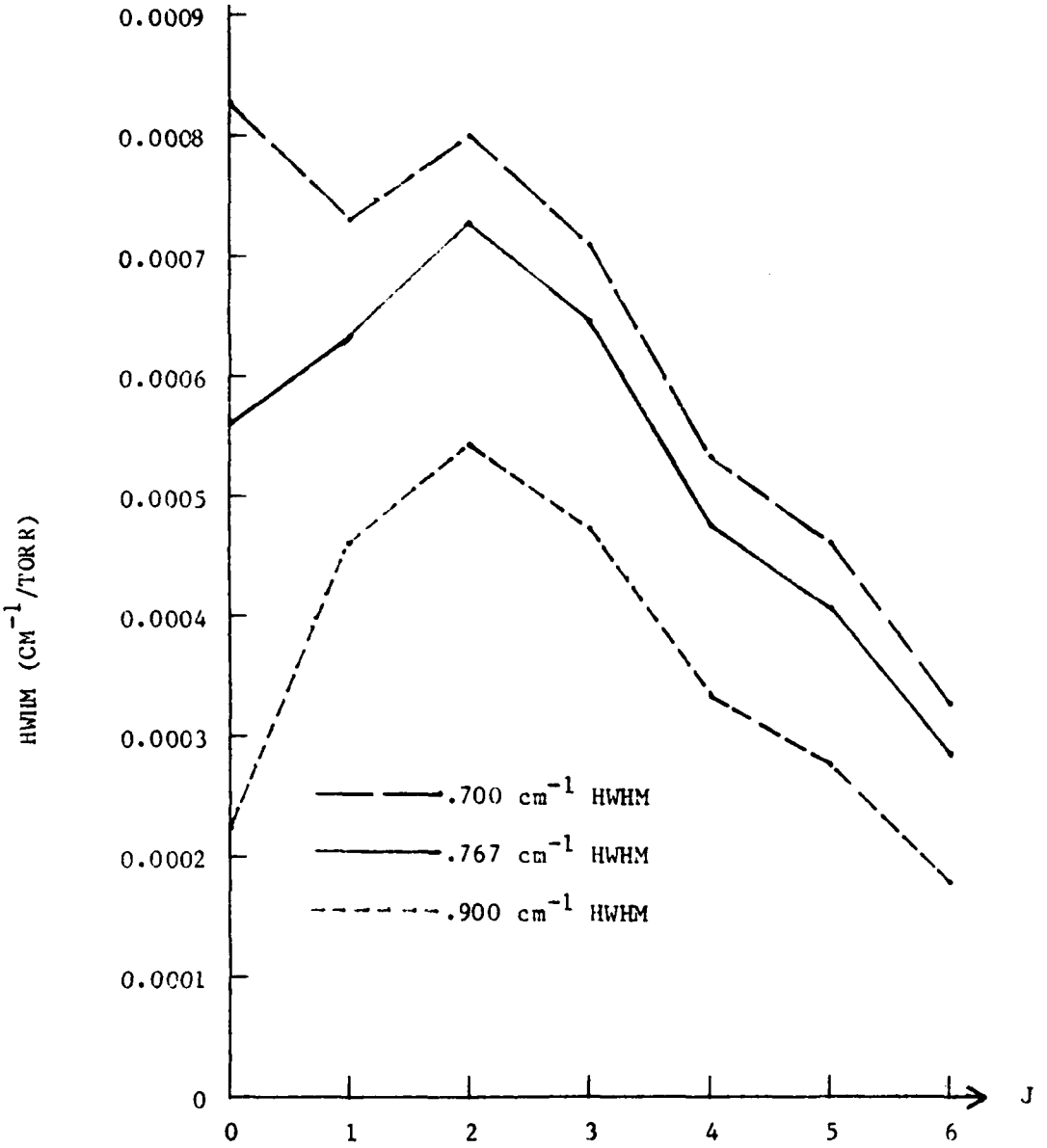

Fig. 29. Pressure-Broadening Coefficients Obtained with an Overestimate and an Underestimate of the Breadth of the Instrument Slit Function. The best estimate of the breadth is .767 cm^{-1} HWHM.

V. Conclusions

The pressure-broadening coefficients of the Q-branch Raman transitions in HF have been determined for the first time. Broad-band Coherent anti-Stokes Raman spectroscopy was used to obtain low-resolution spectra of the Raman transitions at various pressures, then equations for the CARS spectral density were used to find the linewidths of each transition vs. pressure. Accurate knowledge of the effective slit function of the detection equipment is desireable, but not essential. A calibration source is normally used to determine a slit function, but procedures developed here allow it to be determined from the CARS spectra.

It has been verified that the linewidths of the Raman transitions determine the relative magnitudes of the corresponding peaks in the CARS spectra. These magnitudes contain enough linewidth information that the linewidths can be estimated even for transitions which are severly blended in broad-band CARS spectra. Loosely speaking, high resolution equipment was effectively substituted with broad-band CARS and computational analyses.

Appendix: Calculation Details

The required numerical resolution of the calculations is dictated by the Raman susceptibility calculation (Eq 10). Since the equation yields a Lorentzian lineshape, the desired resolution should be several times greater than the minimum linewidth to be encountered. The most narrow transition encountered was approximately 0.02 cm^{-1} HWHM, so a calculation resolution of 0.005 cm^{-1} was desired. This increment would represent a 0.02 HWHM line with at least seven points. However, the available computer memory limited the spectral calculations to 8000 points. In the 60 cm^{-1} range of interest, 8000 points permits a resolution of 0.0075 cm^{-1}. At 50 torr, this resolution is marginal, but smaller resolutions would have required unreasonably complicated software development to overcome the memory deficiency. The extra work was considered unwarranted since the linewidths increase proportionately with pressure and the next lowest pressure measured has linewidths double those of the 50 torr data. Calculations were made at 50 torr regardless but no unusual effects could be discerned.

The first two of four steps of a spectrum calculation, finding the state populations and then χ^2, are performed and χ^2 is stored in an 8000 element array. The third step requires evaluating $S_{as}(\omega_{as})$ (Eq 8). To reduce computation time, only 1000 points are calculated for a resultant resolution of 0.06 cm^{-1}. An integration is computed only at every eigth point since the resulting spectra is smoothed considerably by the probe beam convolution. It may seem at first that a resolution of 0.0075 cm^{-1} is not necessary for the χ^2 calculation since it will be smoothed.

However, the high resolution requirement is necessary because the area under the peaks must be determined accurately since it is those areas that will "weight" the pump beam spectrum and determine the CARS spectrum. A 0.06 cm^{-1} resolution used with 0.02 cm^{-1} lineshapes might straddle the peak and severely underestimate the area. For each of the 1000 points determined by the convolution, the pump beam spectra was represented in 0.0075 cm^{-1} intervals and the integration was performed using the full resolution of the χ^2 array. In other words, the integrations used the χ^2 array and the pump beam profile represented in an array with the same 0.0075 cm^{-1} increment, but only calculated an intensity at 0.06 cm^{-1} intervals. The nonlinear least-squares fitting routines require the the estimation of points that in general fall between the 1000 points calculated. These magnitudes are computed assuming the spectra are linear between the points, an adequate approximation for the smooth resultant profiles.

The fourth and final step is convolving the CARS spectra with the instrument slit function. The slit function was determined to be approximately Lorentzian with a HWHM of 0.8 cm^{-1}, so a numerical resolution of 0.06 cm^{-1} was chosen for finding the final 1000 points. Spectra were calculated using a resolution of 0.0075 cm^{-1} for all integrations and compared with the much faster procedure with 0.06 cm^{-1} interals. No difference could be observed, so the low resolution method was used with confidence.

The convolutions were approximated differently for the pump beam than the slit function. The same quadratic area algorithm was used, but the range of the slit function calculation was larger. The pump beam

lineshape was Gaussian, so the individual area calculations in the convolution were carried out to three HWHM from center. On the other hand, the extensive wings on the Lorentzian slit function required integrating out to ten HWHM from center.

Bibliography

1. Barret, J. J. and R. F. Begley. "Low-Power CW Generation of Coherent Anti-Stokes Raman Radiation in CH_4 Gas," Applied Physics Letters, 27 (2): 129 (1975).

2. Roh, Won B. Coherent Anti-Stokes Raman Scattering of Molecular Gases. Technical Report AFAPL-TR-77-47. AF Aero Propulsion Laboratory, AF Wright Aeronautical Laboratories (AFSC), Wright-Patterson AFB, OH, August 1977.

3. Goss, L. P., D. D. Trump, B. C. MacDonald, and C. L. Switzer. "10 Hz Coherent Anti-Stokes Raman Spectroscopy Apparatus for Turbulent Combustion Studies," Rev. Sci. Instrum., 54 (5): 563-571 (May 1983).

4. Yuratich, M. A. "Effects of Laser Linewidths on Coherent Anti-Stokes Raman Spectroscopy," Molecular Physics, 38 (2): 625-655 (1979).

5. Weber, A. (Editor). Topics in Current Physics: Raman Spectroscopy of Gases and Liquids. New York, Springer-Verlag, 1979.

6. Herzberg, Gerhard. Spectra of Diatomic Molecules. New York, Van Nostrand Reinhold, 1950.

7. Huber, K.P. and G. Herzberg. Molecular Spectra and Molecular Structure": IV. Constants of Diatomic Molecules. New York, Van Nostrand Reinhold, 1979.

8. Wilkins, Roger L. Vibration Rotation Bands of HF and DF. Technical Report TR-0077(2603)-7. Aerospace Corporation, Aero Physcis Lab, El Segundo, CA, September 1977.

9. Anderson, P. W. "Pressure-Broadening in the Microwave and Infrared Regions," Physical Review, 76: 647-661 (1949).

10. Benedict, W. S. and R. Herman, "The Calculation of Self-Broadened Linewidths in Linear Molecules," Journal of Quantitative Spectroscopy and Radiative Transfer, 3: 265-278 (1963).

11. Kim, Hyunyong. "Computer Programming in Physical Chemistry Laboratory: Least-Squares Analysis," Journal of Chemical Education, 47 (2): 126-122 (February 1970).

12. Kuipers, G.A. "The Spectrum of Monomeric Hydrogen Fluoride: Lineshapes, Intensities, and Breadths," Journal of Molecular Spectroscopy, 2 (2): 75-98 (April 1958).

13. Herget, W.F., W.E. Deeds, N.M. Gailar, "Infrared Spectrum of Hydrogen Fluoride: Line Position and Lineshapes. Part II. Treatment of Data and Results," Journal of the Optical Society of America 52 (10): 113-119 (October 1962).

14. Beigang, R., G. Litfin, and R. Schneider "Halfwidths of Pure and Foreign-Gas-Broadened 2.5 um HF Absorbtion Spectra," Physical Review A, 20 (1): 229-232 (1979).

VITA

Lieutenant Richard A. Cleis was born on 5 June 1960 in Bristol, Pennsylvania. He moved west in 1969 and graduated from high school in Newbury Park, California in 1978. He attended the University of Southern California and received the degree of Bachelor of Science in Electrical Engineering in May 1982. Upon graduation, he received a commission in the USAF through the ROTC program and immediately entered the School of Engineering, Air Force Institute of Technology.

REPORT DOCUMENTATION PAGE

RT SECURITY CLASSIFICATION	1b. RESTRICTIVE MARKINGS
RITY CLASSIFICATION AUTHORITY SSIFIED .ASSIFICATION/DOWNGRADING SCHEDULE	3. DISTRIBUTION/AVAILABILITY OF REPORT Approved for public release; distribution unlimited
)RMING ORGANIZATION REPORT NUMBER(S) GEO/PH/83D-2	5. MONITORING ORGANIZATION REPORT NUMBER(S)
E OF PERFORMING ORGANIZATION: ol of Engineering 6b. OFFICE SYMBOL (If applicable): AFIT/EN	7a. NAME OF MONITORING ORGANIZATION
RESS (City, State and ZIP Code) r Force Institute of Technology ight-PATTERSON AFB, Ohio 45433	7b. ADDRESS (City, State and ZIP Code)
E OF FUNDING/SPONSORING ANIZATION: WAL 8b. OFFICE SYMBOL (If applicable): POOC-3	9. PROCUREMENT INSTRUMENT IDENTIFICATION NUMBER
RESS (City, State and ZIP Code) ight-Patterson AFB, Ohio 45433	10. SOURCE OF FUNDING NOS. PROGRAM ELEMENT NO. / PROJECT NO. / TASK NO. / WORK UNIT NO.
E (Include Security Classification) e Box 19	

SONAL AUTHOR(S)
chard A. Cleis, B.S., 2d Lt, USAF

PE OF REPORT	13b. TIME COVERED	14. DATE OF REPORT (Yr., Mo., Day)	15. PAGE COUNT
Thesis	FROM _____ TO _____	1983 December	107

PLEMENTARY NOTATION

COSATI CODES		
	GROUP	SUB. GR.
	04	

18. SUBJECT TERMS (Continue on reverse if necessary and identify by block number)
Molecular spectroscopy; Hydrogen fluoride
Raman spectroscopy; infrared spectroscopy.

TRACT (Continue on reverse if necessary and identify by block number)

Title: MEASUREMENT OF THE LINEWIDTHS OF HYDROGEN FLUORIDE Q-TRANSITIONS USING COHERENT ANTI-STOKES RAMAN SPECTROSCOPY

Theses Advisor: Won B. Roh

Approved for public release: IAW AFR 190-17.
LYNN E. WOLAVER
Dean for Research and Professional Development
Air Force Institute of Technology (ATC)
Wright-Patterson AFB OH 45433
21 Feb 83

RIBUTION/AVAILABILITY OF ABSTRACT SSIFIED/UNLIMITED ☒ SAME AS RPT. ☐ DTIC USERS ☐	21. ABSTRACT SECURITY CLASSIFICATION UNCLASSIFIED
ME OF RESPONSIBLE INDIVIDUAL Won B. Roh, Associate Professor of Physics	22b. TELEPHONE NUMBER (Include Area Code): 255-4498 22c. OFFICE SYMBOL: AFIT/ENP

SECURITY CLASSIFICATION OF THIS PAGE

The measurement of the linewidths of the Hydrogen Fluoride Q-branch vibrational-rotational transitions was performed using coherent anti-Stokes Raman spectroscopy (CARS). A broadband CARS system was used to excite the first seven vibrational-rotational transitions in the Q-branch of HF. Low resolution spectra were recorded on an optical multichannel analyzer at pressures from 50 to 700 torr in 50 torr increments. At each pressure, 1000 measurements were averaged. A computer was programmed to best fit calculated spectra to experimental spectra by adjusting the linewidths. The linewidth of the Q(3) transition was estimated from infrared data then used as a reference in determining the linewidths of the other transition. All lines displayed pressure broadening in the pressure region investigated with relative magnitudes consistent with theory and available infrared data. Although the Q-branch lines of the observed spectra were partially blended, the CARS measurements and calculations permitted consistent linewidth measurements over the experimental pressure range. Accurate knowledge of the instrument slit function permits linewidth measurements without requiring a reference.

END

FILMED

5-85

DTIC